Emissions and In-Cylinder Combustion Characteristics of Fischer-Tropsch and Conventional Diesel Fuels in a Modern CI Engine

by

Alexander G. Sappok

B.S., Mechanical Engineering
Kansas State University, 2004

Submitted to the Department of Mechanical Engineering in Partial Fulfillment of the Requirements for the Degree of

MASTER OF SCIENCE IN MECHANICAL ENGINEERING

AT THE

MASSACHUSETTS INSTITUTE OF TECHNOLOGY

FEBRUARY 2006

Signature of Author: _____

// Department of Mechanical Engineering
January 20, 2006

Certified by: _____

Victor W. Wong
Principle Research Scientist and Lecturer in Mechanical Engineering
Thesis Supervisor

Accepted by: _____

Lallit Anand
Chairman, Department Committee on Graduate Students

(This page intentionally left blank)

Emissions and In-Cylinder Combustion Characteristics of Fischer-Tropsch and Conventional Diesel Fuels in a Modern CI Engine

by

Alexander G. Sappok

Submitted to the Department of Mechanical Engineering
on January 20, 2006 in partial fulfillment of the
requirements for the Degree of Master of Science in
Mechanical Engineering

ABSTRACT

Increasingly stringent emissions regulations, rising oil prices, and an increased focus on environmental awareness are driving the search for clean, alternative fuels. Derived from natural gas, coal, and even biomass Fischer-Tropsch (FT) fuels are one such alternative. The inherently clean nature of FT diesel coupled with the fact that FT diesel exhibits similar physical properties to those of conventional diesel make FT diesel an ideal candidate as both a blending agent with and eventual replacement for conventional petroleum-based diesel fuels.

The potential for emissions reduction with FT diesel fuels in laboratory engine tests and on-road vehicle tests is well documented. While a number of chemical and physical characteristics of FT fuels have been attributed to the observed reduction in emissions, the actual effects of both the fuel properties and in-cylinder combustion characteristics in modern diesel engines are still not well understood. In this study a 2002, six-cylinder, 5.9 liter, Cummins ISB 300 diesel engine, outfitted with an in-cylinder pressure transducer, was subjected to a subset of the Euro III 13-mode test cycle under steady-state operating conditions.

Emissions and in-cylinder pressure measurements were conducted for neat FT diesel, low sulfur diesel (LSD), ultra-low sulfur diesel (ULSD), and a blend of FT/LSD. The experimental results show a significant reduction in regulated emissions with the neat FT fuel and a more than proportional reduction in particulate emissions for the blend. In order to provide further insight into the emissions behavior of the fuels, combustion characteristics were determined from a heat release analysis based on the in-cylinder pressure measurements. In addition, a detailed chemical analysis of the fuels and particulate emissions was carried out. The differences in the measured combustion characteristics and fuel properties were compared to the emissions variations between the fuels studied, and an explanation for the observed emissions behavior of the fuels was developed.

Thesis Supervisor: Victor W. Wong
Title: Principle Research Scientist and Lecturer in Mechanical Engineering

(This page intentionally left blank)

Acknowledgements

A number of people have contributed to making my time at MIT a memorable, always interesting, and extremely rewarding experience. My time at the Institute has afforded me a multitude of opportunities to grow and develop on a number of levels, and for that I am extremely grateful.

I would like to extend my sincerest thanks to my thesis advisor, Dr. Victor Wong, for allowing me the opportunity to spend my time here working on a project that I truly enjoy. Aside from learning to conduct scientific research and the technical experience itself, Dr. Wong has helped me to develop the ability to critically evaluate experimental results. More importantly, I have learned through his example that, more often than not, this analysis can be accomplished with little more than a scrap of paper in under five minutes; however I am still continually amazed by his "back-of-the-envelope" calculations. Lastly, my experience at MIT would not have been nearly as rewarding without the opportunity to work independently and publish and present my work at conferences around the world, and for that I wish to thank Dr. Wong as well.

The contributions of Thane DeWitt and Raymond Phan to the successful completion of this project were immeasurable. Thane's experience, professionalism, sound technical advice, and help in procuring countless parts and supplies contributed greatly to the timely completion of this project. Raymond's help in fabricating and installing numerous components and day-to-day lab operations was invaluable, and I wish to thank him for all of his contributions to the experimental setup. Both Thane and Raymond's cheerful demeanor always brightened my day and made working in the lab that much more enjoyable.

This project would not have been possible without the support of the Integrated Concepts and Research Corporation (ICRC) funded under the DOE Cooperative Agreement No. DE-FC26-01NT41099. I would like to thank Syntroleum for providing the GTL fuel and fuel analysis, and especially Dr. Robert Freerks for his technical comments. Many thanks also go to Michael Blanz and the staff at Cummins Technical Center for their technical support, Jeremy Llaniguez for the initial experimental setup, Joseph Acar for passing on his experience and advice regarding the project, Jeff Jocsak for his help with the heat release programs, and Michael Radovanovic for reviewing my work.

Most of all I would like to thank my family for all of their support and the inspiration they have provided me with every step of the way. I am especially grateful to my parents for the example they set each and every day, and many thanks go to my father for his commission-free technical advice. I am also extremely blessed to have the loving support of my girlfriend, Heidi, whose patience, encouragement, and support has made my time here at MIT that much happier.

Finally, I would like to thank all of my colleagues at the Sloan Automotive Laboratory for making the lab such an enjoyable place to work and for the opportunity to develop many lasting friendships.

(This page intentionally left blank)

Table of Contents

(This page intentionally left blank)

List of Figures

List of Tables

(This page intentionally left blank)

Nomenclature

API	American Petroleum Institute
ASTM	American Society for Testing and Materials
BMEP	Brake Mean Effective Pressure
bTDC	Before Top Dead Center
CA	Crank Angle
CARB	California Air Resource Board
CI	Compression Ignition
CN	Cetane Number
c_p	Specific Heat at Constant Pressure
c_v	Specific Heat at Constant Volume
DAQ	Data Acquisition
DI	Direct Injection
DeNOx	NOx Reduction Trap
DPF	Diesel Particulate Filter
$dU_{\text{int ernal}}$	Change in internal energy
ECM	Electronic Control Module
EGR	Exhaust Gas Recirculation
EOC	End of Combustion
ESC	European Stationary Cycle
EPA	Environmental Protection Agency
FT	Fischer-Tropsch
GC	Gas Chromatography
HCLD	Heated Chemiluminescence Detector
HFID	Heated Flame Ionization Detector
ICRC	Integrated Concepts and Research Corporation
IDI	Indirect Injection
IMEP	Indicated Mean Effective Pressure
LSD	Low Sulfur Diesel
M_f	Molecular weight of the fuel
NDIR	Non-Dispersive Infrared
NOx	Oxides of Nitrogen
n_b	Total number of moles of burned mixture
n_i	Number of moles of species i per mole of O_2
n_u	Total number of moles of unburned mixture
Oxi-Cat	Oxidation Catalyst
P	Cylinder Pressure
PAH	Polycyclic Aromatic Hydrocarbons
PM	Particulate Matter
PPM	Parts per Million
SCR	Selective Catalytic Reduction
SI	Spark Ignition
SLPM	Standard Liters per Minute
SOC	Start of Combustion

SOF	Soluble Organic Fraction
SOI	Start of Ignition
SOL	Solid Carbonaceous Matter
TDC	Top Dead Center
TEM	Transmission Electron Microscopy
TPM	Total Particulate Mass
ULSD	Ultra-Low Sulfur Diesel
V	Cylinder Volume
VI	Virtual Instrument
VGT	Variable Geometry Turbocharger
VOF	Volatile Organic Fraction
y	Molar H/C ratio of the fuel
α	Coefficient to obtain average molecular weight of the fuel
γ	Ratio of specific heats
$\delta Q_{chemical}$	Chemical energy of the fuel
δQ_{HT}	Energy lost through heat transfer
δW	Work done on the piston
θ	Crank angle
λ	Air/fuel ratio
ϕ	Fuel/air equivalence ratio
$\widetilde{x}_i$	Wet mole fraction of species i
x_b	Burned gas fraction
$\widetilde{x}_i^*$	Dry mole fraction of species i
ψ	Molar N/O ratio

1.0 Introduction and Background

1.1 Diesel Engine Fundamentals

The diesel engine technology of today has come a long way since its inception over a century ago by Rudolph Diesel. In his first patent filed in Germany in 1892, Diesel outlined the design for an innovative new internal combustion engine in which combustion was initiated by injecting liquid fuel into air heated solely by compression. This fundamental difference between Diesel's compression ignition (CI) engine and conventional spark ignition (SI) engines of the time yielded an improvement in efficiency of nearly a factor of two when the engine was first introduced [1].

Despite a number of advances in diesel engine technology in the century since diesel introduced his first engine, the fundamental operating principles of the diesel engine have remained virtually unchanged. In its most basic form, a diesel engine is a reciprocating-piston engine employing internal (heterogeneous) mixture formation and autoignition to initiate combustion. During the engine's compression stroke, intake air is compressed to 30 to 55 bar resulting in a temperature increase within the cylinder of 700 to 900°C. Fuel is injected either directly into the cylinder or into an adjacent pre-combustion chamber late in the compression stroke, near piston top dead center (TDC), upon which the elevated temperature within the cylinder causes the fuel to autoignite [2].

Mixture formation in the diesel engine, therefore, plays a vital role in diesel autoignition and subsequent combustion as well as the attainable mean effective pressure [2]. Unlike spark ignition engines that control load by restricting the intake air by means of a throttle plate, load in a diesel engine is controlled by varying the amount of fuel injected per cycle. The absence of any fuel in the cylinder during the compression stroke also eliminates the possibility of uncontrolled auto ignition or engine knock, a major problem limiting the compression ratio of SI engines. As such, the compression ratio in diesel engines can be up to twice that of a conventional SI engine, in the range of 12 to 24 depending upon engine size and aspiration [2].

1.1.1 Diesel Engine Advantages

Due to the nature of the diesel combustion process, diesel engines exhibit a number of advantages over conventional spark ignition engines the most notable of which are: improved efficiency and better fuel economy, lower greenhouse gas and hydrocarbon emissions, higher torque at lower engine speeds, and extended engine life. In addition to the qualities inherent to the engine itself, engine maintenance and fuel costs for diesel engines are also typically lower than the costs associated with comparable SI engines [3].

The significant improvement in efficiency for the diesel engine is attributed primarily to the engine's higher compression ratio, low pumping losses due to the absence of any type of throttle mechanism, overall lean operation, and reduced friction losses. Diesel engines typically run at slower engine speeds than SI engines, due in part, for the need to allow time for the heterogeneous mixture formation and autoignition to occur. The slower engine speeds, thus, contribute to a reduction in friction losses within the power cylinder [3]. Furthermore, the diesel engine's higher efficiency translates into a 20-40% improvement in fuel economy for diesel-powered vehicles when compared to their gasoline-powered equivalents [4].

The very nature of the diesel combustion process also results in a significant amount of heat released earlier and at a faster rate in the expansion stroke than in a gasoline engine. A direct result of the greater amount of heat released early in the expansion stroke is the production of higher torque at lower engine speeds. In order to withstand the higher in-cylinder pressure and faster rate of heat release, diesel engines are typically constructed in a much more robust manner than SI engines. This fact, combined with the reduced friction in the power cylinder, leads to an extension of the useful life of a diesel engine three to four times that of a comparable gasoline engine. Furthermore, many of today's heavy-duty diesel engines are designed for a service life of one million miles before the first overhaul [3].

Aside from the performance advantages, the lean nature of diesel combustion also results in extremely low CO emissions. Furthermore, the absence of any fuel in the cylinder

during the compression stroke reduces the formation of HC emissions from crevice volumes [1]. The low HC and CO emissions eliminate the need for expensive aftertreatment systems to further reduce HC and CO levels such as the three-way catalysts employed with SI engines.

1.1.2 Diesel Engine Disadvantages

While the benefits listed in the previous section combine to make the diesel engine the most efficient internal combustion engine in mass production today, there is still significant room for improvement in a number of key areas. The major disadvantages of the diesel engine are: elevated NOx and particulate emissions, heavy weight and low specific power output, reduced engine speed and low exhaust temperatures, and elevated engine noise levels.

The complex heterogeneous nature of diesel combustion leads to significant NOx and particulate matter (PM) emissions from diesel engines. The problem of reducing both of these emissions simultaneously is, perhaps, the most difficult challenge facing diesel engine development today. Furthermore, the overall lean nature of diesel combustion complicates NOx reduction via exhaust aftertreatment systems, as NOx reduction in an oxygen-rich environment cannot currently be easily achieved [3]. An additional disadvantage of lean combustion in diesel engines is its associated reduction in exhaust temperature, which complicates particulate emissions reduction using particulate filters and traps, since these units require temperatures in excess of 600°C for complete soot oxidation and regeneration [5].

While the problem of reducing NOx and PM emissions is currently the most pressing challenge facing the diesel industry, a number of additional diesel engine design and operating characteristics are the focus of substantial improvement efforts as well. The robust engine design requirements, imposed by the severe nature of the diesel combustion process, lead to increased engine size and weight. As a result, the specific power output of diesel engines is typically only 50% to 65% of that of comparable gasoline engines. An additional consequence of the rapid autoignition event in diesel engines is elevated

engine noise, especially at idle. In an effort to reduce engine noise and emissions, most modern diesel engines are now equipped with precision high-pressure fuel injection systems, which, while effective, also add substantial cost to the engine [3].

1.1.3 Diesel Engine Applications

Despite some apparent disadvantages, the benefits of diesel engines, namely high efficiency and improved fuel economy, durability, and high power output have made the diesel engine the power plant of choice in a large and varied number of applications. Currently diesel engines are used in many industries including transportation, construction, agriculture, and mining, and power a wide range of vehicles from large container ships and locomotives to light-duty passenger cars and agricultural equipment.

Based on a 2000 study titled "Diesel Technology and the American Economy," diesel-powered vehicles transport over 95% of all freight in the United States. Furthermore, based on the fraction of fuel energy consumed by vehicle type, diesel engines power 80% of all buses (transit, intercity, and school), 100% of all freight ships, 100% of all freight trains, and 23% of all passenger trains (transit, commuter, and intercity). In addition, based on the fraction of fuel energy consumed by sector, diesel engines power 83% of all construction equipment, 66% of all agricultural equipment, and 22% of all mining equipment in the U.S. [6].

While diesel engines find widespread use in a number of heavy-duty vehicles, their acceptance in the light-duty and passenger vehicle market in the U.S. has been slow. A market survey conducted by R.L. Polk & Company in 2004 showed that for vehicles offering a choice between gasoline- and diesel-powered versions, 59% of consumers chose diesel engines in the medium-duty truck segment, whereas only 11% chose the diesel-powered version in the light-duty segment, and only 6% chose diesel passenger vehicles. Furthermore, diesel-powered vehicles made up only 3.37% of the new U.S. passenger vehicle market in 2004, up from 2.25% in 2000 [7].

The case for diesel engines in the automotive and passenger vehicle market in Europe and many other parts of the world is quite different from that of the United States. Already in 1990 14% of all new car registrations in Western Europe were diesels, with the number rising to 40% by 2002 and 51.9% by 2004. Based on projected sales estimates, the automotive diesel market share in Europe is expected to extend well over 50% by 2010 [8].

1.2 Project Motivation

The growing number of diesel engines in use in the United States and Europe has prompted concern over the contribution of diesel engines to the overall atmospheric emissions inventory. Combined with increasing evidence demonstrating the adverse health effects posed by diesel particulate (PM) emissions [9], this concern has given rise to increasingly stringent emissions regulations aimed at drastically reducing exhaust emissions from diesel engines. These new regulations are some of the most important factors driving diesel engine development in the United States and Europe today.

In order to meet these strict requirements, engine manufacturers are finding it more and more difficult to reduce emission levels through in-cylinder optimization alone. As a result, exhaust aftertreatment systems and cleaner diesel fuels present additional means for meeting these requirements. The trend toward cleaner fuels for reduced emissions and improved compatibility with aftertreatment devices has led to renewed interest in Fischer-Tropsch (FT) fuels in recent years. Developed in the 1920's by Franz Fischer and Hans Tropsch, the FT process can be used to produce hydrocarbon fuels from a wide range of carbonaceous materials including natural gas, coal, and even biomass. The diesel fuels produced as a result of this process exhibit a number of chemical and physical properties attributed to reduced emissions levels. In addition, FT diesel is completely miscible with conventional diesel making it an ideal candidate as both a blending agent with and eventual replacement for conventional petroleum-based diesel fuels. Furthermore, the current state of global politics and rising oil prices make FT fuels an increasingly attractive alternative to petroleum-based fuels with the potential to reduce U.S. dependence on foreign oil imports as well [10].

1.2.1 Emissions Regulations

Due to the nature of diesel combustion, emissions of unburned hydrocarbons and carbon monoxide are typically low and well below the regulated levels. Emissions of nitrous oxides and particulates are, therefore, the two primary emissions of concern from diesel engines. The contribution of diesel-powered vehicles to the overall U.S. mobile source particulate emissions inventory is presented in Figure 1.1 below.

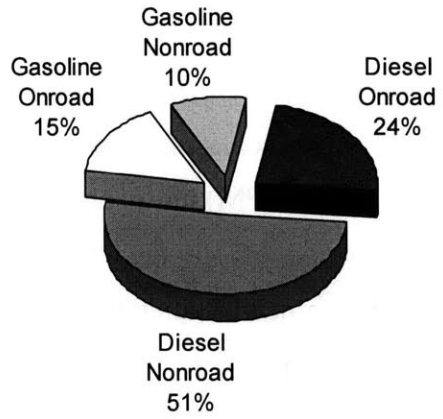

Figure 1.1. 2000 PM-2.5 mobile source emissions inventory [11]

According to the data presented in Figure 1.1, diesel engines accounted for nearly 75% of all mobile source PM-2.5 emissions in the U.S. in 2000 [11]. PM-2.5 is defined as all particulate matter smaller than 2.5 microns. Furthermore, in Germany the daily PM-10 emissions limit of 50 $\mu g/m^3$, which was not to be exceeded on more than 35 days in one calendar year, was exceeded on more than 35 days within the first three months of 2005 in a number of major German cities [12].

Aside from particulates, diesel engine-out NOx exhaust concentrations are comparable to those of gasoline engines [1]. However, SI engines have an advantage over diesels since they are operated near stoichiometric, $\varphi = 1$, in order to utilize a three-way catalyst to simultaneously reduce NOx, HC, and CO emissions. Unlike SI engines, diesels run lean making NOx reduction in an oxygen-rich environment extremely difficult.

In an effort to reduce NOx and PM emission from diesel engines, both the U.S. and EU have implemented increasingly stringent emissions regulations. In the U.S., emissions of NOx and particulates will be reduced by an order of magnitude from the 2002 levels of 2.0 g/hp-hr NOx and 0.1 g/hp-hr PM to the 2007 limits of 0.2 g/hp-hr NOx and 0.01 g/hp-hr PM. Trends in European emission regulations follow those of the U.S., however in general the EU regulations are slightly less stringent, as shown in Figure 1.2 [3]. As a result of these increasingly stringent emissions regulations, NOx and PM emissions will be reduced by over 98% from the 1990 levels by 2010 when the new regulations are completely phased in.

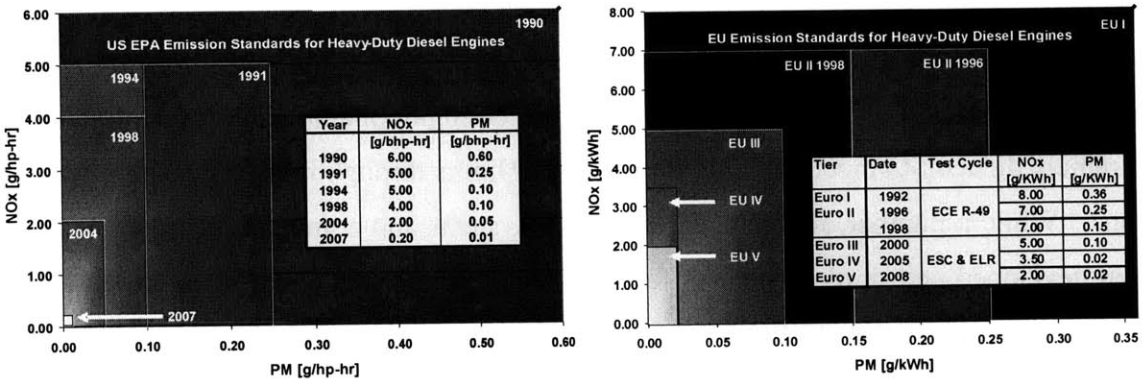

Figure 1.2. U.S. and EU heavy-duty diesel emissions regulations [3]

The significant reduction in allowable NOx and PM emissions from heavy-duty diesel engines is motivated, in part, by growing concern over the adverse environmental and human health effects posed by these emissions. Excessive NOx concentrations in densely populated urban areas contribute significantly to the formation of photochemical smog and ozone [1]. Further, a number of studies have demonstrated the potentially carcinogenic nature of diesel particulates, which can affect humans when the particulates are inhaled and become trapped in the bronchial passages and lungs [13]. In addition, diesel nanoparticles (diameter < 0.1μm) have been the subject of much investigation, especially in Europe, where new studies have demonstrated the potential for these particles to penetrate lung tissue and enter the blood stream, whereby the particles are transported to other parts of the body [14].

1.2.2 Fuel Quality Standards

Along with a decrease in the allowable emissions limits, diesel fuel standards in the U.S. and Europe are changing significantly. Beginning in the U.S. in 2006, the allowable sulfur content in on-road diesel fuels will be limited to 15 PPM, down from the 500 PPM limit set in 1993. Similar to the U.S., new diesel fuel standards will take effect in the EU in 2009, limiting the allowable sulfur content in diesel fuel to 10 PPM. The reduction in fuel sulfur levels is aimed at reducing particulate emissions from diesel engines, as well as improving compatibility with aftertreatment devices that would otherwise be poisoned by higher fuel sulfur levels [3].

1.2.3 Emission Reduction Measures

Despite the reduction in fuel sulfur content, diesel engine manufacturers are finding it extremely difficult to meet the 2007 PM and NOx limits through in-cylinder optimization alone. While a number of advanced engine subsystems and combustion strategies have been developed and implemented to further improve the diesel combustion process and reduce emissions, exhaust aftertreatment systems currently present the only technically feasible and economically attractive means to meet these new emissions limits. Figure 1.3 depicts a number of measures, which have been successfully implemented in the past to meet current emissions regulations.

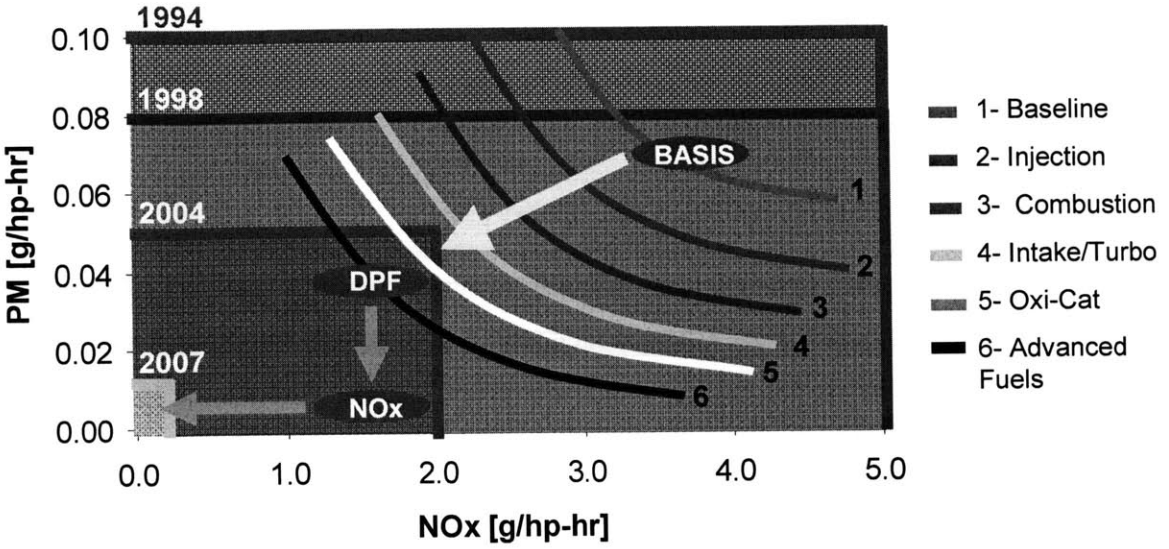

Figure 1.3. U.S. heavy-duty diesel emission reduction measures [15]

According to the trends shown in the Figure 1.3, advances in engine technology such as the development and implementation of high-pressure common rail fuel injection systems, multiple combustion strategies, variable geometry turbochargers, and cooled EGR systems have yielded significant improvements in reducing both NOx and PM emissions to the 2004 levels. While advanced fuel formulations and cleaner diesel fuels present additional emissions reduction potential, it is widely accepted that some form of PM and NOx aftertreatment systems will be required to comply with future emissions regulations.

1.2.4 Emissions Benefits with Fischer-Tropsch Fuels

A number of studies in the open literature have demonstrated the emissions reduction potential of neat Fischer-Tropsch fuels and blends. In addition, the zero-sulfur content of FT fuel has also been shown to permit the use of advanced aftertreatment systems in order to realize an even greater reduction in PM and NOx emissions [16, 17]. While numerous studies have investigated the effect of FT fuels on engine-out emissions, little is understood about the underlying causes for the observed emissions behavior of the fuels, and much work in this area remains. Furthermore, most research with FT fuels has been conducted using older technology engines without many of the advanced subsystems used in toady's modern diesel engines.

A comprehensive literature review covering a wide range of light- and heavy-duty vehicle and engine tests with Fischer-Tropsch fuels was presented by Alleman et al. in 2003. The review cited the FT fuel's near zero sulfur content, low aromatics content, and high cetane number as the major contributors to the reduction in PM and NOx emissions observed with Fischer-Tropsch fuels. In addition, the near zero sulfur content of the fuel enabled the use of state-of-the-art aftertreatment technologies. On the other hand, some of the studies mentioned in the review cited poor cold flow and lubricity properties for the FT fuel, and called for further investigation into the long-term durability implications [18].

One of the earliest significant studies into the effects of Fisher-Tropsch fuels on diesel exhaust emissions was carried out by Schaberg et al. in 1997. In this study, a 12.7-liter, 1991 emission level, DDC series 60 diesel engine was run using four neat test fuels and three fuel blends. Of the four neat fuels, two were Fischer-Tropsch fuels produced by the Sasol Slurry Phase Distillate Process (SSPD), and the remaining two were conventional CARB and US 2-D petroleum-based fuels. In addition to the neat fuels, three blends of various amounts of SSPD in the US 2-D were tested as well. Results showed that the SSPD fuels reduced nearly all regulated emissions as compared to the US 2-D and CARB fuels, with the blends reducing emissions in proportion to the amount of SSPD fuel in the blend. Over all of the test conditions, the SSPD reduced HC, CO, NOx, and PM emissions by 49%, 33%, 27%, and 21% respectively, when compared with the 2-D fuel. In addition, the SSPD reduced the PM volatile organic fraction (VOF) by 34% relative to the 2-D fuel. When compared with the CARB diesel, the SSPD reduced HC, CO, NOx, and PM emissions by 15%, 23%, 15%, and 21%, and yielded a reduction in PM VOF of 29%. Based on the results of the study, it was estimated that a blend of 40% SSPD with the US 2-D would result in equivalent emissions of the CARB fuel [19].

A more recent study carried out by Sirman et al. at Southwest Research Institute in 2000 investigated the fuel effects of six alternative diesel fuels in a modern 2.2L Daimler Benz OM611 engine. The fuels under investigation were a low-sulfur diesel, Fischer-Tropsch

diesel, a California Reference fuel, and three blends. All six fuel formulations were compared against an ASTM D975 low sulfur No. 2 diesel (2DLS) control fuel. The neat FT fuel reduced particulate and NOx emissions by 37% and 6% respectively, and provided the greatest benefits in emissions reduction over all 13 test modes. Furthermore, a 20% blend of FT in ULSD was observed to produce the same NOx reduction as the neat FT fuel as well [20].

In another study, an unmodified 1999 Cummins 5.9 L , turbo-charged, direct injection B-Series engine was tested using a federal low sulfur diesel fuel, CARB diesel, Swedish City 1 diesel fuel, and Syntroleum's FT diesel. The results showed a reduction in emissions with the FT fuel of 41% for HC, 38% for CO, 20% for NOx, and 40% for PM compared to the federal low sulfur diesel [21].

In one of the first studies to modify an engine to take full advantage of the FT fuel properties, May et al. used a modified Power Stroke 7.3 liter turbocharged diesel engine. The engine was modified to take advantage of the high cetane number of the FT fuel by lowering the compression ratio and altering the piston bowl geometry. A cooled EGR system, DeNOx catalyst, and diesel particulate filter were also added. When operated with the FT fuel in the optimized engine configuration, tailpipe-out emissions were reduced to near the 2007 limits [22].

More recently, studies have focused on fuel effects and emissions in conjunction with diesel aftertreatment devices. Thompson et al. tested a wide range of fuels of varying sulfur content including a Fischer-Tropsch and Swedish Class 1 diesel fuel in two advanced light-duty diesel vehicles and three heavy-duty diesel engines covering Euro-3 to Euro-5 technologies. The Euro-4 and Euro-5 engines were equipped with various exhaust aftertreatment systems to control both NOx and PM emissions including diesel particulate filters and SCR/urea systems for NOx control. In all cases, particulate emissions were significantly reduced for the engines equipped with diesel particulate filters. Furthermore, in all of the DPF tests, the impact of the fuel properties, other than sulfur content, on PM emissions was negligible [16].

Frank et al. conducted a similar study in which Fischer-Tropsch diesel, Biodiesel, PuriNOx^{TM}, two Ethanol-Diesel blends, and a number of conventional diesel fuels of varying sulfur content were evaluated using four different exhaust aftertreatment configurations: engine-out, diesel oxidation catalyst, continuously regenerating diesel particulate filter, and EGR-DPF. In general, it was observed that the use of aggressive aftertreatment systems had a much more pronounced effect on emissions than any of the fuels alone. The FT fuel exhibited the lowest PM emissions of all of the fuels tested and also substantially reduced NOx emissions. Only the PuriNOx^{TM} exhibited a greater overall reduction in NOx than the FT [17].

1.3 Project Objectives

While the emissions characteristics of FT fuels are well documented in the literature, the underlying mechanisms responsible for the observed emissions behavior are still not well understood. Furthermore, most of the published studies present results based on experiments conducted using older technology engines, that do not employ such advanced combustion and engine control strategies as multiple injection events and severely retarded injection timing for NOx control. The goal of this work was to investigate the fundamental combustion and emissions characteristics of Fischer-Tropsch diesel in a modern CI engine.

This study concludes the initial work on FT fuel effects that began in 2001 and was subsequently reported on by Llaniguez (S.M. 2003) and Acar (S.M. 2005). This work distinguishes itself from previous studies as it focused solely on the fundamental fuel and combustion interactions and their effect on engine-out emissions, whereas the studies by Llaniguez and Acar tended to focus more on the interaction between the FT fuel and various engine parameters such as EGR rate and injection timing.

The focus of this work was, therefore, to gain a fundamental understanding of the impact of fuel properties, combustion characteristics, and engine operating parameters on regulated emissions from a modern heavy-duty diesel engine. To this end, experiments

were carried out on a 2002 Cummins ISB 300 diesel engine using a standard low sulfur diesel fuel, ultra-low sulfur diesel fuel, Syntroleum Fischer-Tropsch diesel fuel, and a blend of 25% FT/75% LSD by volume. A significantly expanded test matrix was developed to cover a much wider range of engine operating conditions than had been used in previous studies. Moreover, detailed fuel and particulate composition analyses were carried, in order to gain further insight into the impact of fuel properties on emissions. In addition, in-cylinder pressure measurements were also recorded and used to calculate a number of thermodynamic indicators to quantify the observed differences in the combustion characteristics of the fuels.

(This page intentionally left blank)

2.0 Diesel Combustion and Emissions Formation

The diesel combustion process, characterized by its internal heterogeneous mixture formation and autoignition, is a highly complex multi-phase process that significantly affects particulate and NOx emissions. It is, therefore, imperative that any discussion of pollutant formation in diesel engines begin with a thorough review of the diesel combustion process.

2.1 Diesel Combustion Fundamentals

Diesel combustion systems can be divided into two major categories: direct injection (DI) systems, and indirect injection (IDI) systems (also called divided chamber and prechamber systems). These classifications can be further subdivided into various other categories based on combustion chamber geometry and means of fuel injection [1]. The following discussion will focus on the direct injection system, as it is the system employed by the Cummins ISB in this study.

Combustion in a direct injection diesel engine begins when fuel is injected into the hot compressed cylinder gasses. The start of injection and the start of ignition in a diesel engine are separated by a specific amount of time, known as the ignition delay. The length of the ignition delay is influenced by a number of factors, the most important of which are: the cetane number and quality of the fuel, the engine's compression ratio, the cylinder and component temperatures, and the fuel management system [2].

The diesel combustion process begins following the ignition delay and is initiated by the start of ignition. The air-fuel ratio, λ, in a heterogeneous mixture, such as that found in the cylinder following fuel injection, varies from pure air at the spray periphery ($\lambda = \infty$) to pure fuel ($\lambda = 1$) at the center of the spray. However, analogous to the combustion of homogenous mixtures, combustion in a diesel engine only takes place within a small range between $\lambda = 0.3$ and $\lambda = 1.5$. The distribution of the injected fuel throughout the cylinder and mass transport necessary to form the combustible mixture occurs via diffusion and turbulent mixing which is strongly influenced by the following factors: the kinetic energy and small scale turbulence induced by the fuel spray, heat energy within

the cylinder that promotes vaporization of the liquid fuel, combustion chamber geometry and large scale turbulence (swirl), and the combustion process itself [2].

Following the start of ignition, the combustion process proceeds in two distinct phases. In the first phase, "premixed combustion," the fuel injected prior to the star of ignition, which has already mixed with the hot air inside the cylinder to form a combustible mixture, burns rapidly within a few crank angle degrees. The rapid pressure rise and heat release associated with the premixed combustion phase is primarily responsible for the diesel combustion noise. Following the premixed combustion, the fuel injected after the start of ignition combusts in the "diffusion" or "mixing controlled" phase [1].

In many cases heat release continues at a low rate well into the expansion stroke, and a "late combustion" phase is clearly identifiable. This late combustion can be due to a number of factors such as unburned fuel remaining in the cylinder, soot oxidation, and the fact that the kinetics of the final burning process slow down as the temperature of the cylinder drops during expansion [1].

Each distinct phase of the combustion process has a specific effect on emissions formation within the power cylinder as depicted in Figure 2.1 below.

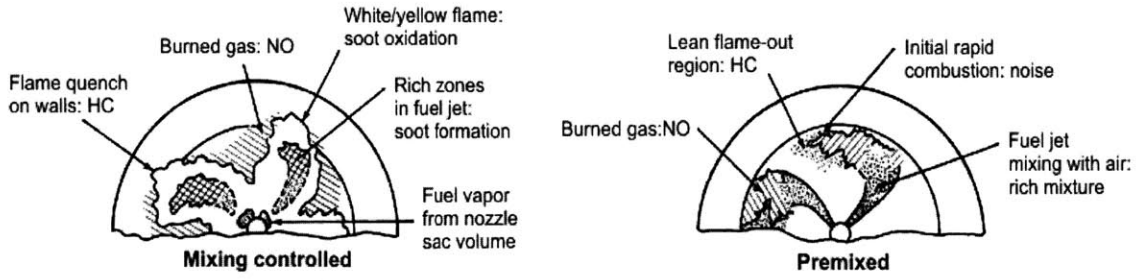

Figure 2.1. Pollutant formation pathways during diesel combustion [3]

The portion of fuel that burns very rapidly within the premixed combustion phase gives rise to the high cylinder temperatures necessary to form NO in the flame front and post-flame gasses. However, due to the small area of the flame front, NO formation in the post-flame typically dominates any flame-front-produced NO.

The majority of diesel soot and particulates are formed in the diffusion phase where fuel rich zones, the result of incomplete mixing, lead to incomplete combustion and the formation of partially combusted carbon in the form of soot. However, the total engine-out PM emissions are typically much lower than the amount of soot formed during the combustion process, as much of the soot is oxidized as it approaches the diffusion flame boundary and during the late combustion phase [1].

A very effective means for reducing NOx and PM emissions in the cylinder is through the use of heavily retarded injection timing and a multiple fuel injection strategy. Both of these combustion strategies influence the rate and shape of the heat release curve, and have a significant impact on engine-out emissions. A comparison of a conventional heat release profile and one in which three separate injection events are employed is shown in Figure 2.2 below.

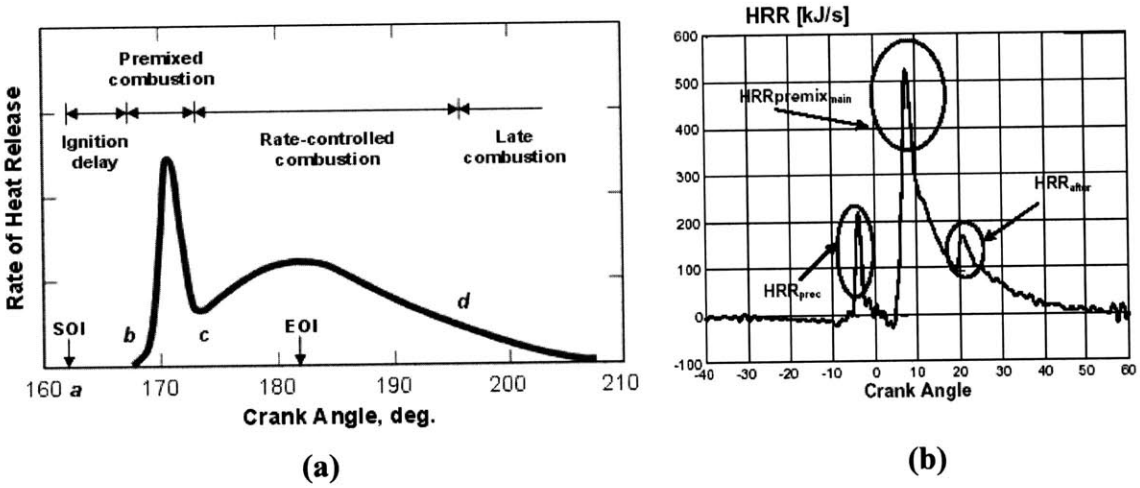

Figure 2.2. Comparison of heat release profiles for (a) conventional DI combustion, [3] and (b) DI combustion with three separate injection events [23]

The heat release profile shown in Figure 2.2 (a) is for a conventional DI diesel engine employing only a single injection event. The characteristic combustion phases are clearly visible in this plot. On the other hand, the heat release profile shown in Figure 2.2 (b) exhibits three distinct peaks corresponding to the heat release for each separate injection event. In most multiple injection strategies, a small amount of fuel is injected during the pre-injection event, which helps to slow the initial pressure and associated temperature

rise within the cylinder. In this way, the pilot-injection not only helps to reduce NOx emissions, but also reduces combustion noise. Due to the small amount of heat released during the post-injection, the rise in cylinder pressure during the main combustion is also slower, thus further reducing combustion noise. Following the main injection, the post-injection is very effective in completing the oxidation process and reducing particulate emissions [23].

Advanced multiple injection strategies, while effective when used properly, can actually increase NOx and PM emissions if not correctly optimized and calibrated. The timing of each injection event, quantity of fuel injected for each event, and separation of injection events are key parameters in such a multiple injection strategy. For example, Mallmo et al. found that the addition of a second pilot injection more than 40° BTDC increased PM emissions by 15%. On the other hand, they also demonstrated that optimized timing of the post-injection reduced PM emissions by more than 30% [23]. Overall, multiple injection strategies give greater freedom to the engine designer when optimizing the combined fuel injection, combustion, and emission control systems.

Despite advanced combustion strategies and fuel injection systems, diesel combustion remains a complex process that significantly influences emissions formation. Due to the inherently heterogeneous nature of the internal mixture formation and autoignition in diesel engines, a truly soot-free engine is impossible to achieve as some soot is always formed in the diffusion phase. However, through the use of advanced fuels and aftertreatment systems, significant reductions in both PM and NOx emissions can be achieved [23].

2.2 Exhaust Composition

Diesel exhaust is a complex mixture of gasses, liquids, and solid aerosol particles, the precise composition of which depends upon on a number of factors. While fuel and lube oil compositions certainly contribute to the overall exhaust composition, the fuel distribution within the cylinder and the manner in which this distribution changes throughout the combustion process also exerts significant influence [11]. Figure 2.3

presents typical values for the major diesel exhaust constituents for an engine operating at full load.

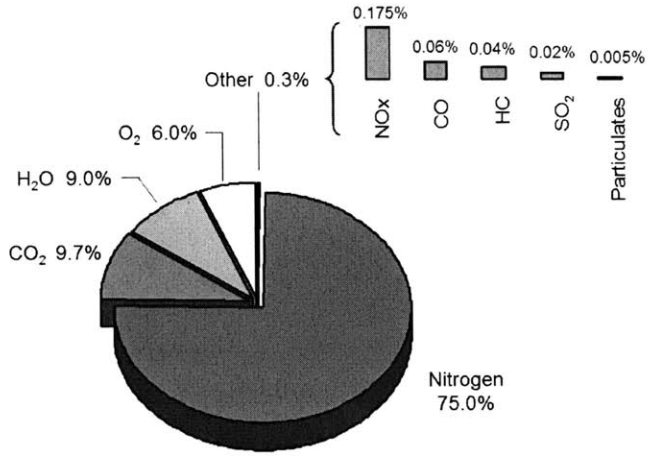

Figure 2.3. Typical diesel exhaust gas composition (Vol. %) at full load [24]

Interestingly, less than 0.3% by volume of the total diesel engine exhaust is composed of regulated pollutant species (CO, HC, NOx, and PM), and of those exhaust constituents, only 0.180% (NOx and PM) contribute significantly to the overall mobile-source atmospheric emissions inventory as described in Section 1.2.1. Furthermore, while PM emissions compose only 0.005% of the total exhaust by volume, they currently pose the greatest concern to human health and the environment [24].

Diesel particulate matter is defined by the U.S. EPA as "all solid matter and condensable species that can be collected on a paper filter from a diluted exhaust sample held at no higher than 52°C" [25]. Diesel particulates are primarily composed of carbonaceous material (soot) on which some organic compounds have become absorbed. The composition of the PM can be divided into three significant categories consisting of the SOL (solid particles or soot), SOF (soluble organic fraction), and SO_4 (sulfates). The SOL is primarily composed of the organic and elemental carbonaceous solid, while the SOF is made up of unburned hydrocarbons originating from the fuel and lubricant that have become absorbed on the soot. The SO_4 originates from sulfur compounds present in the fuel and lubricant, which form SO_2 and small amounts of SO_3 during combustion, and later combine with water and oxygen in the exhaust to form sulfuric acid (H_2SO_4). The

absorption of the sulfuric acid on the PM is the source of particulate sulfates. In addition to the major constituents just listed, liquid phase hydrocarbons and sulfate compounds may also form on the outside of the PM [13]. A schematic depicting the various constituents that comprise the PM is shown in Figure 2.4.

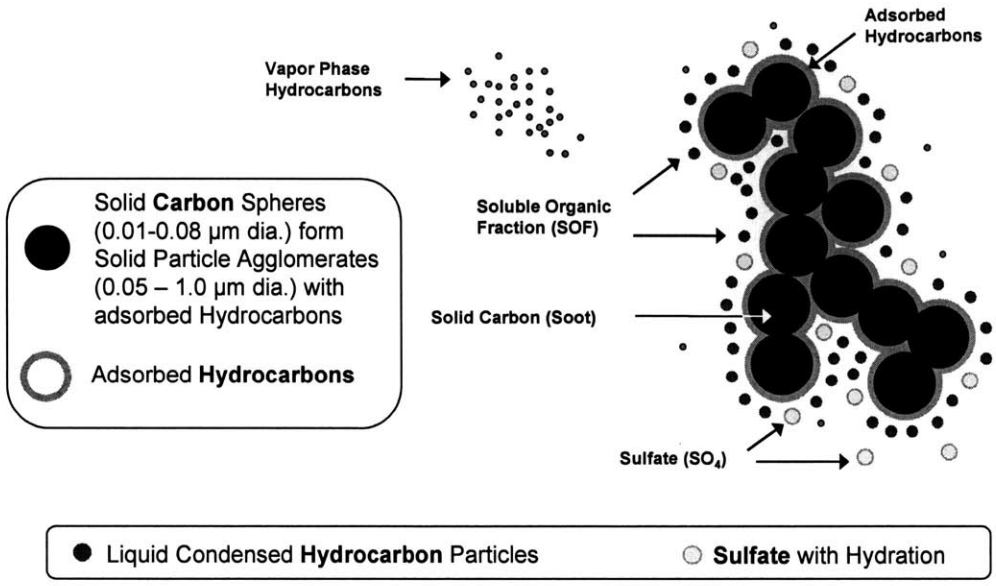

Figure 2.4. Typical diesel particulate composition [13]

As shown in the schematic above, the diesel particulates are composed of collections of small primary particles (spherules). The average diameter of the spherules is in the 10 to 80 nm range, with most between 15 and 30 nm. Particles exist either as clusters or chains of spherules and may contain up to 4,000 individual spherules [1].

In addition to the PM constituents shown in Figure 2.4, the particulates also contain some levels of ash. Ash in diesel particulates originates primarily from metallic compounds in the engine lubricant, wear metal, and fuel additives [26]. Efforts to reduce particulate ash have increased significantly in recent years, as ash accumulation in particulate traps shortens the service life of the trap.

Due to the complex mixture of organic and inorganic compounds in both solid and liquid phases that make up diesel particulate matter, exhaust and PM sampling conditions play an important role in influencing the amount, type, and composition of the PM collected.

The dilution ratio and temperature at which the particulates are collected are the two most important experimental parameters influencing particulate composition. As the dilution ratio increases from unity, the extractable fraction of the particulates increases as well, up to a dilution ratio of approximately 8 to 10. The extractable fraction increases with increasing dilution ratio, since the dilution and subsequent cooling of the exhaust stream promotes the condensation and absorption of liquid and vapor phase hydrocarbons and sulfate compounds onto the soot. Further dilution of the exhaust gasses, above a dilution ratio of approximately 10, causes the extractable fraction to decrease slightly. In the absence of any type of dilution, a dilution ratio of unity, the extractable fraction is extremely small, since the rate of condensation and adsorption of liquid and vapor phase hydrocarbon onto the PM in the hot exhaust gasses is relatively slow [1].

2.2.1 NOx Formation

NOx is a term used to describe the total emissions of NO and NO_2, although NO is generally the predominant oxide of nitrogen produced inside the cylinder. While the primary source of NO is atmospheric nitrogen, fuel nitrogen is also a possible source of NO, however the levels of nitrogen compounds in current fuels are generally negligible [1].

Three important mechanisms contribute to the formation of NO from atmospheric nitrogen and are collectively know as the extended Zeldovich mechanism. The reactions that make up the extended Zeldovich mechanism are listed as follows:

Equation 2.1 $$O + N_2 \leftrightarrow NO + N$$

Equation 2.2 $$N + O_2 \leftrightarrow NO + O$$

Equation 2.3 $$N + OH \leftrightarrow NO + H$$

The large activation energies for the forward reaction in Eq. (2.1) and reverse reactions in Eq. (2.2) and Eq. (2.3) are responsible for the strong temperature dependence of the NO formation rates. Due to the high forward rate constant for the first reaction, Eq. (2.1), it is

generally the rate limiting step in the extended Zeldovich mechanism. The high temperatures required for the reaction to take place at an appreciable rate generally occur in the post-flame gasses during the pre-mixed phase of diesel combustion. While some NO does form in the flame front, this amount is significantly smaller than that generated in the post-flame gasses, since the reaction zone in the flame front itself is extremely thin [1].

Although not insignificant, NO_2 emissions from modern diesel engines account for approximately 10% of the total NOx emissions and play an important role in particulate trap regeneration. While the exact mechanisms responsible for the production and destruction of NO_2 in diesel engines are not as well understood as those for NO, one possible mechanism for the formation of NO_2 from NO is presented below [1]:

Equation 2.4 $$NO + H_2O \rightarrow NO_2 + OH\,.$$

Unless the NO_2 formed in the flame zone is quenched by mixing or some other means, the high temperatures within the vicinity of the flame front will most likely lead to the back-conversion of NO_2 to NO as follows:

Equation 2.5 $$NO_2 + O \rightarrow NO + O_2\,.$$

The validity of the mechanism presented above is supported by experimental data showing the highest NO_2/NO ratio occurring at low load, where quenching due to mixing with cooler gasses within the cylinder is more likely to occur [1].

2.2.2 Particulate Formation

Particulate formation is a complex process involving nucleation, growth, and agglomeration of the particles. Almost simultaneous to these processes, particulate oxidation within the cylinder also takes place as the particulates, in various stages of development, are mixed with fuel hydrocarbons and consumed by the diffusion flame in oxygen-rich regions within the cylinder. While the specific particulate formation

mechanisms are not well understood, a number of theories have been developed to explain the formation of soot precursors. The two most prevalent theories are the Acetylene Theory and Radical Hypothesis [27].

According to the Acetylene Theory, a product of the oxidation of fuel molecules is the formation of acetylene, which forms the building blocks for more complex hydrocarbons and aromatics. The ensuing formation of polycyclic aromatic hydrocarbons (PAH) from the acetylene base molecules forms the precursors to soot and particulates. On the other hand, the Radical Hypothesis assumes that small free-radicals combine to form larger branched hydrocarbons independent of their original composition [27]. A schematic depicting the PM formation pathways proposed by the two theories is shown in Figure 2.5.

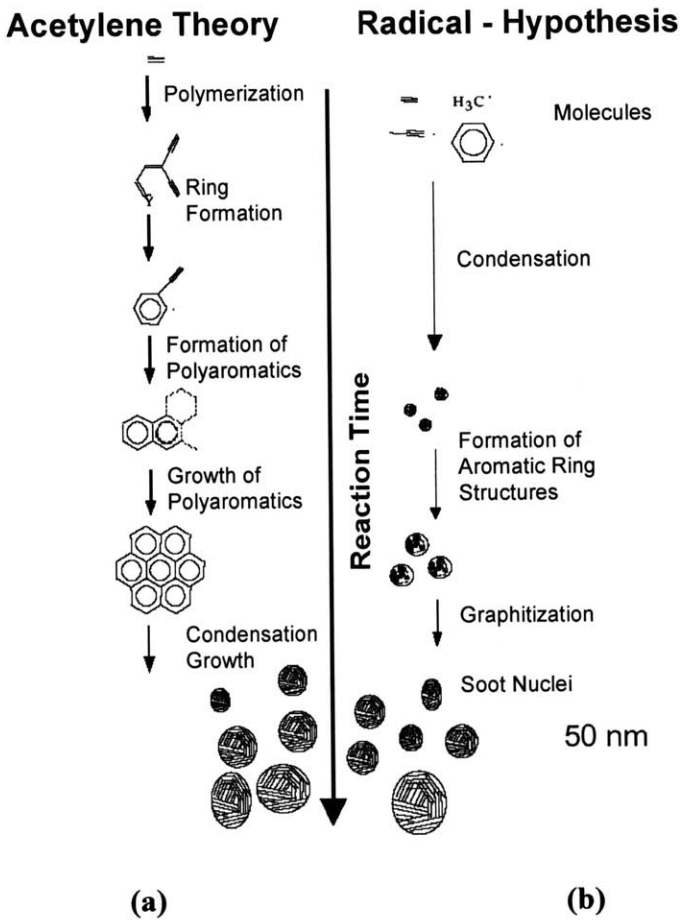

Figure 2.5. Formation mechanisms for diesel particulates in the power cylinder: (a) Acetylene Theory, and (b) Radical Hypothesis [27]

The formation and growth of the particulates, from the soot precursors formed via either of the two theories, follows from the combination of larger polycyclic aromatic hydrocarbons, and the volume of the resulting aggregate increases by means of coagulation and surface growth. Growth on the surface of the primary particles proceeds as carbon atoms form leaf-shaped graphite crystallites, which are randomly packed with their planes parallel to the surface of the primary particles [27].

During the early phases of combustion, the spherical primary particles continue to grow in the manner described above until a diameter of approximately 30 nm is reached. As the cylinder temperature drops during the expansion stroke, the primary particles agglomerate by means of particle-to-particle collisions and, thus, form chain- and grape-like structures with diameters in the range of 70 to 100 nm. Additional cooling results in the absorption and condensation of gaseous species, mostly hydrocarbons, onto the particulates. Figure 2.6 presents TEM images of diesel particulates [27].

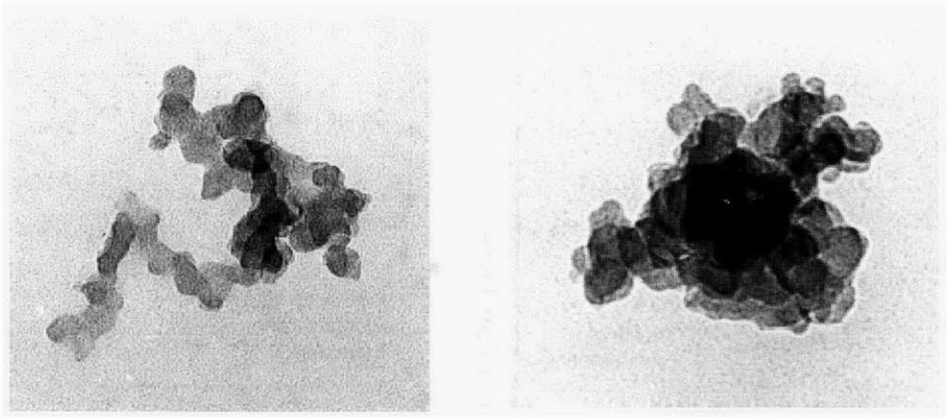

(a) **(b)**

Figure 2.6. TEM diesel particulate images at (a) low and (b) high load [27]

An important distinction in the particulate formation process is the difference between particulate growth via agglomeration and coagulation, and surface growth by means of condensation and absorption. In the former case, growth by agglomeration and coagulation leads to a decrease in the number of soot particles, whereas the soot volume fraction (volume of soot/total volume) remains the same. In the latter case, surface

growth leads to an increase in the amount of soot, while the total number of particulates remains constant [1].

Parallel to the particulate formation processes, oxidation of the newly formed soot precursors and particulate agglomerates is also continually taking place throughout the diesel combustion process. Over 80% of the initially formed particulates are oxidized within the cylinder and never contribute to engine-out PM emissions. The particulate emissions measured at the tailpipe are, therefore, the result of two competing processes: particulate formation and oxidation [27].

(This page intentionally left blank)

3.0 Factors Influencing Diesel Emissions

The emissions characteristics of Fischer-Tropsch fuels are well documented in the literature, and the results of a number of studies [28-36] on FT fuels were presented in a thesis by Llaniguez (S.M. 2003). The work on this project distinguishes from previous studies in two respects. First, the current study was carried out using a modern (MY 2002) advanced diesel engine that has incorporated much of the latest engine technology and emissions control strategies. Second, the author is unaware of any studies to date in which the combustion and emissions characteristics of neat FT fuels and blends have been carried out on an engine employing a multiple injection strategy.

Despite the numerous studies of FT fuels and their effects on engine-out emissions, the underlying causes for the emissions behavior are still not well understood, and much work in this area still remains. It is widely accepted that a number of factors contribute to the emissions behavior of the fuel, the most important of which are: chemical and physical properties of the fuel, combustion characteristics, and interaction with the engine technology.

3.1 Fuel Effects

The intercorrelations between fuel properties make investigation into the effect of a specific property on emissions quite difficult. Relatively few studies have succeeded in adequately decoupling the change in a specific fuel property from changes in additional properties in the test fuel. Furthermore, it is nearly impossible to link changes in emissions to a particular fuel property when a number of properties are varied simultaneously [37]. The literature review compiled by Lee et al. focused solely on those studies where the intercorrelations between the fuel properties were decoupled, allowing for direct comparison between changes in a specific fuel property and engine-out emissions. In this review, the following fuel properties were identified as having a significant effect on diesel emissions: cetane number, fuel sulfur, density, and aromatics.

3.1.1 Cetane Number

Cetane number is the measure of a fuel's tendency to auto-ignite, with higher cetane number fuels exhibiting a shorter ignition delay. Recent studies have shown some benefit to reduced NOx emissions as cetane number was increased, however the impact of cetane number on particulates tends to be much less pronounced and engine specific. The reduced ignition delay with higher cetane number fuels leads to a reduction in pre-mixed combustion and a more gradual temperature rise in the cylinder, thus slowing the rate of NOx formation [38].

3.1.2 Sulfur

One of the most widely investigated diesel fuel parameters, the conversion of fuel sulfur to sulfate following the combustion process contributes to particulate exhaust emissions. Previous studies have shown that the amount of sulfur converted to PM is at least 1-2% of the fuel sulfur content irrespective of the total fuel sulfur level or engine type [39]. In addition to contributing to particulate emissions, fuel sulfur has also been linked to catalyst poisoning, limiting the use of exhaust aftertreatment systems with diesel engines. Furthermore, the production of sulfuric acid from fuel sulfur has detrimental effects on the durability of EGR systems as well [40]. Aside from influencing particulate emissions and its detrimental impact on specific engine subsystems, fuel sulfur is not known to have any significant effect on regulated gaseous engine-out emissions [37].

3.1.3 Density

A number of studies have linked fuel density to particulate emissions. It has been shown that reducing fuel density can lead to a significant reduction in particulate emissions in older technology engines; however the effect is substantially reduced in newer technology engines with advanced injection strategies and improved mixing. In addition to reducing particulates, less dense fuels tend to reduce NOx emissions as well. On the other hand, emissions of CO and HC's may increase as the fuel density is reduced. Aside from emissions, density also directly affects an engine's power output, with less dense fuels leading to reduced power output, all other factors remaining constant [37, 41].

3.1.4 Aromatics

Much of the data regarding the impact of aromatics on emissions in the past presented conflicting results and failed to decouple the effect of the aromatics from density, cetane number, and T90. Despite this fact, it is widely agreed that total aromatics do not contribute significantly to HC, CO, or PM emissions, and only slightly affect NOx emissions. On the other hand, poly-aromatic hydrocarbons (PAH) can have a substantial impact on particulate emissions and a smaller effect on NOx and CO emissions. However, similar to density, the effect of poly-aromatics on emissions is seen to decrease with newer technology engines [37, 40].

3.1.5 Back-End Volatility

While the effect of back-end volatility, T90/T95, on emissions is generally considered minor and heavily dependent on the composition of the back end, this property can have a small effect on engine-out gaseous emissions. A number of studies have shown that reducing back-end volatility can lead to a slight increase in HC and CO emissions along with a decrease in NOx emissions. As mentioned above, T90/T95 has not been shown to have a noticeable effect on PM emissions [37, 43].

3.2 Combustion Characteristics

Although the effects of FT fuel on engine-out emission have been well documented in the literature, there are very few published reports on the combustion characteristics of FT fuel. Furthermore, the author is not aware of any analysis of the combustion behavior of neat FT fuel or FT blends in a modern diesel engine employing a multiple fuel injection strategy and heavily retarded injection timing in addition to a number of other advanced engine subsystems.

Atkinson et al. presented, perhaps, the first detailed combustion analysis of FT fuel in a direct injection diesel engine. In this study, a Navistar T444E (7.3 liter, V8) diesel engine was outfitted with two in-cylinder pressure transducers and subjected to twelve steady-state operating conditions. Over the entire test range, it was found that the higher cetane number of the FT fuel yielded a reduced ignition delay, and thus, reduced fuel

evaporation before ignition. Furthermore, the FT fuel exhibited a slightly longer combustion duration and more uniform heat release rate than the baseline diesel. However, the total time from the start of injection to the end of combustion for each fuel was approximately equivalent. FT fuel was observed to reduce nearly all regulated emissions over the entire engine operating range, with the exception of hydrocarbons at some test conditions. It was also noted that FT fuel reduced the exhaust gas temperature, thus reducing NOx emissions. During the course of the Atkinson study the engine was operated completely stock, with no engine control parameters altered to compensate for the differences in the combustion characteristics of the two fuels [44].

Following the Atkinson study, McMillan and Gautam investigated the combustion and emission characteristics of FT and a federal low-sulfur diesel fuel in a Ricardo single-cylinder four-stroke DI research engine outfitted for in-cylinder pressure measurements. The engine was run at several steady-state operating conditions and timing was varied for each fuel at these conditions as well. McMillan and Gautam cited the higher cetane number and lower density of the FT fuel as primarily responsible for the observed differences in the combustion characteristics. They also observed similar overall burn durations and peak pressures for the two fuels; however the FT did exhibit a slightly shorter 50% to 90% mass fraction burn duration [45]. Consistent with the Atkinson study, nearly all regulated exhaust emissions were reduced with the FT fuel, and the higher cetane number of the FT contributed to its shorter ignition delay.

3.3 Engine Technology

While the fuel properties and combustion characteristics have a significant effect on exhaust emissions, the relative importance of each specific effect can change depending on the type of engine and its operating characteristics. Numerous studies have indicated that the relative impact of fuel properties on emissions decreases with modern technology engines. In addition, Mann et al. noted that fuel effects on engine calibration significantly influenced the observed emissions effects. In this study, seven diesel fuels were tested in a modern electronically controlled direct-injection diesel engine and significant changes in engine calibration settings (most notably EGR rate and injection

timing) were observed [46]. More recently, the effects of multiple injections and injection pressure have also demonstrated a significant effect on engine-out emissions and heat release rate [47, 48].

(This page intentionally left blank)

4.0 Experimental Fuels

The three neat fuels under investigation in this study were a low sulfur diesel containing 400 PPM sulfur, an ultra-low sulfur diesel containing 15 PPM sulfur, and a Fischer-Tropsch synthetic diesel, produced from natural gas, containing zero sulfur. A blend of 25% FT and 75% low sulfur diesel by volume was used as well.

4.1 Number 2 Diesel Fuel

Two standard No. 2 diesel fuels were used to develop a performance and emissions baseline against which the Fisher-Tropsch fuel was compared. The baseline fuels were supplied by Fleetline, and differed primarily in sulfur content with the LSD containing 400 PPM sulfur by volume and the ULSD containing 15 PPM sulfur by volume. According to the information provided in the product literature, these fuels are formulated with "anti-oxidants to reduce volatility and prevent fuel degradation, inhibitors to fight gum and deposit formations in the fuel system, viscosity improvers for fuel injector lubrication and correct spray pattern, and additives for low-temperature operation" [35].

4.1.1 Low Sulfur Diesel Fuel

Fleetline's low sulfur diesel fuel was selected as one of the baseline fuels, as it is representative of typical worst-case fuels currently used in on-road heavy-duty diesel engines. The fuel, thus, provided a reference by which to compare potential improvements in performance and emissions observed with the FT fuel. The 400 PPM fuel sulfur content of the Fleetline low sulfur diesel used in this study still meets the current EPA Low-Sulfur Fuel requirement of no more than 500 PPM sulfur. In addition, according to the ASTM D 975 specifications for No. 2 diesel fuels, it should have a minimum cetane number of 40 and contain no more than 35% aromatics. A detailed listing of the fuel properties and specifications provided by the manufacturer is listed in Table 4.1.

FLEETLINE®

PRODUCT SPECIFICATIONS

PREMIUM LOW-SULFUR DIESEL FUEL

TEST DESCRIPTION	ASTM METHOD	ASTM NO. 2-D STANDARD (D 975)	TYPICAL ANALYSIS
Cetane Number	D 976	40 min.	47
API Gravity at 16°C (60°F)	D 287	30 min.	37
Pour Point, °C (°F)	D 97	–7 (20) max.	–11 (12)*
Cloud Point, °C (°F)	D 2500	–	–10 (14)*
Flash Point (Pensky-Martens), °C (°F)	D 93	52 (125) min.	66 (151)
BTU/Gallon (gross)	--	--	139,200
Sulfur, Weight %	D 1552	0.05 max.	0.04
Viscosity, Saybolt, SUS at 38°C (100°F)	D 2161	32.6-40.1	34.5
Viscosity, Kinematic, cSt at 40°C (104°F)	D 445	1.9-4.1	2.52
Copper Strip Corrosion, 3 Hrs. @ 50°C (122°F)	D 130	3 max.	1
Distillation (Evap.), °C (°F)	D 86		
10% Recovered		--	206 (402)
50% Recovered		–	260 (500)
90% Recovered		282-338 (540-640)	335 (635)
End Point		–	353 (667)
Recovery %		--	98.0
Residue %		--	1.5
Loss %		–	0.5
Carbon Residue, Ramsbottom (10% Bottoms, Weight %)	D 524	0.35 max.	0.05
Water and Sediment, Vol. %	D 1796	0.05 max.	0.001
Ash, Weight %	D 482	0.01 max.	<0.001
Color (Visual)	–	–	Clear to Amber
Date Approved: 3/15/00 (Specification valid only if dated)			

Typical test data are average values only. Minor variations which do not affect performance may occur.

* Adjusted with additives and kerosene blending for winter operation.

DENNIS K. BURKE INC.

Note: Other additives may be added to enhance lubricity when needed.

We can also custom blend fuel to meet customer's specifications.

284 EASTERN AVE. • CHELSEA, MASS. 02150 • PHONE: 1-800-289-2875 • FAX: (617) 884-7638 • WEBSITE: WWW.BURKEOIL.COM

Table 4.1. Manufacturer's specifications for the low sulfur diesel used as one of the baseline fuels

The lower heating value of the low sulfur diesel fuel was not listed in the product literature provided by Fleetline, and repeated attempts to contact the manufacturer were unsuccessful in obtaining the actual heating value. Therefore, the lower heating value for a standard No. 2 diesel fuel given in Syntroleum's S-2 product literature was used to allow for comparison of the lower heating values of the three different fuels used in the experiments. The value given in the Syntroleum brochure is: $Q_{LHV,No.2}$ = 129,400 Btu/gal [49]. In order to convert the heating value from a volumetric to mass basis, the density of the fuel is required. The API (American Petroleum Institute) gravity obtained using the ASTM D 287 method for the low sulfur diesel fuel is given in the manufacturer's specifications in Table 4.1 as 37. The ASTM D 287 method defines API gravity at 16°C as:

Equation 4.1
$$API@16^{\circ}C = \frac{141.5}{s.g.@16^{\circ}C} - 131.5$$

The fuel density was calculated using the given API gravity and Equation (4.1) as $\rho_{No.2}$ = 840 kg/m^3. Using the calculated density gives a lower heating value of $Q_{LHV,No.2}$ = 42.9 MJ/kg. This compares well with heating value data of typical light diesel fuels listed as $Q_{LHV,No.2}$ = 43.2 MJ/kg in [1].

4.1.2 Ultra-Low Sulfur Diesel Fuel

To provide a more realistic baseline for comparison with the FT fuel, tests were also carried out with Fleetline's ultra-low sulfur diesel fuel. This fuel meets the 2006 standard of 15 PPM sulfur by volume, and is representative of the types of diesel fuels that will be in use once the 2006 standards take effect. The fuel properties provided by Fleetline for the ultra-low sulfur diesel are listed in Table 4.2. Aside from a significant difference in sulfur content, the ULSD has a slightly higher cetane number and API gravity than the low sulfur diesel.

FLEETLINE®

PRODUCT SPECIFICATIONS

ULTRA LOW SULFUR DIESEL

TEST DESCRIPTION	ASTM METHOD	ASTM NO. 2-D STANDARD (D 975)	TYPICAL ANALYSIS
Cetane Index (Calculated)	D 976	40 min.	42.7
Cetane Number	D 613	40 min.	50
API Gravity at 16°C (60°F)	D 4053	30 min.	40.3
Density, lbs./gallon	Table 8	–	6.858
Pour Point, °C (°F)	D 97	–6 (20) max.	–30 (–22)
Cloud Point, °C (°F)	D 2500	–	–30 (–22)
Flash Point (Pensky-Martens), °C (°F)	D 93A	52 (125) min.	63 (146)
Heat of Combustion, BTU/gallon	D 240	–	135,514
Viscosity, Saybolt, SUS at 38°C (100°F)	D 2161	32.6-40.1	31.47
Viscosity, Kinematic, cSt at 40°C (104°F)	D 445	1.9-4.1	1.67
Sulfur, parts per million	D 5453	30 max.	15
Nitrogen, parts per million	D 5762	–	5
Corrosion, Copper Strip	D 130	1 max.	1
Alkali or Mineral Acids	D 974	–	neutral
Distillation (Evap.), °C (°F)	D 86		
10% Recovered		–	199 (390)
50% Recovered		–	218 (425)
90% Recovered		282-338 (540-640)	248 (478)
End Point		–	269 (517)
Recovery %		–	98.0
Residue %		–	1.4
Loss %		–	0.6
Carbon Residue, Wt. % (10% Bottoms)	D 524	0.35 max.	0.15
Water and Sediment, Vol. %	D 1796	0.05 max.	0.00
Ash, Weight %	D 482	0.01 max.	0.00
Color (Visual)	D 1500	(Clear to Amber)	< 0.5
Date Approved: 2/15/04 (Specification valid only if dated)			

Note: Premium Additive Package includes cetane improvers, lubricity enhancers and detergents.

FLEETLINE
DENNIS K. BURKE INC.

Typical test data are average values only. Minor variations which do not affect performance may occur.

284 EASTERN AVE. • CHELSEA, MASS. 02150 • PHONE: 1-800-289-2875 • FAX: (617) 884-7638 • WEBSITE: WWW.BURKEOIL.COM

Table 4.2. Manufacturer's specifications for the ultra-low sulfur diesel used as one of the baseline fuels.

The purpose of using the ULSD fuel is twofold. First, to allow for evaluation of the fuel sulfur effect on emissions and, second, to compare FT fuel to a fuel that will be widely available in the future.

Once again, the lower heating value of the ultra-low sulfur diesel fuel was not listed in the table provided by Fleetline. In order to compare the lower heating value of the ULSD to the other fuels used in this study, the lower heating value for a standard No. 2 diesel fuel, $Q_{LHV,No.2}$ = 129,400 Btu/gal, given in Syntroleum's S-2 product literature was used once more [49]. The conversion of the heating value from a volumetric basis to SI units on a mass basis follows the same procedure outlined in Section 4.1.1. Accounting for the measured fuel density of 845 kg/m^3, yields a lower heating value for the ULSD of $Q_{LHV,No.2}$ = 42.7 MJ/kg [36]. This value also compares well with heating value data for typical light diesel fuels listed as $Q_{LHV,No.2}$ = 43.2 MJ/kg in [1].

4.1.3 No. 2 Diesel Combustion Equation

In order to compare differences in the combustion characteristics between the No. 2 diesel fuels and the Syntroleum S-2 FT diesel, a simplified chemical composition of $CH_{1.8}$ and a molecular weight of 170 g/mol [1] was used in order to write the ideal combustion equation (using the simplified chemical composition) for both the LSD and ULSD baseline No. 2 diesel fuels as follows:

Equation 4.2
$$12.3CH_{1.8} + \frac{17.835}{\phi}(O_2 + 3.773N_2) \rightarrow 12.3CO_2 + 11.07H_20 + 17.835\left(\frac{1}{\phi} - 1\right)O_2 + \frac{67.29}{\phi}N_2$$

Based on Equation 4.2, the air/fuel ratio for stoichiometric combustion for both of the baseline No. 2 diesel fuels is 14.50:1. This matches the accepted stoichiometric air/fuel ratio for light diesel fuels given in [1].

4.2 Fischer-Tropsch Diesel

The trend toward cleaner fuels for reduced emissions and improved compatibility with aftertreatment devices has led to renewed interest in Fischer-Tropsch fuels in recent years. Developed in the 1920's by Franz Fischer and Hans Tropsch, the FT process can

be used to produce hydrocarbon fuels from a wide range of carbonaceous materials. This process consists of four major steps and is shown in Figure 4.1 below.

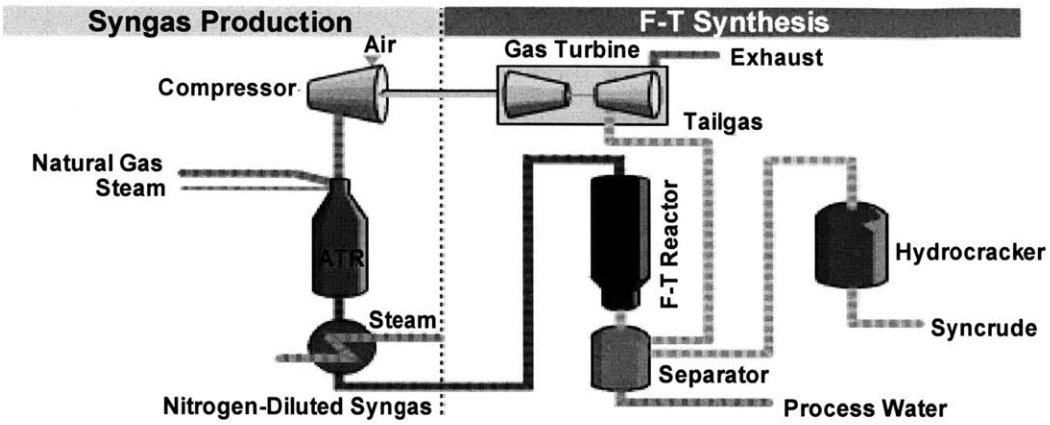

Figure 4.1. Production of Fischer-Tropsch fuels via the Syntroleum Process™ [49]

The first step is the production of synthesis gas (CO and H_2) from the feedstock, typically natural gas, coal, or biomass. This step is followed by the purification of the synthesis gas, since the FT process relies heavily on the use of catalysts, and any sulfur in the synthesis gas can poison the catalysts, thus reducing fuel production. The third step is the FT catalysis process in which the synthesis gas is converted to heavy, straight-chain liquid hydrocarbons and waxes. The final step in the process consists of refining the heavy hydrocarbons by means of hydrocracking, isomerization, fractionation, and distillation to produce the desired fuel [41]. For a detailed description of the specific steps and reactions involved in the Fischer-Tropsch synthesis process, the reader is referred to [35].

4.2.1 Syntroleum FT Diesel Fuel Properties

The Fischer-Tropsch fuel (S-2) used in this study was provided by the Syntroleum Corporation. Syntroleum S-2 is produced using the Syntroleum Process™ described in the previous section. Utilizing a unique auto-thermal-reformer (ATR) to produce the synthesis gas from natural gas and untreated air reduces the overall production costs and makes Syntroleum S-2 fuel economically marketable [35].

While the zero sulfur content of the S-2 FT fuel provides a number of benefits in terms of particulate emissions reduction and improved compatibility with exhaust aftertreatment systems, the absence of the sulfur also reduces the lubricity properties of the fuel, which may have deleterious effects on the fuel injection system. In order to improve the lubricity properties of the fuel, 300 PPM of a lubricity additive manufactured by Lubrizol was blended with the fuel prior to shipping to MIT. The Lubrizol additive is not believed to significantly affect the combustion or emissions characteristics of the S-2 fuel.

The diesel fuels produced as a result of the Syntroleum Process ^{TM} exhibit a number of chemical and physical properties attributed to reduced emissions levels, namely zero sulfur content, low aromatics and olefins content, high cetane rating (74.4), and reduced density. In addition, S-2 diesel has a viscosity similar to that of standard No. 2 diesel, allowing the fuel to be used in current technology engines with no modifications to the fuel handling and injection system. The S-2 diesel used in this study meets or exceeds the ASTM requirements for typical diesel fuel oils, which are given in Table 4.3 below.

ASTM D 975 Requirements for Diesel Fuel Oils

Property	Test Method*	Low Sulfur No. 1-D	No. 1-D	Low Sulfur No. 2-D	No. 2-D	No. 4-D
Flash point, °C, min	D 93	38	38	52	52	55
Water and sediment, % vol, max	D 2709 D 1796	0.05	0.05	0.05	0.05	0.50
Distillation temperature, °C, 90% vol recovered min max	D 86	 288	 288	 282 338	 282 338	
Kinematic viscosity, 40°C, cSt min max	D 445	 1.3 2.4	 1.3 2.4	 1.9 4.1	 1.9 4.1	 5.5 24.0
Ash, % mass, max	D 482	0.01	0.01	0.01	0.01	0.1
Sulfur, % mass, max	D 2622	0.05	0.50	0.05	0.50	2.00
Copper strip corrosion, 3 hr at 50°C, max rating	D 130	No. 3	No. 3	No. 3	No. 3	
Cetane number, min	D 613	40	40	40	40	30
One of the following: 1) Cetane index, min 2) Aromaticity, % vol, max	 D 976 D 1319	 40 35		 40 35		
Ramsbottom carbon residue on 10% distillation residue,	D 524	0.15	0.15	0.35	0.35	

* All "Dxx" methods are ASTM standards.

Table 4.3. ASTM D 975 requirements for diesel fuel oils

Furthermore, FT diesel is completely miscible with conventional diesel making it an ideal candidate as both a blending agent with and eventual replacement for conventional petroleum-based diesel fuels. Additional fuel properties provided by Syntroleum for the two batches of S-2 FT fuel used during this study are presented in Table 4.4 and 4.5.

Certificate of Analysis Syntroleum

SYNTROLEUM® S-2 SYNTHETIC DIESEL FUEL		Grade S2—Summer Climate diesel fuel with Cloud Point between -20°C and -29°C		
SYNTHETIC DIESEL FUEL OIL—SUMMER GRADE BATCH 5 LOT 1		ISO Container Number: 124015-1		
PHYSICAL PROPERTIES	TEST METHOD	UNITS	S-2 S2 SPECIFICATION	ACTUAL
Flash Point, min	D93	°C(°F)	52 (125)	58(136)
Distillation, 10% Vo. Recovered	D86	°C	Report	191
Distillation, 50% Vol Recovered	D86	°C	Report	243
Distillation, 90% Vol Recovered	D86	°C	282-338	307
Kinematic Viscosity @ 40°C	ASTM D-445	cSt	1.9-2.5	2.0
Ash	ASTM D-482	% mass	<0.01	<0.001
Cloud Point Min/Max	D5771	°C(°F)	-20 to -29°C	-25
Conductivity	ASTM D-2624	pS	250-450	276
Density @ 15°C	ASTM D-4052	kg/L	0.76-0.78	0.77
API	ASTM D-4052	°	49-54	52.2
Appearance	Visual		Clear & Bright	Clear & Bright
Sulfur	ASTM D 4045	ppm	<1	
Cetane Number	ASTM D-613		>70	
Copper Strip Corrosion	D 130		No. 1	
Water and Sediments	ASTM D-2709	% vol	< 0.05	
Ramsbottom Carbon	D524	% mass	<0.1	
Aromatics Content**	ASTM D 5292-93	Mol %	<0.1	
Or Cetane Index	D976 or D4737		>70	
Lubricity, HFRR@60°C	ASTM D6079	Microns	300-460	

Table 4.4. S-2 fuel properties for the first batch of Fischer-Tropsch diesel tested

Aside from minor variations in physical properties such as flash point, kinematic viscosity, and distillation there were no major differences between the two batches of Syntroleum S-2. Furthermore, the differences in physical properties are so small that their effect on the combustion and emissions behavior of the fuels is negligible.

SYNTROLEUM® S-2 SYNTHETIC DIESEL FUEL		Grade S2—Summer Climate diesel fuel with Cloud Point between -20°C and -29°C		
SYNTHETIC DIESEL FUEL OIL—SUMMER GRADE BATCH 11 LOT 8		ISO Container Number: 124260-0		
PHYSICAL PROPERTIES	TEST METHOD	UNITS	S-2 S2 SPECIFICATION	ACTUAL
Flash Point, min	D93	°C(°F)	52 (125)	61 (142)
Distillation, 10% Vo. Recovered	D86	°C	Report	196
Distillation, 50% Vol Recovered	D86	°C	Report	254
Distillation, 90% Vol Recovered	D86	°C	282-338	308
Kinematic Viscosity @ 40°C	ASTM D-445	cSt	1.9-2.5	2.2
Ash, max	ASTM D-482	% mass	<0.01	<0.0001
Cloud Point	D5771	°C	-20 to -29°C	-24
Conductivity	ASTM D-2624	pS	250-450	363
Density	ASTM D-4052	kg/L	0.76-0.78	0.77
API	ASTM D-4052	°	49-54	51.5
Appearance	Visual		Clear & Bright	Clear & Bright
Sulfur	ASTM D 4045	ppm	<1	
Cetane Number	ASTM D-613		>70	
Copper Strip Corrosion	D 130		No. 1	
Water and Sediments	ASTM D-2709	% vol	< 0.05	
Ramsbottom Carbon	D524	% mass	<0.1	
Aromatics Content	ASTM D 5292-93	Mol %	<0.1	
Or Cetane Index	D976 or D4737		>70	
Lubricity, HFRR@60°C	ASTM D6079	Microns	300-460	

Table 4.5. S-2 fuel properties for the second batch of Fischer-Tropsch diesel tested

The lower heating value of Syntroleum S-2 was calculated using data provided by Syntroleum and values listed in Table 4.4 and Table 4.5. The product literature for Syntroleum S-2 gives a lower heating value of $Q_{LHV,S-2}$ = 121,500 Btu/gal. The lower heating value was then converted to SI units and a mass basis using the S-2 density listed as ρ_{S-2} = 775 kg/m^3. The resulting lower heating value of $Q_{LHV,S-2}$ = 43.7 MJ/kg is substantially greater than that of the baseline fuels on a mass basis. However, the significantly lower density of the S-2 fuel results in a reduction in the lower heating value on a volumetric basis by approximately 6.0% as compared to the baseline fuels.

4.2.2 Syntroleum FT Diesel Combustion Equation

Syntroleum provided additional S-2 fuel properties and specifications necessary to carry out the combustion calculations. The molecular weight of the FT fuel is 205 g/mol, and the fuel is composed primarily of 84.9% carbon and 15.1% hydrogen. No significant

quantities of impurities such as oxygen or nitrogen were detected in the fuel. Based on the fuel composition data provided by Syntroleum, the reduced chemical C:H ratio for the S-2 diesel fuel is 2.12. Based on the simplified fuel composition, the ideal combustion equation for Syntroleum S-2 is:

Equation 4.3 $$14.49CH_{2.12}+\frac{22.17}{\phi}(O_2+3.773N_2)\rightarrow 14.49CO_2+15.36H_20+22.17\left(\frac{1}{\phi}-1\right)O_2+\frac{83.65}{\phi}N_2$$

Equation 4.3 yields an air/fuel ratio of 14.95:1 for the stoichiometric combustion of Syntroleum S-2 diesel.

4.3 Fuel Blends

In addition to the three neat fuels, fuel blends were studied in order to gain a better understanding of how varying fuel properties affect emissions reductions. Furthermore, this allowed direct quantification of the effect of fuel sulfur level on particulate emissions as well. A blend of 25% FT diesel and 75% low sulfur diesel was used in order to realize the greatest benefit of using the FT fuel as a blending agent.

4.3.1 25% FT - 75% Low Sulfur Diesel Blend

This blend was studied to determine whether or not the major advantages of FT fuel could be realized if the FT fuel comprised only a small portion of the engine's fuel. Previous studies have demonstrated that the effect on the emissions trends of FT/D-2 blends is not linear with respect to the portion of FT in the blend, with most of the benefit realized with less than 50% FT in the blend by volume [35, 36]. In order to realize the greatest benefit of using the FT fuel as a blending agent, a 3:1 by volume LSD to FT fuel blending ratio was chosen.

The lower heating value and ideal combustion equation for the blend were determined from the figures for the baseline LSD and FT fuel properties presented above in Section 4.1.1 and Section 4.2.1. The conversion of 25% by volume FT fuel to a mass basis yielded 23.5% FT fuel by mass, giving a fuel density for the blend of 824 kg/m^3. Using the calculated fuel density, the lower heating value for the blend was calculated to be

$Q_{LHV,\ BL}$ = 43.1 MJ/kg. Furthermore, the 25% molar fraction of FT gave a simplified chemical composition for the blend of $CH_{1.9}$. Based on the simplified chemical composition, the ideal combustion equation is given as:

Equation 4.4
$$12.88CH_{1.9}+\frac{19.0}{\phi}(O_2+3.773N_2)\rightarrow 12.88CO_2+12.24H_20+19.0\left(\frac{1}{\phi}-1\right)O_2+\frac{71.69}{\phi}N_2$$

From Equation 4.4, the stoichiometric air-fuel ratio for the blend is 14.61:1, which lies between the calculated air/fuel ratio for the neat LSD and FT fuels, as could be expected.

4.4 Fuels Analysis

In order to verify the fuel properties provided by the manufacturers, and provide further insight into the observed combustion and emissions differences between the fuels, a sample of each of the fuels tested was sent to Syntroleum for analysis. A specific comparison of the fuel properties analyzed by Syntroleum is presented in Table 4.6.

	Fleetline Fuel LSD (400ppm)	Fleetline Fuel ULSD (15ppm)	Syntroleum S-2
Flash point, °F	130	139	142
Viscosity @40°C	2.777	2.288	2.2
Cloud Point, °C	-13	-24	-25
Freezing Point,°C	-10.5	-18.5	---
Density,15°C	0.851	0.82	0.7701
Sp Gr, 15°C	0.855	0.824	0.775
API, 60°F	33.95	40.16	51.06
Distillation Data			
D2887,IBP °F	225	254	246
D2887, 5%	335	321	330
D2887,10%	369	343	357
D2887,20%	409	368	400
D2887,30%	442	389	435
D2887,40%	473	410	467
D2887,50%	502	428	498
D2887,60%	534	449	528
D2887,70%	576	467	561
D2887,80%	622	491	594
D2887,90%	673	517	640
D2887,95%	703	540	675
D2887,FBP	758	652	741

Table 4.6. Fuel properties comparison as determined from the analysis carried out by Syntroleum

The results of the Syntroleum analysis match the data provided by Fleetline reasonably well, however the values provided by Fleetline are only the results of typical values computed from an average of a number of samples, and minor variations are to be expected.

Of specific interest to this study is the distillation data presented in the chart comparing the distillation curves for the three different fuels in Figure 4.2. It is quite clear from the chart that the distillation curve for the FT fuel is very similar to that of the low sulfur (400 PPM) diesel. Furthermore, the ultra-low sulfur diesel (15 PPM) contains a significantly greater amount of the lower boiling point (higher volatility) fraction, especially near the back end.

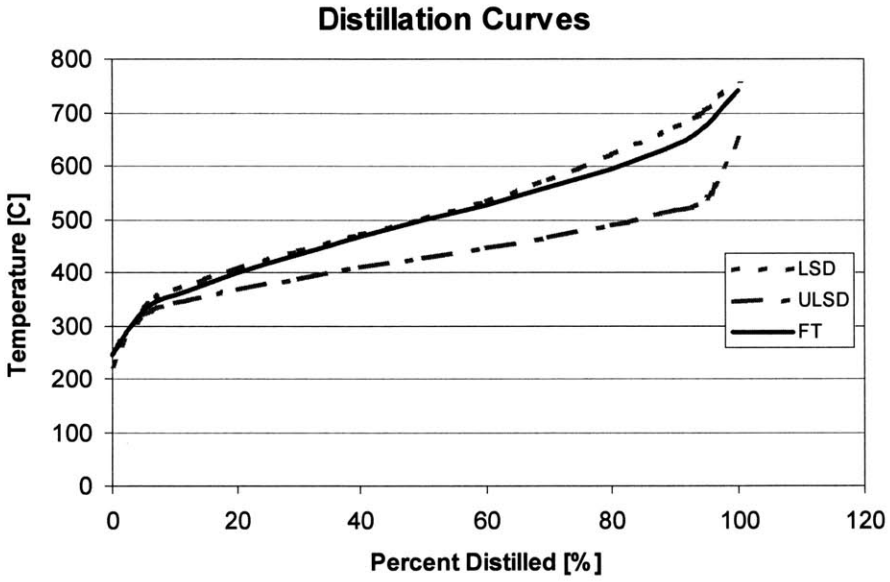

Figure 4.2. Distillation curves for each of the three fuels tested

In addition to verifying the distillation curves, Syntroleum also analyzed the fuel samples using gas chromatography. The gas chromatograms present the results of their analysis and are shown Figure 4.3 and Figure 4.4.

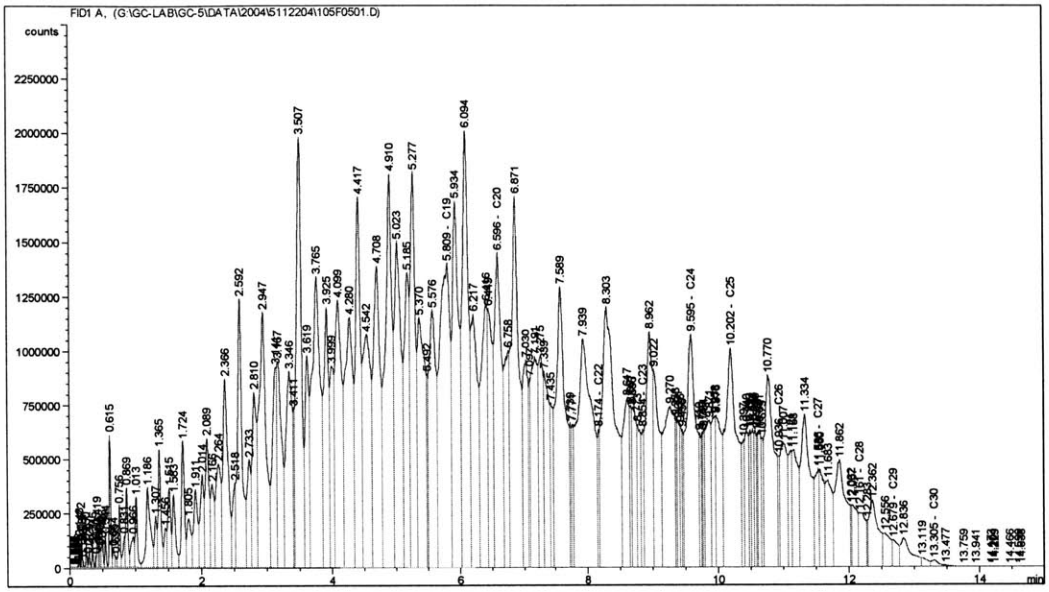

Figure 4.3. GC trace for the 400 PPM low sulfur diesel

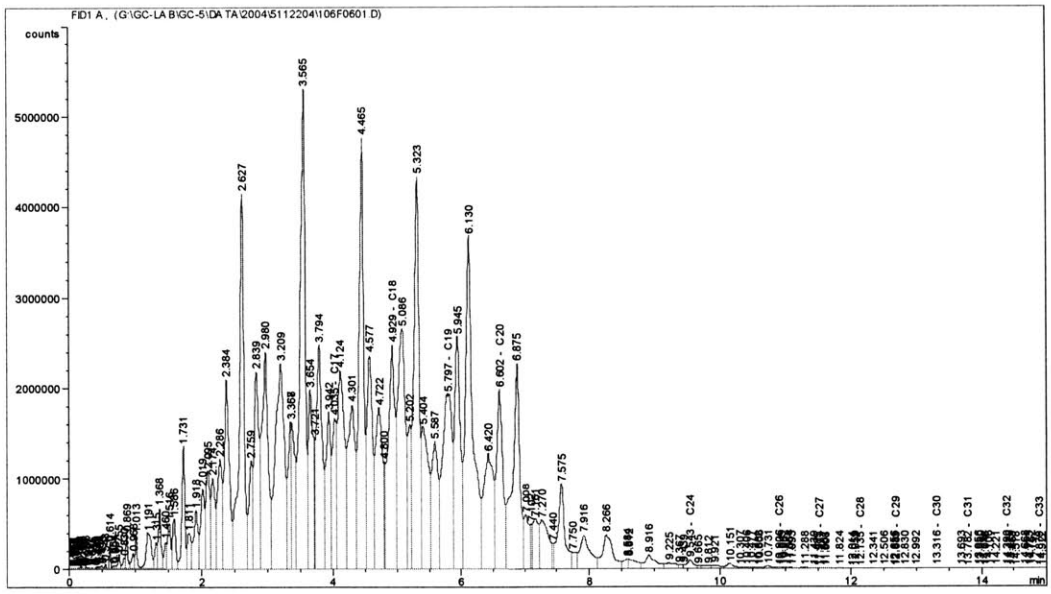

Figure 4.4. GC trace for the 15 PPM ultra-low sulfur diesel

Unfortunately the gas chromatograms for Syntroleum's S-2 fuel were not available prior to the conclusion of this study, however based on the distillation curves presented in Figure 4.2, the GC trace for the FT is expected to be similar to that of the LSD with a

slightly lower heavy hydrocarbon concentration near the back end. From the two gas chromatograms for the low sulfur and ultra-low sulfur diesel, it is apparent that the ULSD contained a significantly greater portion of light hydrocarbons, a trend that was observed in the distillation curves for the two fuels as well. The lack of peaks on the right side of the spectrum for the ULSD indicate the absence of an appreciable number of heavy hydrocarbons (high carbon number compounds). Heavier compounds elute from the column more slowly, and, thus, appear toward the latter end of the spectrum. The distribution of hydrocarbon compounds in the LSD was much more uniformly distributed over the entire range of the GC trace and included a wide range of both light- and heavy-hydrocarbons, as indicated by the large number of peaks at later elusion times.

5.0 Experimental Setup

While the engine and test bed were installed an setup for two prior studies by Llaniguez (S.M. 2003) and Acar (S.M. 2005), substantial changes to the data acquisition and gaseous and particulate emissions sampling systems were made in this study. For a detailed description of the engine setup the reader is referred to [35]. Additional details and diagrams related to the experimental setup are also presented in Appendix A.

5.1 Engine

The engine used in this study was a pre-production development engine based on the Cummins 2002 ISB 300 platform. The Cummins ISB 300 is a turbocharged, 6-cylinder, 5.9-liter, four-stroke, direct injection diesel engine. The engine is rated at 224 kW (300 hp) at 2500 rpm and 890 N-m (660 lb-ft) at 1600 rpm. Appendix B presents additional engine performance data. The ISB300 is certified to meet 2002 EPA emissions standards, and employs a number of advanced subsystems such as a Bosch common rail high-pressure fuel injection system, Holset variable geometry turbocharger, and cooled EGR. In addition to these subsystems, the engine also utilizes a multiple fuel injection strategy to further optimize the combustion process with three injection events (pre-, main-, and post-injection) per cycle. All of the advanced subsystems are electronically controlled by an electronic control module (ECM) (version CM 850) calibrated to meet 2002 emissions limits when operating with an EPA No. 2 diesel fuel. Table 5.1 lists the engine specifications.

Number Of Cylinders	6
Combustion System	Direct Injection
Aspiration	Turbocharged
Stroked (Displaced) Volume [liters]	5.9
Bore/ Stroke [mm]	102/120
Connecting Rod Length [mm]	192
Crank Radius [mm]	60
Compression Ratio	17.2
Valve Timing	IVO = 9.5° bTDC | IVC = 23.5° aBDC
	EVO = 142.0 °aTDC | EVC = 18.0° aTDC
Injection Nozzle	O.D. = 158 μm, L = 1.00 mm
	8 Sac-less (VCO) Nozzles Per Injector

Table 5.1. Pre-production Cummins ISB 300 engine details [35]

5.2 Engine Control Software

The ISB 300 engine provided by Cummins was fully electronically controlled and came equipped with an unlocked ECM. In addition, Cummins also provided their proprietary in-house software, Calibration Terminal (CalTerm) version 7.63, allowing for engine calibration changes and real-time monitoring and modification of engine parameters. Throughout the duration of this study, the stock 300-horsepower calibration provided by Cummins was uploaded into the ECM and no modifications to any engine control parameters were made. This calibration was based on a standard No. 2 diesel fuel and was used for the following two reasons: (1) to ensure the engine would run on the 2002 EPA-emission-certified performance maps, and (2) to evaluate the performance of the Fischer-Tropsch fuels and blends in a modern engine with an unmodified control system.

While CalTerm allows for the monitoring and modification of hundreds of engine parameters, unlike prior studies, no parameters were modified during the tests carried out in this investigation. Despite this fact, CalTerm was used to monitor and log a number of engine control parameters of interest such as charge flow, pilot injection quantity and timing, post injection quantity and timing, EGR fraction, boost pressure, and common-rail accumulator pressure, among others. Furthermore, CalTerm proved invaluable as a diagnostic tool aiding in the diagnosis of occasional engine problems by providing real-time logging and display of fault codes.

5.3 Dynamometer Setup and Controller

The engine was directly connected to a Digalog AE 250 eddy current dynamometer via a drive shaft assembly and two Spicer 1710 Series flange yokes capable of withstanding 1220 N-m under steady state operation and spikes of up to 6500 N-m [35]. The Digalog AE 250 is rated up to 250 kW, and was used to load the engine. In order to control engine load, a Watlow Series 96 process controller was wired into the engine's control system. Furthermore, a Digalog Model 1022A-STD dynamometer controller regulated engine speed. Torque was measured using a Maywood Instruments U4000, 500 kg load cell, and torque data was continually recorded using the National Instruments data acquisition system described in the following section.

5.4 Data Acquisition System

The engine was heavily instrumented and all measurements were recorded using National Instruments data acquisition (DAQ) hardware and software. A high-speed PCI-6024E DAQ board comprised the heart of the system, and was connected to a SCXI-1000 multiplexing chassis. A 32-channel thermocouple module (SCXI-1102B) containing a fixed 200 Hz low-pass filter was installed in the multiplexing chassis, and used to acquire most slow-speed data. In addition, a general 32-channel module (SCXI-1100) containing a 10 kHz low-pass filter was also installed in the multiplexing chassis to accommodate both high- and low-speed data acquisition. TBX-1303 terminal blocks were connected to both the SCXI-1102B and SCXI-1100, and incoming signals were wired directly to the terminal blocks. The slow-speed measurements consisted primarily of data from various thermocouples, pressure transducers, and flow meters in addition to the engine control parameters monitored in CalTerm. A detailed list of the parameters that were monitored is shown in Table C.1 of the appendix.

Aside from the two modules mentioned above, an additional 32-channel SCXI-1102B module was also installed in the multiplexing chassis during the course of this investigation to accommodate additional input signals from various emissions analyzers, exhaust thermocouples, and pressure transducers. This module also contained a fixed 200 Hz low-pass filter, and was connected to a TBX-1303 terminal block equipped with cold-junction-compensation sensors to correctly scale the thermocouple signals. The addition of the above-mentioned data acquisition hardware allowed for the acquisition and monitoring of over 96 input signals from various auxiliary sensors mounted on the engine and exhaust system.

In order to correctly monitor and record data from all of the auxiliary sensors as well as the emissions analyzers, the original National Instruments Labview data acquisition programs written by Llaniguez (S.M. 2003) were modified. Entirely new programs to monitor exhaust conditions were written as well, and these are shown in Figure C.1 and Figure C.2 of the appendix.

5.4.1 High-Speed In-Cylinder Pressure Measurements

The high-speed data consisted mainly of in-cylinder pressure, crank angle, and manifold air pressure measurements. The in-cylinder pressure measurements were performed using an AVL QC33C quartz, piezo-electric pressure transducer mounted in cylinder number 6. A Kistler 5010B charge amplifier converted the transducer's small current output to a voltage signal, and the transducer was liquid cooled using a Bernard Model 2500SS MIG welder cooler.

A BEI high-resolution (1800 pulse-per-revolution, 0.2° resolution) crank angle encoder mounted onto the tone wheel recorded engine-position-indexing signals, and provided information on top dead center of cylinder 6. In addition, the encoder also triggered the start of data acquisition at the same point of an engine revolution, but not necessarily the same stroke. In order provide more precise engine-position data on which stroke of the four-stroke cycle each piston was going through, data from Hall-Effect sensors on both the camshaft and tone wheel were monitored as well. This ensured correct phasing of the in-cylinder pressure signal [35].

5.4.2 Pressure Transducer Calibration and Encoder Phasing

In order to obtain meaningful results from the high-speed in-cylinder pressure measurements, correct phasing of the pressure signal is of utmost importance. Two methods were used to correctly adjust the phasing of the start of the high-speed data recording with respect to TDC. The method used as a first approximation to set the proper phasing was to adjust the encoder so that the reference signal on the crankshaft tone wheel occurred 60.0° bTDC [35]. Once the encoder was set at this approximate position, the peak pressure was determined from a motoring pressure trace and 0.4° were added due to heat transfer and blow-by effects. This was the procedure recommended by Cummins and resulted in a more precise determination of TDC.

In order to obtain the motoring pressure trace for TDC determination, the engine was fired and only fueling to cylinder number 6 was cut. Fueling to this cylinder was cut by setting the engine parameter FSI_x_ExtCylMask_c to 001F (hexadecimal representation

of cylinder 6) so that the motoring pressure traces could be recorded. The motoring traces were thus recorded and fine adjustments to the encoder made until proper phasing of the signal was achieved. As a final check for correct phasing, the log-pressure versus log-volume curves were plotted for the motoring pressure traces to verify that the compression and expansion lines did not cross [35].

5.5 Fuel Flow Measurements and Fuel Handling System

The system used to measure fuel flow rates consists of an Ohaus Scout II Pro balance and a four-liter beaker used to hold a given quantity of fuel. Fuel was supplied to the engine from the beaker via a three-way ball valve to allow for selection of either the beaker or fuel tank as the fuel source. Likewise, the fuel return to the beaker was also controlled via a second three-way ball valve. The return line was also used to refill the beaker when the supply line was shut off. The balance was connected directly to the serial port of the data acquisition computer and fuel mass was monitored and recorded every second.

The duration of the fuel flow measurements was limited by the size of the beaker, approximately one gallon, necessitating that fuel flow data only be taken when gaseous emissions and slow-speed data were recorded to allow sufficient time for the beaker to be refilled. Additional corrective measures to compensate for temperature variations such as the counter-flow heat exchangers installed by Llaniguez and Acar were retained, although no longer necessary, as the mass flow of the fuel was measured directly by the balance.

All of the diesel fuel was contained in two separate 81.4-liter (22-gallon) ATL Inc. SP122B racing fuel cells. The first fuel cell was used to hold only the LSD, ULSD, and fuel blends while the second fuel cell was only used for the neat FT diesel. This was done to prevent any cross contamination between the neat FT fuel and baseline diesel fuels. A fuel control bulkhead consisting of a series of three-way valves allowed for switching between the individual fuel tanks. Additional valves in the bulkhead made it possible to bypass the entire return system in order to drain and purge the system when changing fuels. The fuel change procedure is described in detail in Section 6.3.1. All

connections on the entire fuel system were made with stainless-steel braided Teflon lines to ensure trouble-free operation and comply with laboratory safety regulations.

5.6 Intake Air Measurement and Air Handling Systems

Intake airflow measurements were carried out using an Eldridge Products, Inc. Series 8732 thermal mass flow meter installed just after the air filter and before the turbocharger inlet. Following the turbocharger, a Spearco Universal Air/Liquid Intercooler cooled the pressurized intake air before it entered the engine's intake manifold. Cooling water was supplied to the intercooler at a constant flow rate directly from the laboratory's water supply and recovery system. As a result, the intercooler tended to over-cool the intake air when the engine was operated at light loads, and not cool enough at extremely high loads. A gate valve controlled the flow of cooling water to the core of the charge-air cooler, and was used as a rough means to control the cooling capacity of the intercooler.

The intercooler was connected to the engine via 7.54 cm (3") I.D. silicone rubber hose, rated to a maximum temperature of 170°C. Despite these measures, the engine was never operated at rated speed and load due to problems experienced by Llaniguez and Acar in previous tests with the durability of the intake air hoses and cooling capacity of the intercooler at these conditions. Intake air temperature and relative humidity were also continually monitored via a Omega Digital Thermo-Hygrometer that was also wired into the data acquisition system.

5.7 Gaseous Emissions Analyzers

A gas analyzer system was designed and fabricated at the Sloan Automotive Laboratory. This system is capable of measuring exhaust gas concentrations in both the raw exhaust stream and dilution tunnel, as well as in the intake manifold to determine the EGR fraction. In this study, all gaseous emissions comparisons were based on measurements sampled from the raw exhaust using heated sample lines and filters to prevent any water from condensing out of the exhaust stream. Figure 5.1 shows a schematic of the emission sampling system and general experimental setup as it looked at the beginning of this study.

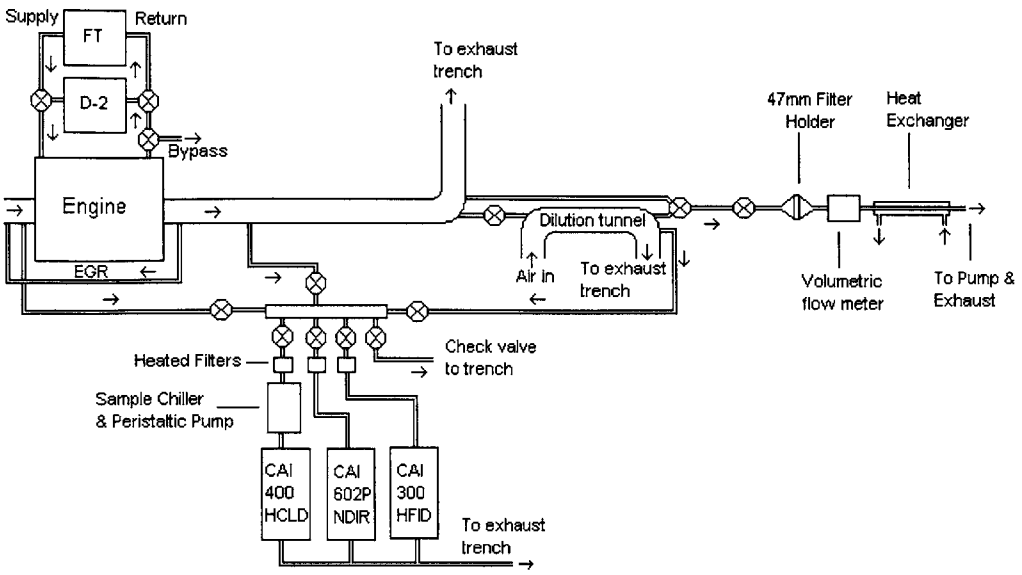

Figure 5.1. Emission sampling system schematic

A full suite of California Analytical Instruments (CAI) emissions analyzers comprised the heart of the gaseous emissions sampling system and enabled measurement of HC, NO/NOx, CO_2, CO, and O_2 exhaust concentrations. Following the completion of the work by Acar, the entire gaseous emissions and particulate sampling system was rebuilt, and new $CO/CO_2/O_2$ and SO_2 analyzers were installed.

Hydrocarbon emissions were measured using a CAI Model 300-HFID. The Model 300-HFID was calibrated with 300 PPM and 30 PPM propane (C_3H_8) span gasses and zeroed using highly purified compressed nitrogen gas. This calibration resulted in a total effective range of 0 – 900 PPM of C_1; however, during the experiments the HC analyzer was left on the 0 – 30 PPM range since HC emissions from the engine were extremely low. The operating principle of the 300 HFID is based on a flame ionization detector, whereby a flame ionizes the sample stream and electrodes in the instrument measure the particles. A mixture of 40% hydrogen, 60% helium, and hydrocarbon-free air was used to fuel the flame in the Model 300-HFID. The output of the HC analyzer was fed into the DAQ system, and the voltage signal was converted back to a PPM concentration and recorded.

A California Analytical Instruments Model 400 HCLD Heated Chemiluminescence NO_x analyzer was used to measure NO/NO_x concentrations in the raw exhaust. The analyzer works by using a photodiode detector and chemiluminescence to generate a low DC current proportional to the amount of NO in the sample gas. To calibrate the Model 400, a calibration gas of 296 PPM of NO and a zero gas of high-grade nitrogen was used. The output of the NOx analyzer was fed into the DAQ system, and the voltage signal was converted back to a PPM concentration and recorded.

A recently installed CAI 602P Non-Dispersive Infrared (NDIR) analyzer replaced the Horiba MEXA 554 JU for CO_2 measurements in previous studies. In addition to CO_2, the NDIR analyzer is also capable of measuring CO and O_2 concentration in the sample gas. The NDIR gas analyzer utilizes the basic principle that each gas component exhibits a unique absorption line spectrum in the infrared region to measure sample gas concentration. The analyzer was calibrated using the following span gas concentrations: 20.0% CO_2, 0.302% CO, and 20.0% O_2. Highly purified nitrogen gas was used to zero the analyzer as well. In addition, gas concentrations of 6.60% CO_2, 2.50% CO, and 4.115% O_2 were also used to verify correct analyzer operation. The output signals from each of the three channels ($CO/CO_2/O_2$) were wired into the DAQ system.

All of the above-mentioned gaseous emissions analyzers were mounted in a newly fabricated analyzer rack. The rack was designed to accommodate up to four different input sample lines to allow either simultaneous measurement of all gaseous emissions of interest or individual measurement of emissions from up to four different sample points. In addition to the analyzers, the rack houses a number of sample preparation and conditioning systems. The samples for all of the CAI instruments were carried from their respective sample points on the engine/exhaust system to the analyzer rack via heated sample lines. A detailed schematic of the gaseous emissions measurement system designed and fabricated for this project is shown in Figure 5.2.

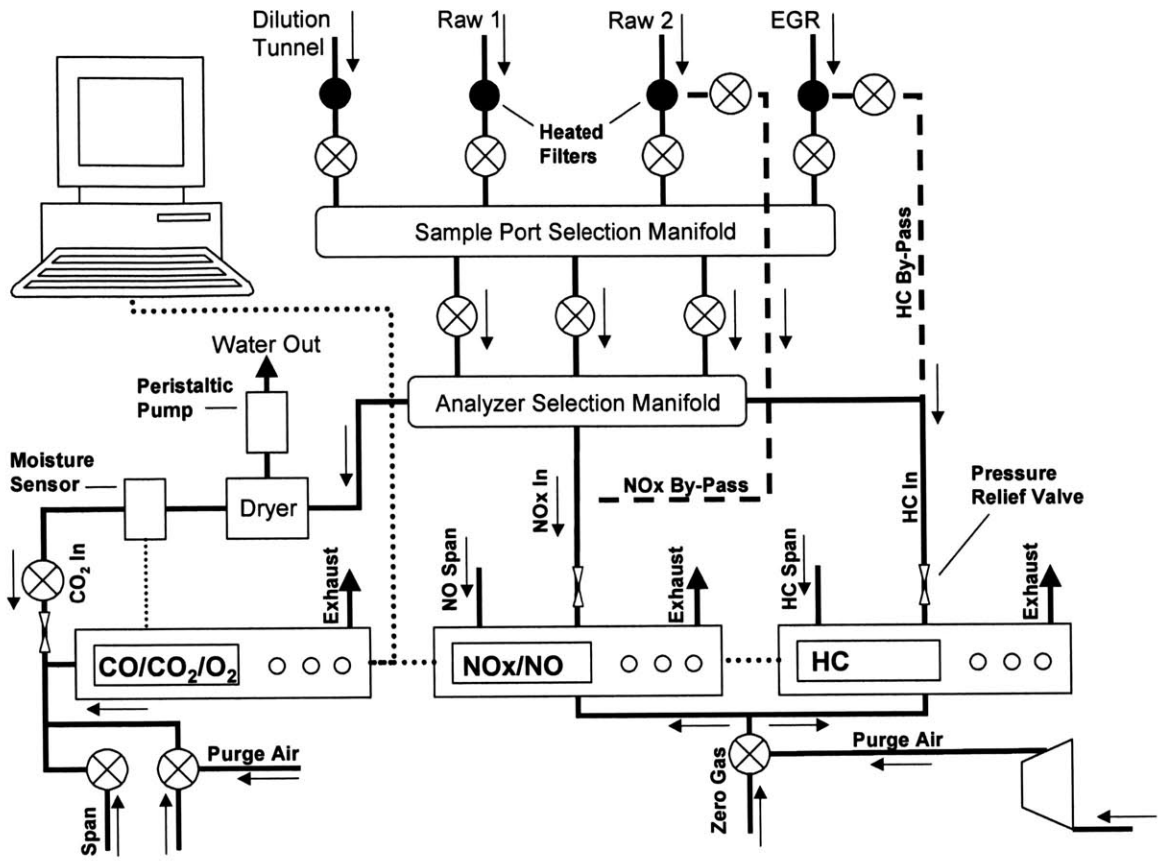

Figure 5.2. Gaseous emissions sampling system

The heated sample lines enter the rear of the analyzer rack and are connected directly to three individual Universal Analyzers Model 270S heated stack filters and one M&C Products Series FT heated filter. The Universal analyzers filters employ 2-micron ceramic filter elements to remove any large particulate matter that can clog sample and capillary tubes within the gas analyzers, and the M&C filter employs a slightly larger 3-micron filter element. A series of heated stainless steel lines connect the heated filters to one of two manifolds. The first manifold, and corresponding bulkhead mounted on the front panel of the analyzer rack, control sample port selection (Dilution tunnel, Raw1, Raw2, and EGR). The second manifold and corresponding bulkhead enable analyzer selection and control zero gas, span gas, and purge airflow.

Each CAI analyzer is also equipped with its own internal sample pump to facilitate sample gas transport from the engine through the heated lines to the analyzers. Early

attempts to simultaneously run all of the analyzers on the same sample line resulted in extremely low sample flow rates and erroneous measurements due to interaction of the various sample pumps. In order to allow for simultaneous emissions sampling, two by-pass lines were added to the gas analyzer system as shown in Figure 5.2. The by-pass lines allow the sample gas to circumvent the common manifolds and flow directly into each of the three gas analyzers, thus eliminating the problem of negative pump interference.

In order to reduce the amount of zero gas consumed during analyzer warm-up and shut down, as well as to provide a convenient means for flushing the analyzer system before shut-down, a purge air system was also installed in the analyzer rack. The system consists of a Gast rotary vane vacuum pump used to pull ambient air into the system and additional bulkhead connections to direct the purge air to each of the analyzers and associated piping.

5.7.1 Sample Preparation

As the HC and NOx measurements were carried out wet, the sample gasses for these analyzers were routed directly from the bulkhead, via heated lines to the sample inlet port of the analyzers. Stainless steel tubing was used for all connections within the gas analyzer system, and all lines, manifolds, and valves were heated using Omegalux rope heaters controlled by two Powerstat variable autotransformers.

On the other hand, since the CO_2, CO, and O_2 emissions must be measured dry to avoid interference between any moisture in the exhaust stream and the optical measurement systems in the analyzer, the sample stream is first passed through a Universal Analyzers Model 520 single stage sample chiller to cool the sample to 3.5°C and remove any water vapor present in the sample stream. The water that accumulates in the sample chiller is then removed with a Universal Analyzers Model 7015-20 peristaltic pump. Furthermore, a secondary moisture sensor/filter assembly provides an additional check before the cool dry gas stream is routed into the NDIR analyzer.

5.7.2 Gaseous Emissions Sample Points

Gaseous emissions were sampled from three different locations on the engine/exhaust system in this study. All engine-out emissions were sampled from the raw exhaust stream at a sample point 10 pipe diameters away from the nearest elbow to ensure fully developed flow at the sample point. Additionally, emissions were also sampled from the intake manifold and mini-dilution tunnel. Intake manifold sampling consisted primarily of CO_2 concentration measurements in order to calculate the EGR fraction. The intake manifold emissions sample point was installed 304.8 mm (12") from the EGR valve. For the gaseous emissions measurements taken from the mini-dilution tunnel, a sample point was installed 762.0 mm (30") away from the tunnel inlet to ensure fully developed flow at the sampling point. CO_2 concentration measurements in the dilution tunnel were used to compute dilution ratio by comparing the raw and dilute CO_2 measurements. Furthermore, the new sampling system enabled the verification of both the dilution ratio and EGR fraction, based on CO_2 measurements, with NOx measurements in these locations as well.

5.7.3 Sulfur Dioxide Measurements

An Antek Model 6000SE SO_2 analyzer was installed following the first round of testing. The Model 6000SE utilized two pyro furnaces each at 1000°C to convert any sulfur on the particulates and in the exhaust stream to SO_2 for measurement via UV fluorescence. As any NO present in the sample stream can adversely influence the SO_2 measurements, (100 PPM NO is detected as 1 PPM SO_2) the Antek is also equipped with an ozone generator to convert the NO to NO_2, which then no longer interferes with the analyzer. For a detailed description of the SO_2 analyzer and its principle of operation, the reader is referred to [26].

The Antek is capable of detecting SO_2 levels in the exhaust down to 250 ppb_v. Depending upon the fuel sulfur concentration, the Antek was calibrated using SO_2 span gas concentrations of 1.96 PPM, 5.23 PPM, and 32.29 PPM. Furthermore, breathing quality compressed air was used as the zero gas for the Antek. SO_2 emissions were sampled from the same locations as the other analyzers as described in Section 5.7.2,

using heated sample lines to maintain as closely as possible the raw exhaust gas composition. An additional sample point for raw exhaust emissions was added downstream of the original raw exhaust sample point to accommodate the Antek's longer heated sample line. Although SO_2 emissions were primarily sampled from this second raw exhaust sample point, other sample points were occasionally used to verify correct analyzer operation and to double-check readings. A detailed schematic of the test bed with the SO_2 analyzer and second raw exhaust sample point is depicted in Figure 5.3.

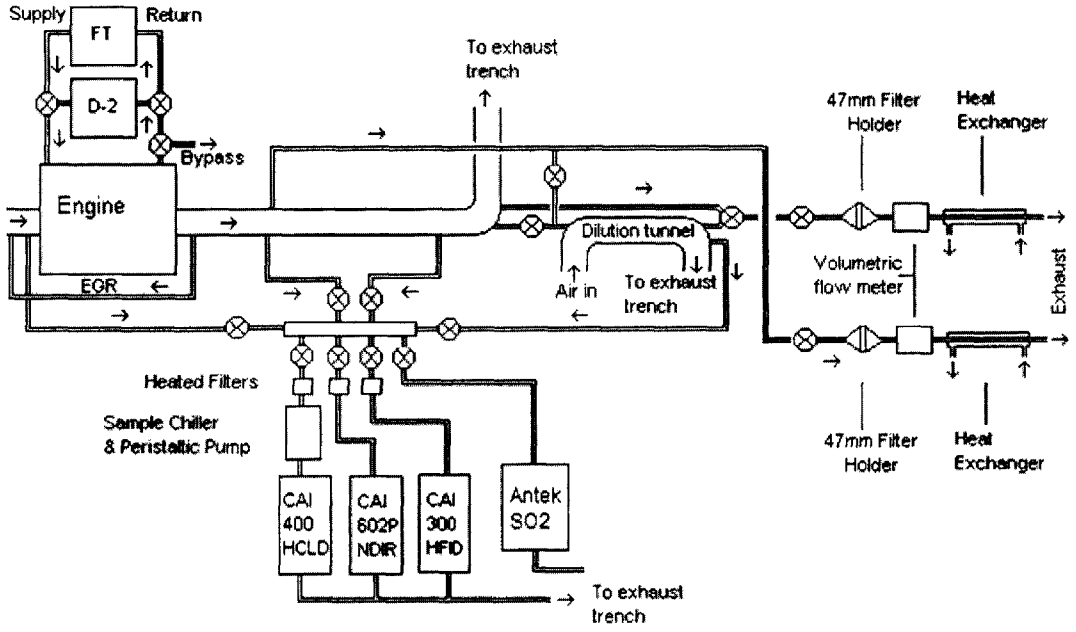

Figure 5.3. Modified test bed showing addition of SO_2 analyzer, second raw exhaust emissions sampling point, and modified PM sampling system

The modifications to the particulate sampling system shown in Figure 5.3 are presented in detail in Section 5.9.

5.8 Mini-Dilution Tunnel

Particulate Matter is defined by the EPA as all solid matter and condensable species that can be collected on a paper filter from a diluted exhaust sample held at no higher than 52°C [25]. In order to conform with the EPA mandated particulate sampling procedure and cool the exhaust to 52°C, some form of a dilution tunnel must be employed. Dilution

tunnels introduce a given portion of ambient air into some or all of the exhaust stream. The mixing of ambient air with the hot diesel exhaust serves two purposes. First, it helps to cool the gasses to below 52°C, and, second, it simulates particle transformations (i.e. agglomeration, adsorption, and nucleation) that occur naturally on the road after the PM leaves the tailpipe.

The size of the dilution tunnel used in this study was limited by the available space in the test cell, and as a result, a mini-dilution tunnel was used that only dilutes a fraction of the exhaust stream. The tunnel is composed of 7.54 cm (3") O.D. stainless steel tubing, and is connected to the engine's exhaust system via a 1.88 cm (¾") O.D. stainless steel tube. A high-temperature ball valve and a Spencer Model 1001-½SS blower control exhaust flow to the tunnel. The blower maintains the pressure inside the tunnel below atmospheric, and ambient air is drawn into the tunnel through a HEPA filter element mounted near the raw exhaust inlet on the dilution tunnel system. The tunnel is 0.762 m (30") long from the raw exhaust inlet to the tunnel outlet to ensure fully developed flow and complete mixing of the raw exhaust and ambient air.

As mentioned in Section 5.7.2, the dilution ratio was measured by comparing the CO_2 readings in the tunnel to the CO_2 readings in the raw exhaust. Additional checks of the dilution ratio were also made by monitoring both raw and dilute NO/NOx readings.

5.9 Gravimetric Particulate Matter Sampling System

The gravimetric particulate matter sampling system was set up to accommodate both raw and dilute particulate samples. Dilute samples were drawn directly from the dilution tunnel, whereas raw samples were routed from a location on the exhaust system before the dilution tunnel via heated stainless steel sample lines to the particulate sampling system. Heated sample lines were used when sampling raw exhaust to prevent water from condensing out of the exhaust stream and onto the filter and tube walls.

Pall Corporation stainless steel 47mm filter holders were used to hold Pallflex® Fiberfilm Model T60A20 glass fiber filters, on which the particulate samples were collected. The Pallflex® Model T60A20 filters are recommended by the EPA for use in gravimetric filter measurements [50]. Additionally, the Model T60A20 filters can also withstand the elevated temperatures encountered during raw exhaust sampling, as they are rated for temperatures up to 315.5°C.

Exhaust gas was drawn through the particulate sampling system by a Gast Model 0823 rotary vane vacuum pump, and the sample flow through the paper filter was measured via an Omega FVL-1611 volumetric flow meter installed downstream of the filter holder assembly. The Omega FVL-1611 is capable of measuring flow rates up to 250 SLPM. The output from the flow meter was fed directly into the data acquisition system, and the flow rates were monitored and recorded continuously for the entire duration of the particulate collection.

In order to verify compliance with EPA dilute particulate sampling procedures, thermocouples were installed at locations slightly in front of the 47mm filter holders. The temperature readings were also fed into the National Instruments data acquisition system.

Shortly after the initial round of testing, the Gast rotary vane vacuum pump failed due to excessive water accumulation within the pump and the elevated temperatures to which the pump had been subjected during raw particulate sampling. Following the failure of the pump, the entire particulate sampling system was rebuilt. In addition to installing a larger and more robust rotary vane vacuum pump, Gast Model 1423, a number of protective measures were taken to prevent future pump failure as well.

The installation of the larger Model 1423 vacuum pump enabled a maximum flow rate of 13.2 CFM at 25 in Hg vacuum. The significantly higher flow rate of the pump allowed for the installation of a second particulate collection system in parallel with the original system, which reduced overall PM collection times by 50%. Secondary 10-micron Gast

canister filters were also installed directly after the filter holder assemblies as an additional protective measure to ensure that no particulates would enter the new vacuum pump. Custom counter-flow heat exchangers were also designed and fabricated at the Sloan Automotive Laboratory and installed immediately after the canister filers. The heat exchangers were capable of cooling the sample gasses to between 20°C to 30°C, well below the pump's maximum allowable inlet temperature specified by the manufacturer. Following the heat exchangers and immediately before the pump, two SMC Model AMJ4000-N04B water separators were installed as well. The water separators are designed to remove any remaining moisture in the gas stream that did not condense in the heat exchangers. A schematic of the rebuilt particulate sampling system is shown in Figure 5.4.

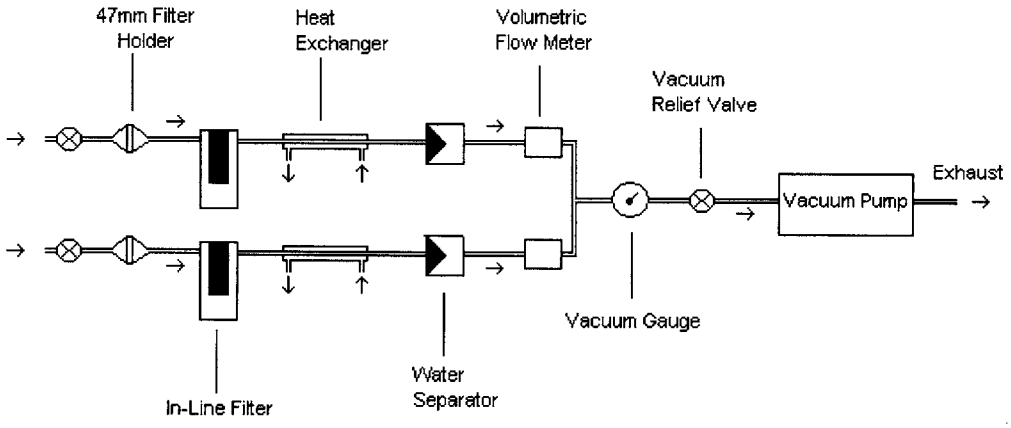

Figure 5.4. Dual branch particulate sampling system with sample conditioning systems in place

(This page intentionally left blank)

6.0 Experimental Test Matrix and Procedure

The experimental work covered in this thesis can be subdivided into three major rounds of testing. The first round focused specifically on the emissions characteristics of the four fuels and a select number of engine operating conditions. The second round of testing covered a significantly larger number of engine operating conditions but focused more on in-cylinder pressure measurements and combustion characteristics of the fuels. Finally, the last round of testing focused solely on the low sulfur diesel and FT fuel, and consisted of a more in-depth gaseous and emissions characterization of these two fuels.

6.1 Engine Operation

In the present study, the stock 300 horsepower calibration provided by Cummins was uploaded into the ECM and no additional modifications to any control parameters were made. In some cases it was, however, necessary to override the stock control settings during engine warm-up, as the engine would shift from the stock control algorithm to a condensation protection algorithm. The engine control system on the ISB 300 monitors intake manifold temperature, intake manifold pressure, airflow, EGR flow, and a number of other parameters to infer if water may be condensing in the intake manifold or EGR system. When the engine is first started and the intake manifold temperature is excessively cold as the charge air cooler is still warming up, oftentimes the engine control algorithm would switch to the condensation protection mode. As a result, the EGR valve closed completely to prevent excessive corrosion of the aluminum components, and the engine switched to a completely different set of operating tables. However, since the engine was operated in a controlled laboratory environment, this was in actuality often not the case. To expedite engine warm-up, the condensation protection algorithm was oftentimes manually overridden to return the engine to the stock control settings. Furthermore, the gate valve controlling the flow of cooling water to the intercooler was also closed, which further helped to expedite engine warm-up. The testing was carried out using the stock calibration to provide the worst-case scenario for a modern engine that switches to FT fuel without properly calibrating the ECM to account for the change in fuel properties.

6.1.1 Experimental Test Matrix

The test matrix of engine operating conditions for this study was based on a subset of the Euro-III 13-Mode Stationary Test Cycle. The European Stationary Cycle (ESC) consists of 13 operating conditions representative of actual on-road driving conditions and is used by Cummins as well. A subset of the Euro-III test modes used in the initial round of emissions testing is listed in Table 6.1. The engine speeds for each test mode A, B, and C are defined as follows:

Equation 6.1 $$A = RPM_{low} + 0.25*(RPM_{high} - RPM_{low})$$

Equation 6.2 $$B = RPM_{low} + 0.50*(RPM_{high} - RPM_{low})$$

Equation 6.3 $$C = RPM_{low} + 0.75*(RPM_{high} - RPM_{low})$$

where RPM_{high}, is defined by calculating the highest engine speed above the rated speed where 70% of the maximum net power occurs, and RPM_{low}, is defined by calculating the lowest engine speed below the rated speed where 50% of the maximum net power occurs. Based on the engine's torque and power curves provided by Cummins and presented in Appendix B, Eq. (6.1) through Eq. (6.3) yield the following values for the three test mode speeds: A = 1682 rpm, B = 2013 rpm, and C = 2345 rpm [35]. Table 6.1 below shows the initial test matrix, which formed the basis for the emissions tests.

Mode	Speed [RPM]	Load [N-m]	BMEP [kPa]
A25	1682	224	477
A50	1682	470	1001
B50	2013	447	952
*A50 is actually 53% load			

Table 6.1. Initial test matrix

The test matrix shown above represents the three steady-state speed and load points that were used to evaluate the fuel effects on engine-out emissions. The number following the letters for the speed modes in Table 6.1 indicates the percent of maximum engine load

at which the engine was operated for a given speed. The A50 test point at 53% load was retained from the previous work of Llaniguez and Acar to allow for direct comparison of the results. The initial test matrix was chosen for the following two reasons: to verify the initial results observed in the last reporting period for the fuel blends, and to reduce dilute particulate collection times, as the test points represent operating conditions producing a relatively large amount of particulate emissions.

6.1.2 Expanded Test Matrix

Following the initial round of testing, the test matrix was expanded to 10 steady-state speed-load points for each fuel to represent a larger portion of the engine's operating range. Similar to the initial test matrix, the expanded test matrix is comprised of a subset of the Euro III 13-mode test cycle. The specific operating conditions are listed in Table 6.2.

Mode	Speed [RPM]	Load [N-m]	BMEP [kPa]
Z25	1200	180	383
A25	1682	224	477
A50	1682	470	1001
A75	1682	671	1429
B25	2013	223	475
B50	2013	447	952
B75	2013	669	1425
C25	2345	217	462
C50	2345	433	922
C75	2345	650	1384
*A50 is actually 53% load			

Table 6.2. Expanded test matrix used to evaluate combustion characteristics

Due to the lengthy sampling times necessary to collect a significant amount of dilute particulates for gravimetric analysis, combined with the fact that diesel particulate emissions are fairly well documented in the literature [12, 41, 51] and the previous work on this engine [35, 36], exhaust emissions measurements were not continued with the expanded test matrix. The focus of the study, thus, shifted to a detailed combustion analysis.

This test matrix was designed to complement the data previously collected in several ways. As can be seen in Tables 6.1 and 6.2, there is significant overlap in the A25, A50, and B50 conditions. The purpose of this overlap is two-fold: to provide an opportunity to correlate results of the combustion analysis with previous emissions data, and to allow for a direct comparison of the 400 PPM and 15 PPM sulfur fuel to the FT fuel. The expanded test matrix extends the scope of the work to cover a full range of engine operating conditions, and it encompasses relatively high speed and load test conditions not covered in previous work.

Data sets recorded in the experiments and presented here adhere to a prescribed naming convention that indicates the fuel used and the engine operating parameters. A two to four letter prefix indicates the type of fuel for the data set. FT, BL, LSD, and ULSD represent Fischer-Tropsch, FT/400 PPM blend, low sulfur diesel (400 PPM), and ultra-low sulfur diesel (15 PPM) respectively. Following the fuel specification, the general operating condition is indicated by the letter corresponding to the speed and two digits representing the percent load for that speed, as outlined in Table 6.2. Unlike the previous studies, all other engine control parameters such as EGR rate and injection timing were maintained at their respective stock settings and no changes to the stock engine calibration were made.

6.2 Particulate Matter Sampling Conditions

Unlike previous work [35, 36], all of the particulate data used to characterize the emissions trends were sampled from the exhaust stream after first passing through the mini-dilution tunnel. Although the sampling times required to collect a comparable amount of dilute particulates are approximately 6 times longer when compared with the raw sampling method, only dilute particulates were sampled during the first round of testing in order to reduce the error and uncertainty inherent to the raw sampling method.

Before each test, the Pallflex filter papers were placed in individual plastic Petri dishes and conditioned for at least 56 hours in accordance with protocol recommended by the

EPA [50]. Filters that were later sent to the emission/chemistry laboratory of a major engine manufacturer for analysis were placed in glass dishes rather than the plastic Petri dishes, since, according to Cummins, certain chemicals in the plastic dishes can leach out onto the filter paper and affect the results.

All filter preparation and conditioning were carried out in a climate-controlled environment where the temperature was between the EPA mandated range of 68° – 86°C and relative humidity of 30% – 70%. Despite the carefully controlled conditions, it was found that daily variation in temperature and humidity, especially when comparing samples collected in the summer and winter months, had a significant effect on filter mass. To correct for variations in environmental conditions, a set of four control filters in plastic Petri dishes were kept in the sample preparation room at all times and used to compute a correction factor based on the weight variation of the control filters in the period between clean and loaded filter weighing.

6.2.1 Dilute Exhaust Sampling

All dilute particulate sampling was carried out with dilution ratios between 9 and 12, and the dilution ratio was computed by measuring the CO_2 concentration in both the raw and dilute exhaust stream. Additional checks of the dilution ratio were made by measuring the dilute and raw NOx concentrations as well. The temperature of the exhaust before each sample filter was carefully monitored to ensure that the particulate samples were collected below 52°C. Typical PM collection temperatures ranged between 45°C and 52°C, and sample times were typically around 30 minutes to collect at least 2.0 mg of sample. Filters sitting idle in the climate-controlled sample preparation room could vary in weight by $\pm$ 0.5 mg. Despite corrective measures taken to reduce sample variability and the use of control filters to account for changes in filter weight due to environmental effects, the best way to minimize sampling error was to collect as much of a sample and as many samples at one test condition as possible.

As mentioned in the previous section, new filter papers were allowed to condition in individual Petri dishes in a climate-controlled room for at least 56 hours prior to use.

After the conditioning period, four particulate samples were taken consecutively for 30 minutes each in order to collect a statistically significant number of samples and calculate a meaningful average. After the filter papers were loaded, they were again allowed to condition for at least 56 hours in the climate-controlled room in order to dry the paper and settle the particulates.

6.2.2 Raw Exhaust Sampling

While all of the particulate emission trends and comparison of PM emission levels of the various fuels are based on dilute particulate samples, some raw particulate sampling was carried out in the last round of testing to gain a better understanding of the composition of the particulates as they existed in the undiluted exhaust stream. As a result, the extractable fraction was significantly reduced, since the hot, undiluted exhaust conditions between the turbo outlet and PM sampling port are not conducive to the condensation of various gaseous species and light hydrocarbons onto the PM.

Typical temperatures just in front of the sample collection filter ranged from 70°C to 90°C for the raw particulate samples. Furthermore, the sampling times necessary to collect a sufficient amount of raw PM for analysis was significantly reduced for the raw particulate samples, with a sampling time of approximately 10 minutes yielding up to 5.0 mg of raw PM collected on the filter for the LSD fuel. This reduction in sampling time is due to the fact that, in the case of dilute sampling, only a portion of the PM that enters the dilution tunnel is actually sampled, with the rest returned back to the exhaust trench. On the other hand, in the case of raw sampling, all of exhaust pulled through the sample port is routed directly to the filter. However, if this were not the case and equal amounts of raw and dilute particulates were sampled, the dilute sample weight would be significantly higher due to the effects of nucleation, condensation, and absorption in the dilution tunnel.

Generally, the dilute sampling method produced more consistent results and was the only sampling method that ensured the sample stream was cooled to below 52°C in accordance with the EPA particulate sampling guidelines. Despite this fact, the dilute

sampling method still leaves much room for improvement, specifically in the areas of filter conditioning, handling, and weighing.

6.2.3 Filter Processing

Following at least 56 hours of filter conditioning in the individual glass or plastic Petri dishes, the clean sample filters were weighed using a Mettler Toledo Model AG285 balance accurate to $\pm$ 0.01 mg. Each filter was weighed 3 times, along with the control filters, prior to use. Following sample collection, all particulate samples were returned to the sample conditioning room for storage prior to final weighing. After at least 56 hours in the sample conditioning room, the loaded filters were reweighed to determine the mass of PM collected. The control filters were also reweighed at this time and used to correct for any changes in the room's temperature and humidity.

6.3 Engine Operation during Experiments

Before beginning each round of testing, all of the gas analyzers and associated heated filters, lines, and sample conditioning systems were allowed to warm up for one hour. Following the initial analyzer warm-up phase, each analyzer was calibrated with the appropriate zero and span gasses covering the instrument's expected operating range. The analyzers were then flushed with zero gas and purge air for at least one more hour prior to taking any measurements. After all of the gas analyzers were calibrated, the clean sample filters for particulate collection were weighed and retrieved from the climate-controlled sample conditioning room.

Following the weighing of the clean sample filters, the engine was started and allowed to idle for five minutes as the National Instruments and CalTerm software programs were started. At this point, initial checks of key engine operating parameters were made using CalTerm to verify proper engine operation. Following the initial checks, the appropriate engine speed was set using the Digalog dynamometer controller. Load on the engine was then slowly increased until the predetermined load set point was reached using the Watlow controller. The engine was run at the specified test condition until normal operating oil and coolant temperatures were reached, and all engine subsystems had

settled into steady state operation. This time also allowed the filter holders and particulate sampling apparatus to reach operating temperature. As mentioned in Section 6.1, the condensation protection control algorithm was occasionally overridden to expedite the warm-up process; however, all engine control parameters were returned to their stock settings before any measurements were taken.

Once the engine reached its normal operating temperature at the specified test condition, a 60-second scan of all slow-speed engine data including fuel flow was initiated. This 60-second scan of the slow-speed engine data was only taken once for each operating condition. After the slow-speed scan, three 30-second scans of the gas analyzers were run. During these scans all gaseous emissions were sampled simultaneously from the raw exhaust, including HC, NO, NOx, CO, CO_2, and O_2. In the third round of testing, SO_2 emissions were sampled from the raw exhaust as well, as the Antek SO_2 analyzer became available. Following the gaseous emissions measurements in the raw exhaust, CO_2 measurements were taken from the intake manifold and dilution tunnel as well. During all of the emissions measurements, the engine's fuel was drawn from the fuel beaker instead of the tank, in order to obtain fuel consumption figures for each test condition.

Once the emissions scans were complete, the first particulate filter samples were collected. During the particulate sampling, flow data for the exhaust through the filters, as well as filter temperature data were recorded using the data acquisition system in addition to actual engine operating data. Between each of the four particulate samples, another round of emissions and fuel consumption data was recorded and the particulate sampling process was repeated. For each test condition, five sets of emissions and fuel consumption data were taken in between four dilute particulate samples.

After all of the emissions and particulate samples were taken at a particular test condition, the high-speed in-cylinder pressure measurements were initiated. The high-speed data consisted of a 10-cycle and a 100-cylce high-speed scans to record in-cylinder pressure data. Both the 10-cycle and the 100-cycle scans were taken at the end of all tests, which was approximately 2.5 hours after the first slow-speed scan. Following the

high-speed scans, the engine's operating conditions (speed and load) were adjusted to the next test condition, and the entire test procedure outlined above was repeated.

This same procedure was also used during the third round of testing when raw particulate samples were collected. The only notable change in the test procedure was the addition of the second particulate sample filter allowing for the simultaneous collection of two raw PM samples. Furthermore, SO_2 data was recorded along with all other gaseous emissions. Aside from the raw PM sampling and the inclusion of the SO_2 measurements, no other changes to the basic test procedure were made.

It should also be noted that the particulate and emissions measurements were not continued for the expanded test matrix. During these tests only the 60-second scan of all slow-speed engine data, including fuel flow, was taken. Following the slow-speed data, the 10-cyle and 100-cycle high-speed in-cylinder pressure measurements were taken. This process (alternating slow- and high-speed scans) was repeated four times for each test condition in order to collect enough data to calculate meaningful averages for each test condition.

Upon completion of data collection, the engine was slowly ramped down to idle and all heated exhaust sample lines were disconnected from the exhaust system and turned off. The engine was then allowed to idle for 5 to 10 minutes before being shut down using CalTerm. All gas analyzers were purged with ambient air and allowed to cool down for at least one hour prior to shut down. Lastly, all particulate samples were returned to the sample conditioning room to allow the samples to settle.

6.3.1 Fuel Change Procedure

Fuel changes were initiated following the completion of a full round of testing for each fuel under investigation. Testing began with the FT fuel (zero sulfur content), and subsequent fuel tests were carried out in the order of increasing fuel sulfur content. The fuels were tested in this order for the purpose of reducing the potential for residual sulfur

in the fuel system leftover from a high sulfur fuel to contaminate the ultra-low sulfur and FT fuels.

In order to minimize cross-contamination of the FT and standard No. 2 diesel fuels, the engine is equipped with two separate ATL fuel cells. Despite this setup, a number of additional precautions were taken when switching from one fuel to another. First, the supply and return valves on the bulkhead controlling fuel routing were switched to the desired fuel source. In addition, the bypass valve was opened and the engine's electronic fuel lift pump was run to purge any remaining fuel from the supply-side of the system. At this point, the engine's fuel filter was removed and replaced to prevent any cross-contamination of fuel sulfur. In order to purge any remaining fuel from the return side of the system, the lift pump was again run with the return line disconnected from its respective tank, and all fuel was routed to a waste fuel container. As a further precaution, the return line was left connected to the waste fuel container for the first few minutes of engine operation with the new fuel to fully eliminate the possibility of any cross-contamination.

6.3.2 Oil Change Procedure

All engine tests for the current reporting period were carried out using a standard 15W-40 heavy-duty diesel oil as recommended by Cummins. Routine oil and filter changes were carried out at the manufacturer's prescribed maintenance intervals. Furthermore, new and used oil samples were collected and sent to the emission/chemistry laboratory of a major engine manufacturer for analysis.

6.4 Data Processing and Reduction

All gaseous and particulate emissions values reported in this study were normalized in units of power and time (g/hp-hr) to allow for direct comparison of the various fuels over a wide range of engine operating conditions. Furthermore, as not all gaseous emissions were measured on the same basis (wet or dry), the conversion on the emissions values to the same basis required a significant amount of data processing.

6.4.1 Gaseous Emissions Data Processing

Since the HC, NO, and NOx emissions were measured wet and the CO, CO_2, and O_2 emissions were measured dry, with any water in the exhaust removed via the sample chiller, the CO, CO_2, and O_2 concentrations were all converted to a wet basis. This also enabled direct comparison with the Cummins ESC data, which was reported on a wet basis as well. In order to convert all of the emissions values measured on a dry basis to a wet basis, the water content in the intake and exhaust had to be estimated.

The conversion of the emissions values measured on a dry basis to a wet basis is as follows. If the average molecular formula of the fuel is defined as $(CH_y)_\alpha$, where y is the molar H/C ratio of the fuel, then the molecular weight, M_f, of the fuel is given by [1]:

Equation 6.4
$$M_f = \alpha(12 + y)$$

where α is the coefficient used to multiply the average molecular weight of the simplified chemical composition to equal M_f. Since the Cummins ISB employs a cooled EGR system to reduce NOx emissions, a fraction of the exhaust gasses is routed back into the intake manifold where it is mixed with the fresh intake charge. The moles of the major species in the intake mixture with EGR can be estimated via the following equation written per mole of O_2 [1]:

Equation 6.5
$$(1-x_b)\left[\frac{4}{M_f}(1+2\varepsilon)\phi(CH_y)_\alpha + O_2 + \psi N_2\right] + x_b(n_{CO_2} + n_{H_2O} + n_{CO} + n_{H_2} + n_{N_2} + n_{O_2})$$

where x_b is the burned gas fraction, ε is defined as 4/(4+y), ϕ is the fuel/air equivalence ratio, n_i is the number of moles of species *i* per mole of O_2, and ψ is the molar N/O ratio (3.773 for air). The mole fractions of the individual species are obtained by dividing by the total number of moles of unburned mixture, n_u, [1].

Equation 6.6

$$n_u = (1 - x_b)\left[\frac{4(1+2\varepsilon)\phi}{M_f} + 1 + \psi\right] + x_b n_b$$

where n_b, the total number of moles of burned mixture, is given by the following equation for a lean mixture [1]:

Equation 6.7

$$n_b = (1-\varepsilon)\phi + 1 + \psi \ .$$

Since the engine is turbocharged, it is assumed that the residual gas fraction is negligible in the equations presented above. However, since the engine employs EGR, x_b, was initially set equal to the EGR fraction, which was computed from the measured CO_2 concentrations in the intake manifold and exhaust system [35].

Once the correct water content in the intake mixture (air, fuel, and burned gas fraction) was calculated, the water vapor mole fraction in the exhaust was found from the ideal combustion equations for each fuel. The equations presented above were then iterated with the newly determined EGR fraction until a steady-state value was reached. Based on the water vapor mole fraction in the exhaust, the dry-basis CO, CO_2, and O_2 values were converted to a wet basis as follows:

Equation 6.8

$$\tilde{x}_i = (1 - \tilde{x}_{H_2O})\tilde{x}_i^*$$

where $\tilde{x}_i$ is the wet mole fraction of species *i*, and $\tilde{x}_i^*$ is the dry mole fraction of species *i*, [1]. As an additional check of the accuracy of the calculations presented above, the measured air/fuel ratio based on the air and fuel flow measurements was compared against the air/fuel ratio computed using the exhaust emissions measurements and the two were found to be in good agreement.

6.4.2 Particulate Emissions Data Processing

Only a portion of the raw exhaust was diverted into the mini-dilution tunnel and collected via the particulate sampling system. Therefore, the mass of the particulates collected on the filter papers had to be converted to a total engine-out PM emissions rate. This was accomplished by using the measured sample flow data recorded from the Omega FVL-1611 volumetric flow meter and the dilution ratio computed from the CO_2 concentrations measured in the dilution tunnel and exhaust system.

The PM sample flow rate data was averaged over the entire sampling period, since the flow rate decreased with time as the filters were loaded. The sample flow rate across the filter was then used to compute the actual particulate emissions from the engine normalized in units of power and time (g/hp-hr) to allow for direct comparison over a range of operating conditions.

6.5 Heat Release Analysis

The major thermodynamic indicators used in this study to quantify the specific aspects of the combustion process were calculated via a simple single-zone heat release analysis. The analysis is based on the First Law of Thermodynamics and assumes a single zone of uniform products in a closed system between intake valve closing (IVC) and exhaust valve opening (EVO). The gas properties in the cylinder are calculated using the ideal gas relationships and the gas constant for air. Due to the nature of this simple single zone model, heat loss through crevice effects, and other non-uniformities within the cylinder the model can only produce approximate results. The following form of the First Law forms the basis of the model:

Equation 6.9

$$dU_{internal} = \delta Q_{chemical} - \delta Q_{HT} - \delta W$$

where $\delta Q_{chemical}$ is the calculated chemical energy of the fuel, δQ_{HT} is the energy lost through heat transfer, and δW is the work. In order to apply the First Law directly to in-cylinder pressure data, the differential forms of some of the terms were rewritten on a crank-angle basis, since the pressure and volume data were recorded referenced to a

signal from the crank-angle encoder [35]. The following form of the First Law was applied directly to the experimental data:

Equation 6.10
$$\frac{\delta Q_{chemical}}{d\theta} = \frac{1}{\gamma - 1} V \frac{dP}{d\theta} + \frac{\gamma}{\gamma - 1} P \frac{dV}{d\theta} + \frac{\delta Q_{HT}}{d\theta}$$

where V is the cylinder volume, P is the cylinder pressure, and γ is the ratio of specific heats (c_p/c_v). The heat transfer term in Eq. (6.10) was calculated from a Nusselt-Reynolds number correlation similar to that used to model steady turbulent pipe flow. Reference [52] provides further detailed information on the heat transfer model.

6.5.1 In-Cylinder Pressure Signal and Data Processing

The in-cylinder pressure signal from the crank angle encoder was first processed using a 10 kHz hardware filter in the National Instruments SCXI data acquisition module. The 10 kHz filter setting was selected to filter some noise, while at the same time preventing the possibility of introducing phase-shift errors in the pressure signals due to poor low-pass filter response [35].

In addition to the hardware filtering, a simple software filter was created in MatLab to further process the data prior to carrying out the heat release and combustion analysis. This code essentially employs a Discrete Fourier Transform to convert between the time and frequency domains and computes and filters the signal at and above the Nyquist frequency to eliminate the problem of alias frequencies. An example of the output from the in-cylinder pressure data filter program is shown in Figure 6.1 for 9 cycles at the A50 test condition (1682 rpm, 447 N-m). For the sake of clarity, only 9 cycles are shown in the graphs in Figure 6.1, however all cylinder pressure data presented in this report were averaged over 100 cycles to minimize the effects of cycle-to-cycle variation.

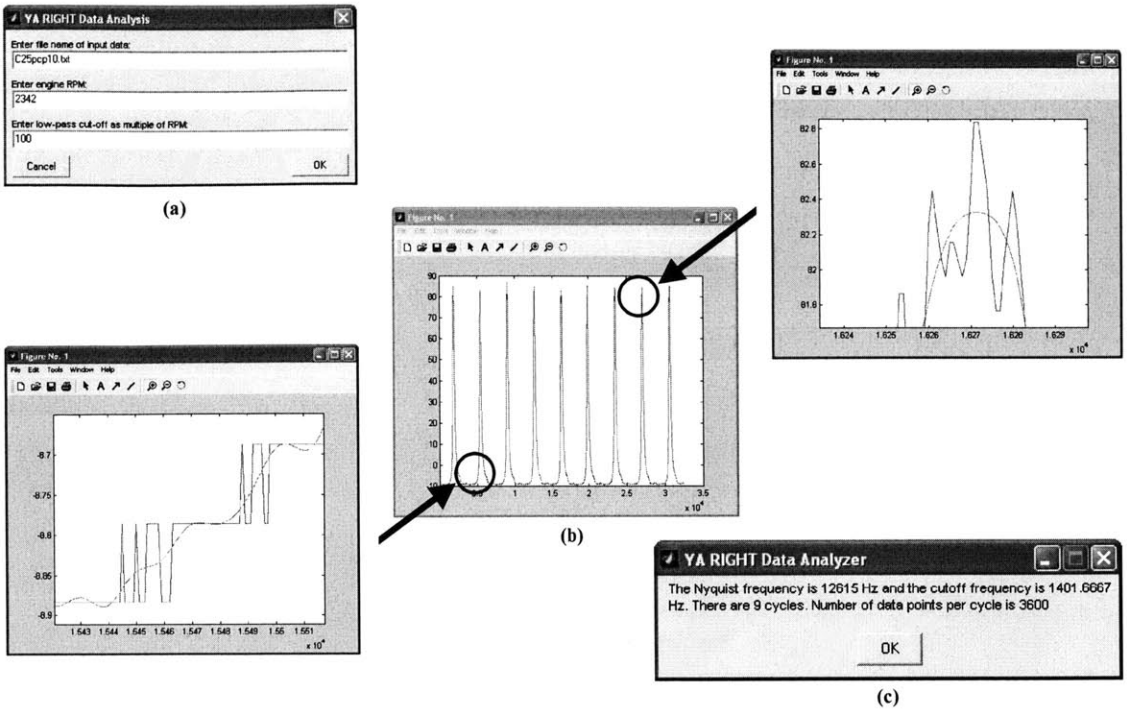

Figure 6.1. Example of MatLab cylinder pressure filter program with FT fuel at the A50 test condition showing (a) input file prompt and frequency cutoff specification, (b) raw and filtered pressure data, and (c) calculation of Nyquist and cutoff frequencies.

The filtered output from the MatLab code was then input into the FORTRAN heat release program to calculate the various thermodynamic indicators of interest. The heat release program employs the simple First Law model presented in Section 6.5 to calculate a number of thermodynamic indicators to characterize the combustion process. In addition to the pressure data filtered using the MatLab program described above, a second data file containing specific fuel properties and engine operating parameters was also input into the heat release program. The relevant portions of the FORTRAN and MatLab codes employed in the processing of the in-cylinder pressure data, as well as the relevant input parameters, are presented in Appendix D.

(This page intentionally left blank)

7.0 Experimental Results

This chapter presents the results of the combustion and emissions measurements, along with the detailed particulate analysis. The results provide considerable insight into the major factors influencing the observed emissions trends.

7.1 Emissions Characteristics

Due to the overall lean operation of diesel engines, in addition to the advanced subsystems and combustion strategy of the Cummins ISB, emissions of carbon monoxide are fairly low. The compression of only air during the compression stroke eliminates several major sources of unburned hydrocarbons, thus HC emissions from diesel engines are usually within acceptable levels. Therefore, the focus of the following discussion is primarily on the NO_x and PM emissions trends; however, some experimental data covering other emissions of interest are presented as well.

7.1.1 Particulate Emissions

The specific particulate emissions rates for the three initial test conditions under investigation are shown in Figure 7.1.

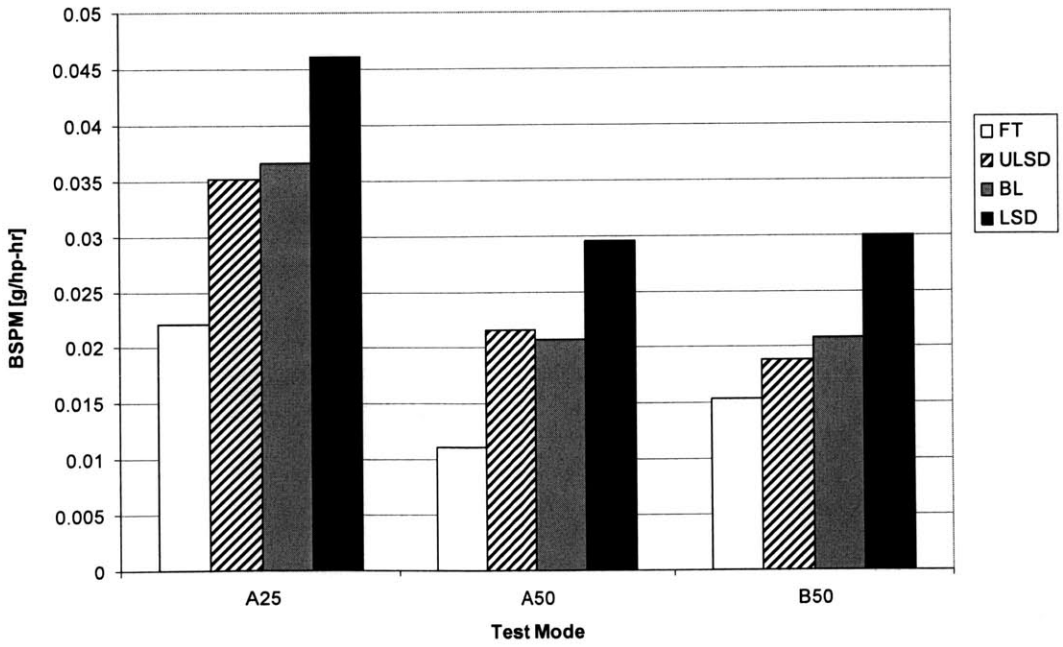

Figure 7.1. Specific particulate emissions

The amount of particulate matter that exits the engine is due to two competing processes: the extent of particulate formation and oxidation. Both the FT fuel and the blends reduced regulated emissions for each test condition. The fuel effects were most pronounced in regards to particulate emissions, where the FT fuel alone reduced particulate emissions by 54% on average as compared to the baseline fuel over all three test conditions. The blend performed nearly as well as the ultra-low sulfur diesel in reducing particulate emissions, with both fuels reducing particulates by an average of 28% compared to the baseline fuel. The fact that the blend produced approximately half the particulate reduction of using neat FT fuel alone suggests a more than proportional benefit of using the blend.

7.1.2 NOx Emissions

It is well understood that the principle factor driving NO_x formation is in-cylinder temperature during combustion. The extended Zeldovich mechanism is very sensitive to temperature, and NO_x control techniques typically attempt to lower peak cylinder temperatures. Based on this fact, it is not surprising that the fuel effect on NOx emissions is much less pronounced. The greatest reduction in NOx emissions was observed with the FT fuel, which reduced NOx by approximately 12% as compared to the low sulfur diesel. The blend and ultra-low sulfur diesel reduced NOx emissions only slightly, on the order of 2% and 4% respectively. The specific NOx emissions rates for the three initial test conditions are depicted in Figure 7.2.

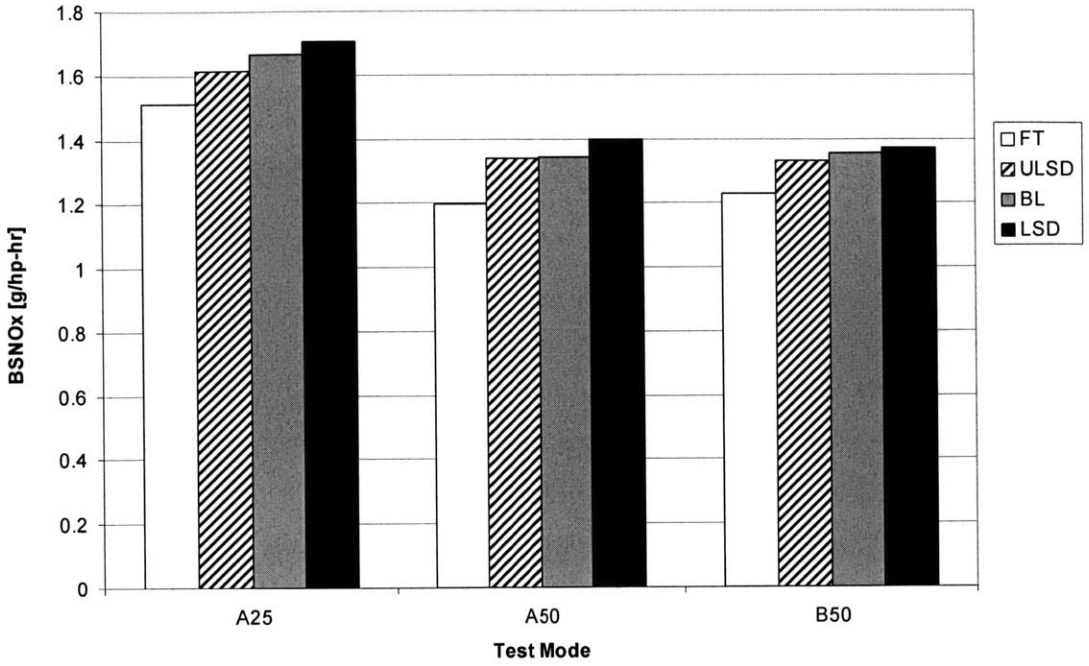

Figure 7.2. Specific NOx emissions

The average exhaust temperatures measured from thermocouples located just outside each exhaust port are plotted in Figure 7.3.

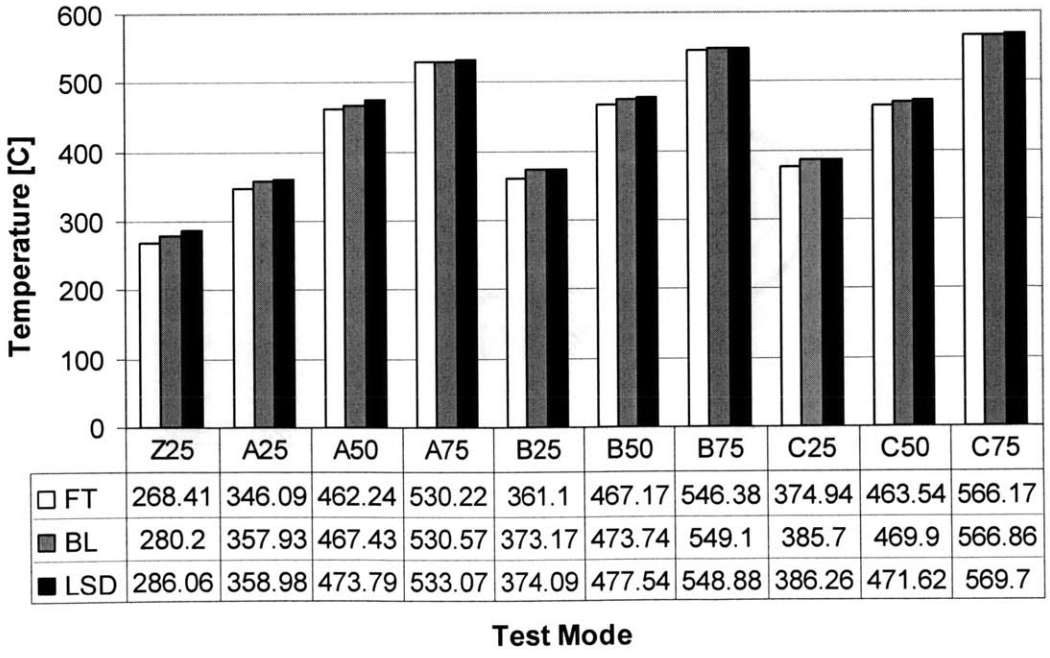

	Z25	A25	A50	A75	B25	B50	B75	C25	C50	C75
FT	268.41	346.09	462.24	530.22	361.1	467.17	546.38	374.94	463.54	566.17
BL	280.2	357.93	467.43	530.57	373.17	473.74	549.1	385.7	469.9	566.86
LSD	286.06	358.98	473.79	533.07	374.09	477.54	548.88	386.26	471.62	569.7

Figure 7.3. Average measured exhaust temperature

The FT fuel exhibited a slightly lower exhaust temperature for each test condition, with values ranging from a maximum temperature reduction of 17.6°C to a minimum reduction of 2.5°C. The blend exhibited only a slight decrease in exhaust temperature relative to that of the baseline fuel.

The effect of the FT fuel and blend on reducing the measured exhaust and corresponding cylinder temperatures is most likely the primary factor contributing to the reduction in NOx emissions. This observation confirms the temperature sensitivity of the extended Zeldovich mechanism as primarily responsible for the majority of the NOx formation in the power cylinder.

7.1.3 Hydrocarbon Emissions

As can be seen from Figure 7.4, the effect of the fuels on hydrocarbon emissions was varied.

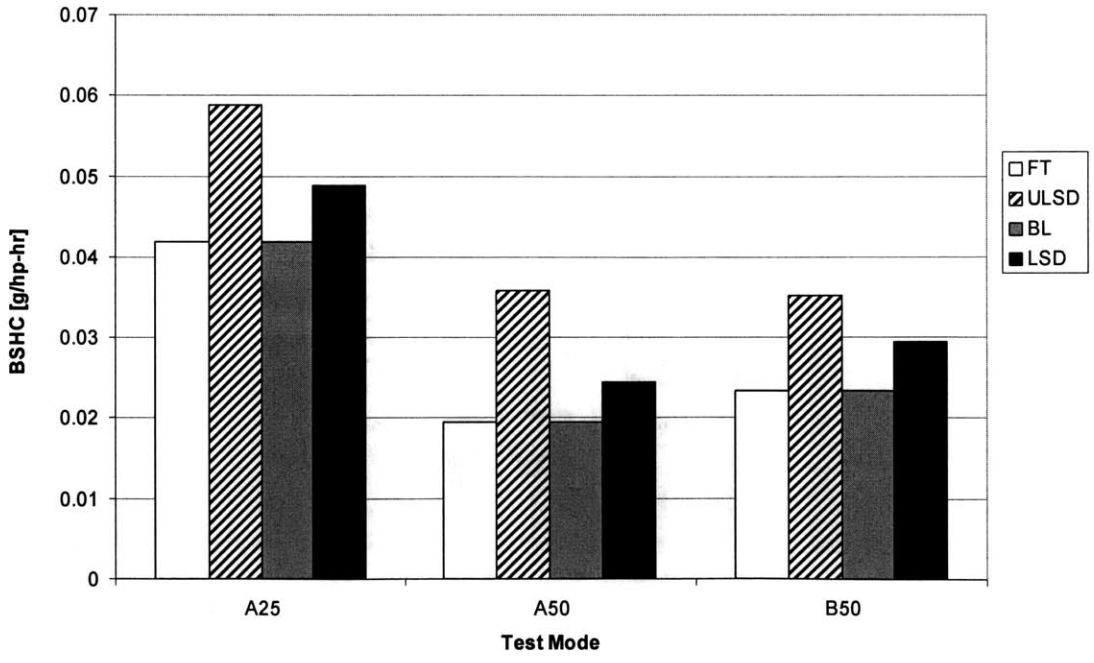

Figure 7.4. Specific hydrocarbon emissions

The FT and blend yielded approximately the same reduction in HC emissions, while the ULSD increased hydrocarbon emissions by nearly 15% on average when compared with the baseline low sulfur diesel. Hydrocarbon emissions are the product of a number of factors related to fuel properties, cylinder geometry, combustion characteristics, and a multitude of additional factors. It is, therefore, quite difficult to attribute the observed differences in HC emissions to any one specific factor. While a number of fuel property interactions may be responsible for the trend, the most likely cause is due to the higher volatility of the ULSD, as depicted by the distillation curves shown in Figure 4.2.

7.1.4 Detailed Emissions Summary

Following the initial round of testing, a more detailed emissions sweep was carried out over a much wider range of engine operating conditions. The engine operating conditions covered nearly all modes of the Euro-III 13-mode test cycle, with the exception of the 100% load points. In addition to the gaseous emissions measured in the previous round of testing (CO, CO_2, O_2, HC, NO, and NOx), measurements of the SO_2 concentration in the exhaust were carried out as well. However, unlike the previous round of testing, the complete emissions mapping was conducted only with the low sulfur diesel and Fischer-Tropsch diesel. The percent difference between the emissions levels for the FT and LSD are presented in Table 7.1 below.

	CO_2	H_2O	O_2	N_2	CO	HC	NO	NO_2	H_2	SO_2	NOx	PM
Test Condition	[%]	[%]	[%]	[%]	[%]	[%]	[%]	[%]	[%]	[%]	[%]	[%]
A25	-9.3	20.6	-9.5	-4.1	10.2	-31.9	-25.8	-25.0	46.5	-99.9	-25.8	-56.0
A50	-4.4	8.8	-1.9	0.0	22.5	-32.9	-20.4	-27.9	39.5	-100.1	-20.8	-40.6
A75	-3.0	9.3	-1.0	1.0	-37.0	-21.1	-22.3	56.4	-29.1	-98.1	-20.1	-24.3
B25	-3.2	9.6	-0.3	0.6	33.3	-45.7	-11.6	-6.0	51.0	-97.7	-10.9	-50.1
B50	-3.9	7.0	2.2	1.4	33.9	-47.9	-9.0	-4.3	49.2	-98.1	-8.6	-56.0
B75	-2.2	7.0	-0.6	0.8	-37.9	-31.6	-19.3	31.1	-32.1	-97.0	-16.8	-45.7
C25	-5.5	6.4	-0.7	-0.7	26.5	-49.2	-15.5	2.2	42.4	-95.1	-12.9	-53.8
C50	-5.5	4.4	2.1	0.3	51.7	-53.2	-10.4	40.3	67.4	-96.4	-6.6	-58.9
Z25	-13.0	1.9	-1.6	-3.4	6.8	-48.8	-8.8	5.6	25.1	-93.1	-8.0	0.0
Average	-5.56	8.33	-1.27	-0.46	12.21	-40.27	-15.90	8.05	28.88	-97.28	-14.51	-48.16

Table 7.1. Difference in measured and calculated exhaust constituents for the Fischer-Tropsch and low sulfur diesel fuel

Negative values in the table indicate a decrease in emissions with the FT fuel, whereas positive values indicate an increase. The NO_2 emissions values used in the calculations presented in the table were determined from the difference in the measured NOx and NO emissions values. Furthermore, the water content in the exhaust was estimated using the procedure outlined in Section 6.4.1, and concentrations of all other gaseous species that were not measured in the exhaust directly (N_2 and H_2) were calculated from the actual combustion equation for the appropriate fuel.

Consistent with the emissions trends observed during the initial round of testing, the data shows an average reduction in PM emissions with the FT fuel of nearly 50% as compared to the baseline low-sulfur diesel. Emissions of sulfur dioxide for the FT fuel were on average 97% lower than with the LSD. The large reduction in SO_2 emissions is due to the fact that FT diesel contains zero sulfur, whereas the LSD contains 400 PPM sulfur. The low levels of SO_2 emissions that were measured for the FT fuel are attributed to the sulfur contained in the lubricant oil. NOx and HC emission agree well with those reported for the initial round of testing, with reductions in NOx and HC by 15% and 40% on average. Furthermore, emissions of CO_2 decreased with the FT fuel by approximately 5% on average. Although an average increase in CO levels of 12% was observed with the FT, the CO levels measured with both fuels were extremely low, near the lower detection limit of the analyzer, and the increase in CO levels with the FT warrants further investigation.

7.2 Particulate Analysis

In order to determine more precisely the effect of various fuels on particulate composition, all particulate samples were sent to the emission/chemistry laboratory of a major engine manufacturer for detailed analysis. Prior to analysis, all samples were conditioned and reweighed in a strictly controlled environment at the engine manufacturer's emission/chemistry laboratory to confirm the particulate mass values determined at MIT. Following the conditioning and weighing, the samples were analyzed to determine the contribution of sulfates (SO_4), nitrates (NO_3), and soluble organic fraction (SOF) to the total particulate mass (TPM). As nitrates are not of primary

interest, and since the nitrate levels were extremely low, their contribution to the TPM is neglected in the following sections. Once total SOF and SO_4 were known, and neglecting the contribution of the nitrates, the SOL (non-soluble fraction or soot) was calculated from the total particulate mass as follows:

Equation 7.1 $$TPM = SOL + SOF + SO_4$$

The SOL is important as it consists of the basic solid carbonaceous particles formed during combustion [13]. The following sections present the results of the detailed PM analysis.

7.2.1 PM Constituent Distribution

An overview of the results of the particulate analysis for each of the three test conditions is presented in Figures 7.5 through 7.7.

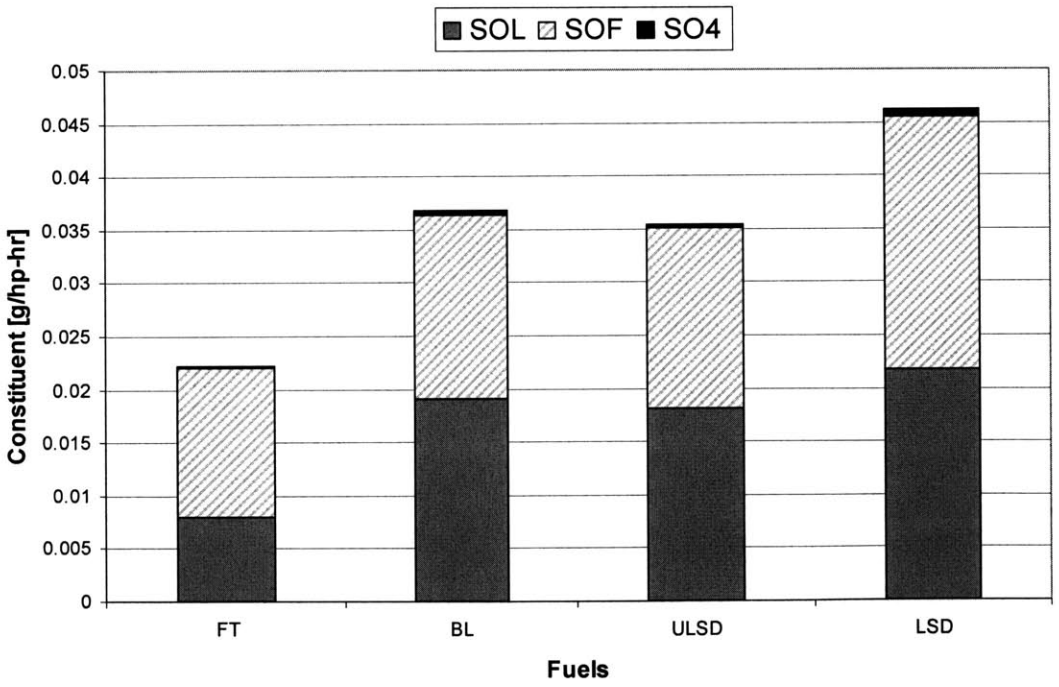

Figure 7.5. Distribution of particulate constituents collected at an engine operating condition of 1682 rpm, 474 kPa BMEP

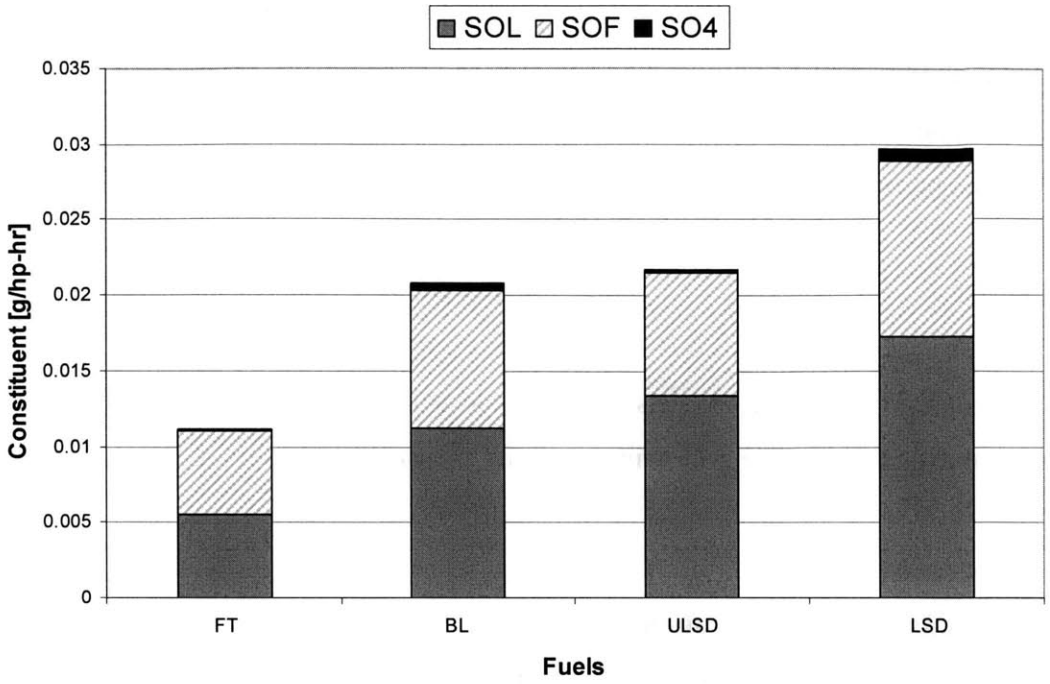

Figure 7.6. Distribution of particulate constituents collected at an engine operating condition of 1682 rpm, 1000 kPa BMEP

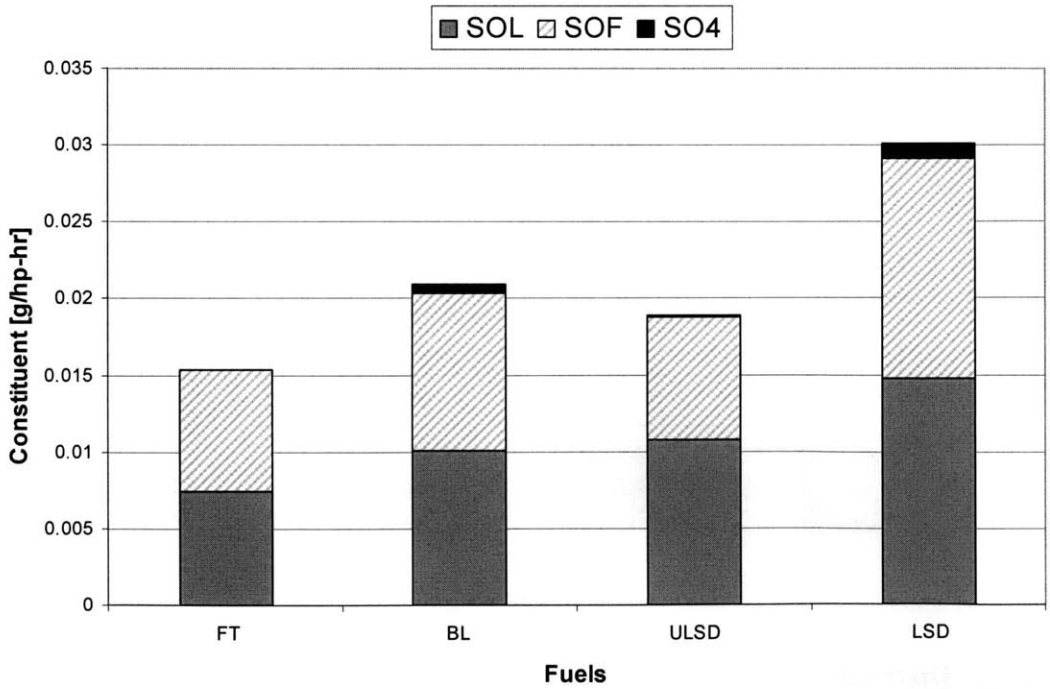

Figure 7.7. Distribution of particulate constituents collected at an engine operating condition of 2011 rpm, 947 kPa BMEP

Of particular interest is the apparently small contribution of sulfate to the total particulate mass, which ranged from a minimum of 0.64% to a maximum of 3.05% of the TPM. A simple calculation of the fuel sulfur to sulfate conversion rate, based on the known fuel sulfur content and fuel consumption rate, yielded a range from a low of 0.22% for the FT/LSD blend to a high of 1.94% for the ULSD. Furthermore, the sulfur to sulfate conversion rates of the blend and low sulfur diesel comprised the low end of the range (0.22% to 0.43%) while the ultra-low sulfur diesel made up the high end (0.52% to 1.94%). These values are suspect as previous studies have shown that the amount of fuel sulfur converted to PM is at least 1-2% of the fuel sulfur content irrespective of the total fuel sulfur level or engine type [39]. Despite this discrepancy, the relative trends observed in the data still hold considerable merit.

The fuel sulfur to sulfate conversion rates were observed to vary directly with load, however the trends differed for each of the fuels tested. The fuel sulfur to sulfate conversion rates for both the blend and low sulfur diesel tended to increase with increasing load, while the conversion rates for the ultra-low sulfur diesel exhibited the opposite behavior.

In general, the contribution of the SOF to the total particulate mass decreased with increasing load, while SOL and SO_4 increased. This trend is consistent with other published reports in the literature [53].

7.2.2 Non-Soluble Fraction and Soot

The SOL contribution to the total particulate mass ranged from 43.7% for the FT fuel to 54.4% for the ULSD. On average, over all of the test conditions, the FT fuel reduced SOL by 60.6%, the ULSD reduced SOL by 22.1%, and the blend reduced SOL by 26.16% as compared to the baseline low-sulfur diesel. A comparison of the solid fraction for each of the fuels over all of the test conditions is shown in Figure 7.8.

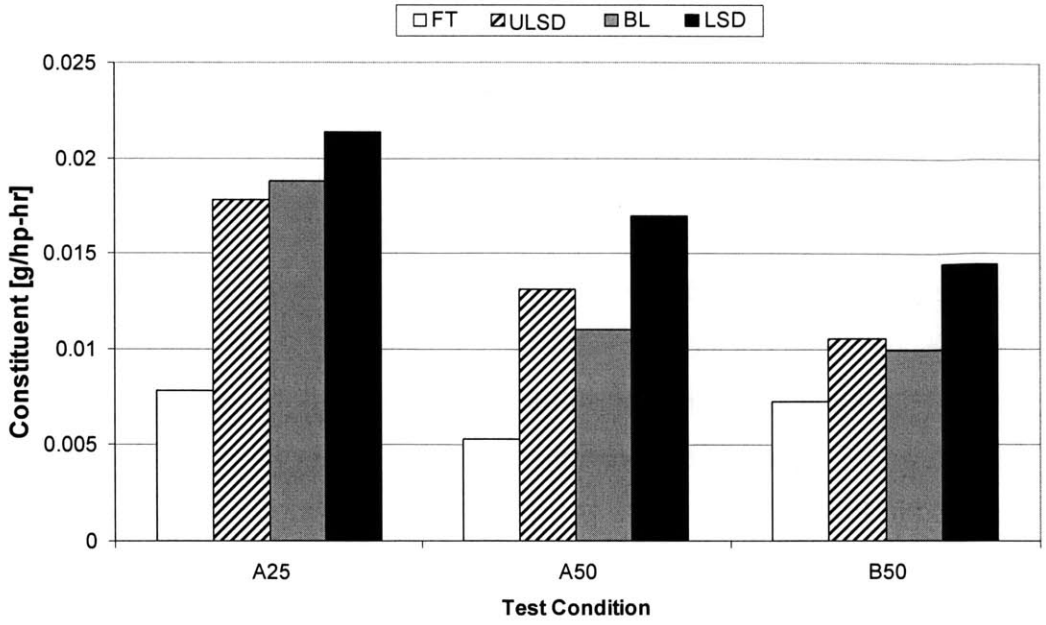

Figure 7.8. Comparison of solid non-soluble fraction

Estimates based on the simplified chemical composition of the fuels, molecular weight, and carbon content provided by the manufacturers gives a lower carbon content of 9.8% by weight for the FT fuel as compared to the LSD. As demonstrated in the figure above, the blend yielded a more than proportional reduction in SOL by approximately 43.0% as compared to the reduction obtained with the FT fuel alone.

7.2.3 Soluble Organic Fraction

The soluble organic fraction was determined via supercritical fluid extraction using CO_2 as the working fluid. This method is believed to produce more consistent results than those achieved by performing the soxhlet extraction using dichloromethane. The trends observed in the SOF are very similar to those presented in the previous section for the SOL. The SOF contribution to the total particulate mass ranged from 41.8% for the ULSD to 55.7% for the FT fuel. While the FT fuel yielded proportionally the greatest contribution of SOF to the TPM, it still produced an average reduction in SOF of 46.0% as compared to the baseline LSD. The blend and ULSD both yielded average reductions in SOF of 26.2% and 34.2% respectively, over the baseline fuel.

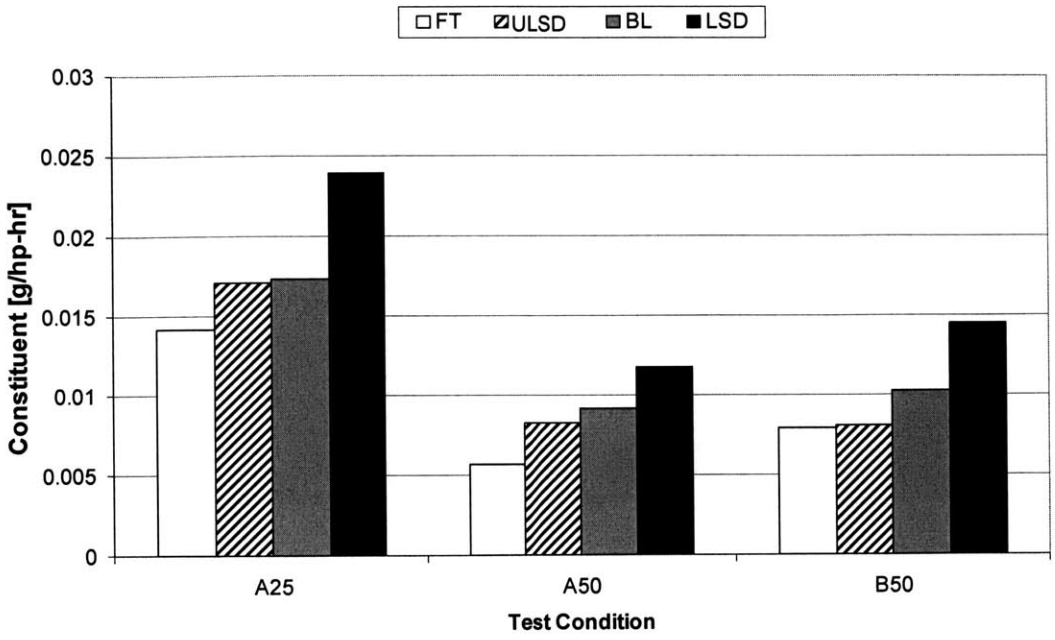

Figure 7.9. Comparison of soluble organic fraction

As shown in Figure 7.9, the blend yielded a more than proportional reduction in SOF, by approximately 56.9%, when compared with the reduction obtained using the FT fuel alone.

7.2.4 Sulfates

The sulfate contribution to the TPM was determined via ion chromatography. As discussed in Section 7.2.1, the low absolute magnitudes of the SO_4 values (between 0.22% and 3.05% of the TPM) are suspect, as they do not correlate well to the accepted fuel sulfur to sulfate conversion rates presented in the literature. Nonetheless, the relative trends are still quite valid. As was expected, the FT fuel and ULSD contributed least to the SO_4, as these fuels contained little to no sulfur. The blend and LSD, on the other hand, contained considerably more sulfur, 305.9 PPM and 400 PPM sulfur by weight respectively. Figure 7.10 presents the particulate sulfate levels generated by each of the fuels.

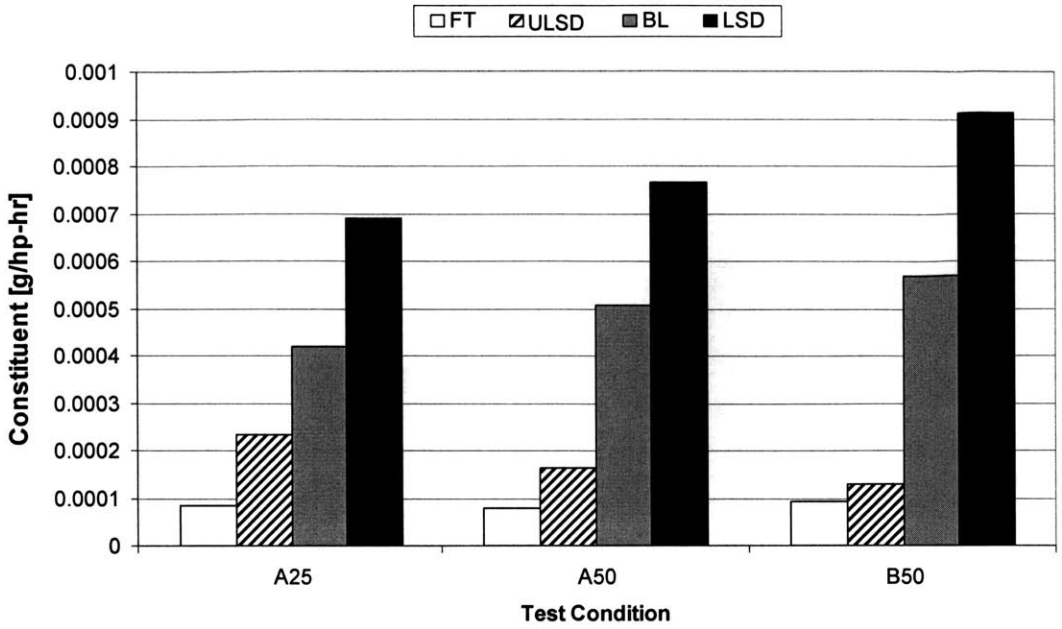

Figure 7.10. Comparison of sulfate contribution to TPM

On average, the FT fuel reduced SO_4 by 89.1%, the ULSD reduced SO_4 by 76.9%, and the blend reduced SO_4 by 37.0% as compared to the baseline low-sulfur diesel. As demonstrated in Figure 7.10, the blend yielded a more than proportional reduction in SO_4 by approximately 41.5% as compared to the reduction obtained with the FT fuel alone. Despite these significant reductions in SO_4, the impact to the overall particulate mass was nearly negligible due to the small contribution of the SO_4 to the TPM.

The contribution of sulfur in the engine lube oil to the total particulate sulfate is depicted in Figures 7.11 through 7.13 for each of the three test conditions. The zero sulfur nature of the FT fuel allowed for the simple and straightforward determination of the lube oil contribution, as any SO_4 in the PM must be attributed to the lube oil.

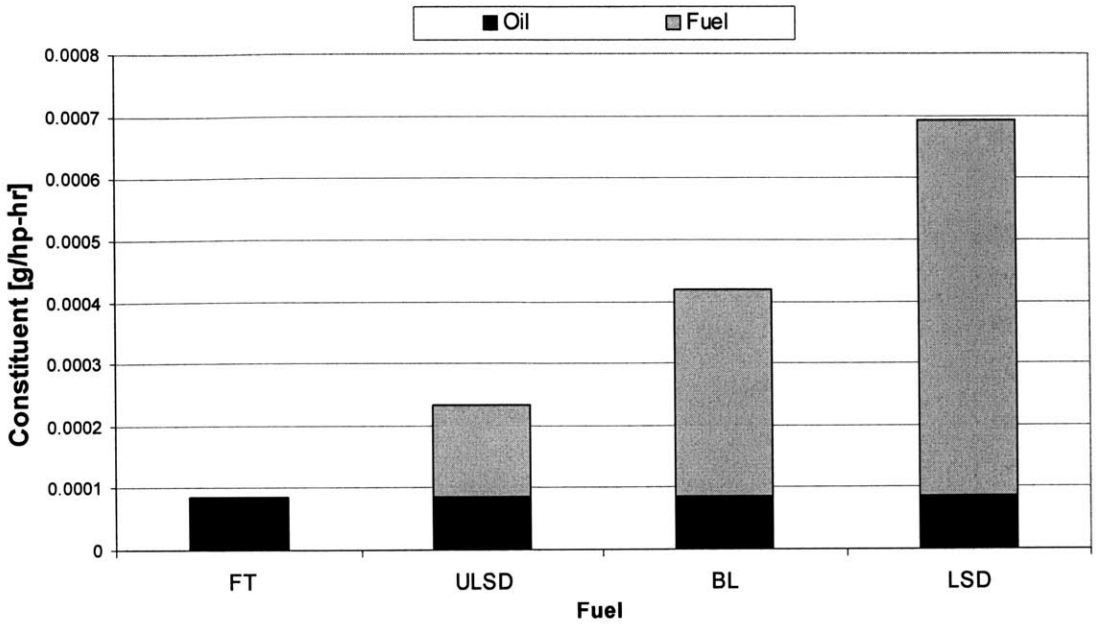

Figure 7.11. Comparison of lubricant oil and fuel contribution to particulate sulfate at a test condition of 1682 rpm, 474 kPa BMEP

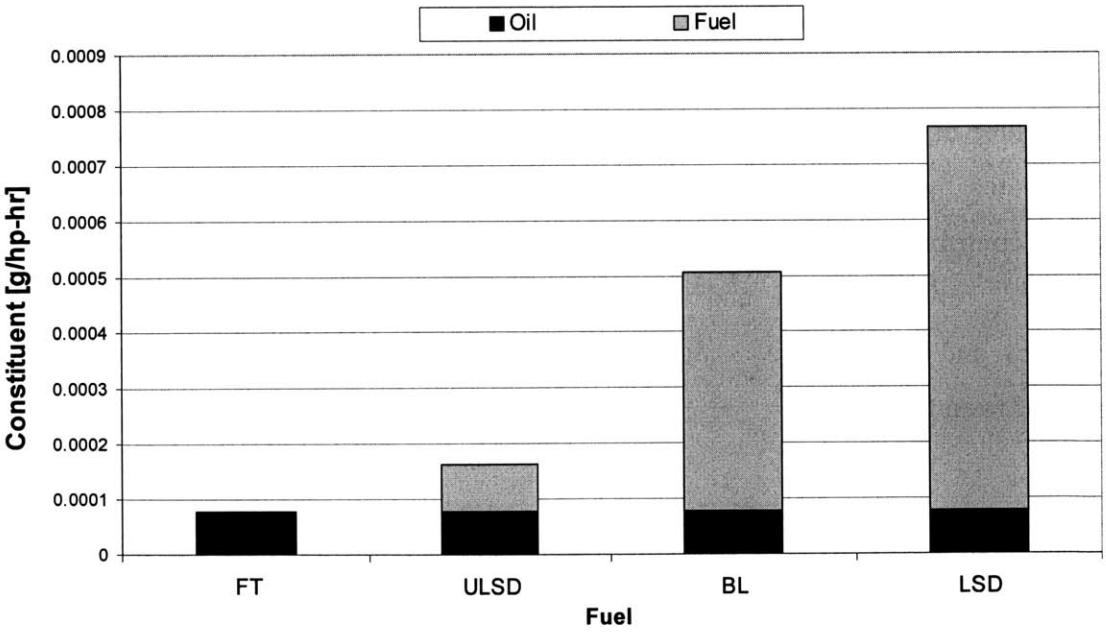

Figure 7.12. Comparison of lubricant oil and fuel contribution to particulate sulfate at a test condition of 1682 rpm, 1000 kPa BMEP

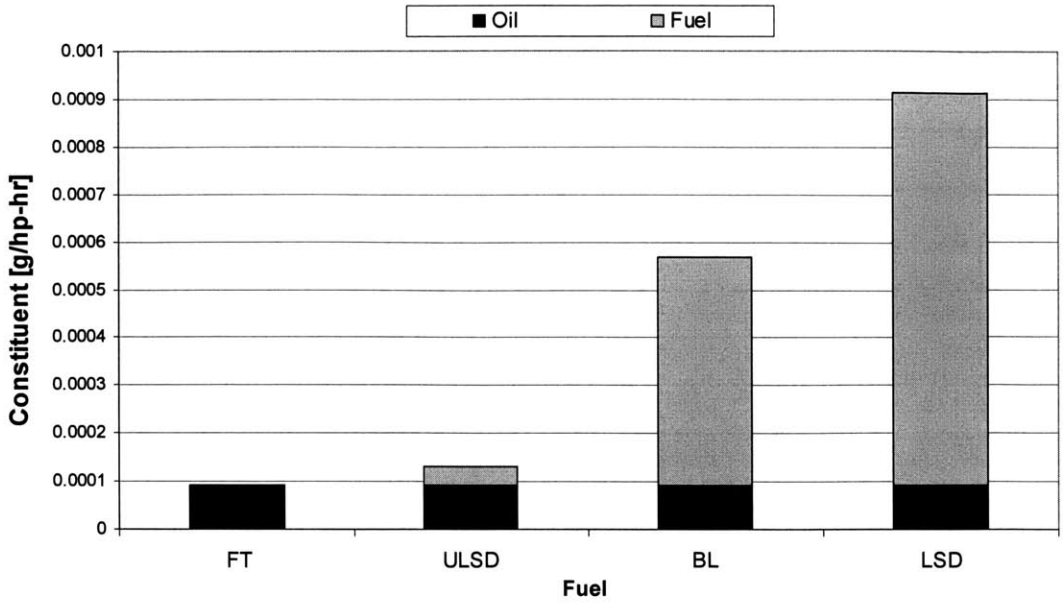

Figure 7.13. Comparison of lubricant oil and fuel contribution to particulate sulfate at a test condition of 2011 rpm, 947 kPa BMEP

Although the absolute magnitude of the lube oil-derived SO_4 increased with increased engine speed and load, a result of the associated increase in lube oil consumption, the relative lube oil contribution to the total SO_4 declined as the increase in oil consumption was negated by the significantly larger increase in fuel consumption. On average the lube oil contributed between 13.9% and 24.9% of the SO_4 determined from the LSD PM emissions, between 63.3% and 74.3% of the SO_4 determined from the ULSD PM emissions, and between 17.9% and 35.7% of the SO_4 determined from the PM emissions observed from the blend.

7.2.5 Comparison to Raw Particulate Measurements

In order to verify the results of the first PM analysis, as well as to determine the effect of dilution ratio on PM composition, a second batch of particulate samples was sent to the same engine manufacturer's emission/chemistry laboratory for analysis. The average particulate composition is shown in Figure 7.14.

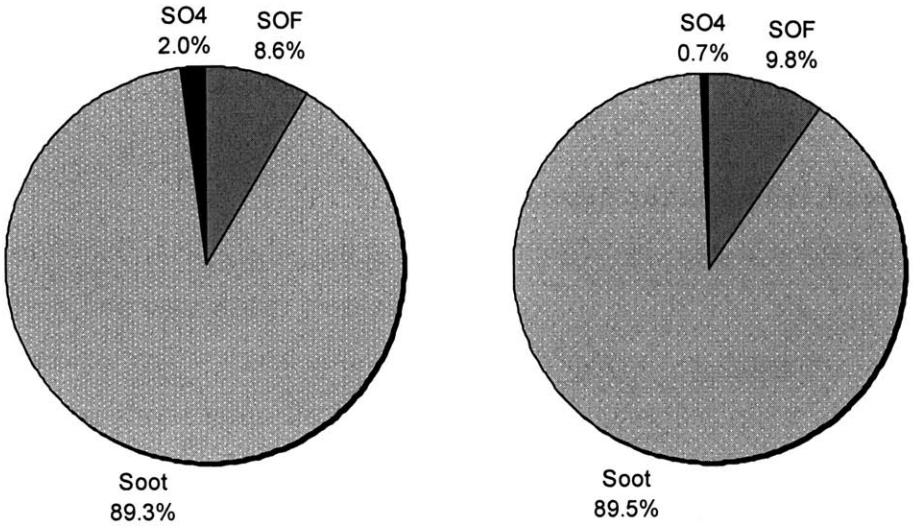

Figure 7.14. Particulate composition for (a) low sulfur diesel, and (b) Fischer-Tropsch fuel. All particulate samples were collected from the raw undiluted exhaust at an engine operating condition of 1682 rpm, 474 kPa BMEP.

All of the samples in the second batch were collected from the raw exhaust without the use of the dilution tunnel. Furthermore, all of the paper filters used in the second batch were stored in glass Petri dishes, rather than the plastic dishes typically used to store the filters, as it was believed that some chemicals in the plastic could leach into the filter paper, potentially affecting the results of the analysis.

The results of the second analysis confirm the initial results with respect to the sulfate contribution to the total particulate mass. In the case of the FT particulates, the SO_4 content was reduced by nearly a factor of three when compared to the LSD particulates. However, as a result of the raw sampling, the soluble organic fraction is quite small in both cases, as the hot raw exhaust conditions are not conducive to the condensation of various gaseous species onto the PM. While the FT particulates do exhibit a slightly higher soluble organic fraction and a significantly lower overall sulfate content than the LSD particulates, due to the differences in fuel composition, the differences in the hot undiluted exhaust stream are minimal. In both cases the particulate composition is very

similar, consisting primarily of non-soluble carbonaceous soot. Typically raw particulate samples contain a significantly higher portion of SOL than equivalent dilute PM samples due to the elevated temperatures at which the samples are collected [53].

7.2.6 Detailed Exhaust Sulfur Accounting

Based on the measured gaseous SO_2 emissions and the sulfate contribution to the total particulate mass, the total sulfur content of the exhaust (particulate and gaseous) was calculated and compared to the expected exhaust sulfur levels. The expected exhaust sulfur levels were computed using the known fuel and oil sulfur levels and fuel and oil consumption rates. While the fuel consumption rates were measured directly for each test condition, no direct measurements of oil consumption were made. The contribution of the sulfur in the lubricating oil to the total exhaust sulfur levels was estimated in two different ways. One means of estimating the lube oil sulfur contribution was to use the gaseous and particulate sulfur levels measured using the FT fuel. Since the FT diesel contains no sulfur, it was assumed that any SO_2 in the exhaust and any sulfates on the FT particulates were due to the lube oil sulfur. Table 7.2 lists the contribution of the gaseous and particulate sulfur levels to the total measured sulfur emissions with the FT fuel.

FT	Speed	BMEP	Sulfur: Gaseous SO_2	Sulfur: PM Sulfates	Total Sulfur (Oil Contribution)
	[rpm]	[kPa]	[g/hr]	[g/hr]	[g/hr]
A25	1681	477	0.00	0.03	0.03
A50	1684	955	0.00	0.03	0.03
A75	1684	1388	0.11	0.05	0.16
B25	2012	483	0.06	0.02	0.09
B50	2016	951	0.10	0.03	0.12
B75	2013	1407	0.21	0.05	0.26
C25	2344	456	0.16	0.03	0.19
C50	2351	901	0.21	0.02	0.24

Table 7.2. Breakdown of total sulfur emissions for the FT fuel

The second means of estimating the contribution of the lube oil sulfur to the total exhaust sulfur levels, was by using the oil consumption rates for the Cummins ISB determined in a previous thesis by Plumley. In this thesis, Plumley gives the measured oil sulfur

concentration as 4,200 PPM_w and oil consumption rates for the A50 and B75 test conditions as 5.8 g/hr and 7.5 g/hr respectively for the Cummins ISB 300 [26].

LSD	Speed	BMEP	Sulfur: Gaseous SO2	Sulfur: PM Sulfates	Total Measured Sulfur (Fuel +Lube)	Total Expected Sulfur (Fuel +Lube)	Percent Sulfur Accounted For
	[rpm]	[kPa]	[g/hr]	[g/hr]	[g/hr]	[g/hr]	
A25	1679	483	2.23	0.17	2.40	3.68	65.1%
A50	1681	951	3.97	0.13	4.10	5.95	69.0%
A75	1686	1415	5.79	0.19	5.98	8.73	68.5%
B25	2012	476	2.84	0.13	2.97	4.63	64.1%
B50	2017	945	4.93	0.17	5.09	7.55	67.5%
B75	2013	1416	7.08	0.24	7.32	10.37	70.6%
C25	2342	457	3.25	0.16	3.41	5.57	61.2%
C50	2345	919	5.98	0.16	6.14	8.99	68.3%

Table 7.3. Breakdown of total sulfur emissions for the LSD

Once the expected lube oil sulfur emission rates were known, the total expected exhaust sulfur levels were calculated as the sum of the fuel and lube oil sulfur contributions. The breakdown of the total sulfur emissions for the LSD is given in Table 7.3. The contribution of the lube oil sulfur to the expected sulfur levels in the Table 7.3 was estimated from the FT sulfur data presented in Table 7.2. As can be seen from the table, only 65% to 70% of the expected exhaust sulfur could be accounted for based on the gaseous SO_2 and PM sulfate concentration measurements alone.

In order to verify the difference in the measured and expected exhaust sulfur levels, the estimated lube sulfur contribution based on the measured FT sulfur levels were compared with those calculated using the lube oil consumption rates given by Plumley. In both cases, the lube oil sulfur contribution to the total exhaust sulfur levels was extremely small due to the low lube oil sulfur content and small rate of engine oil consumption.

A comparison of the measured and expected exhaust sulfur levels for the A50 test condition is given in Figure 7.15. In this case, the sulfur contribution of the lube oil estimates based on the measured FT data and oil consumption data given by Plumley agree very well.

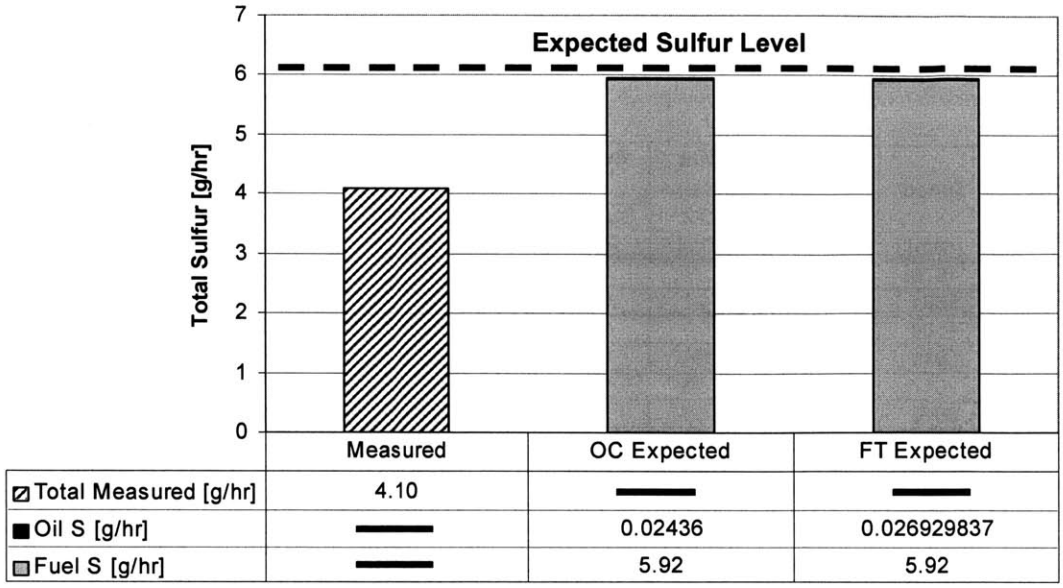

Figure 7.15. Measured and expected sulfur emissions with the 400 PPM low sulfur diesel at 1682 rpm and 951 kPa BMEP. FT corrected and OC corrected indicate lube oil sulfur contribution estimates based on the measured FT data and oil consumption rates given by Plumley respectively.

On the other hand, the sulfur contribution of the lube oil estimates based on the measured FT data and oil consumption data given by Plumley for the B75 test condition differ substantially as shown in Figure 7.16. However, once again, the contribution of the lube oil-derived sulfur is small in comparison to the fuel sulfur contribution.

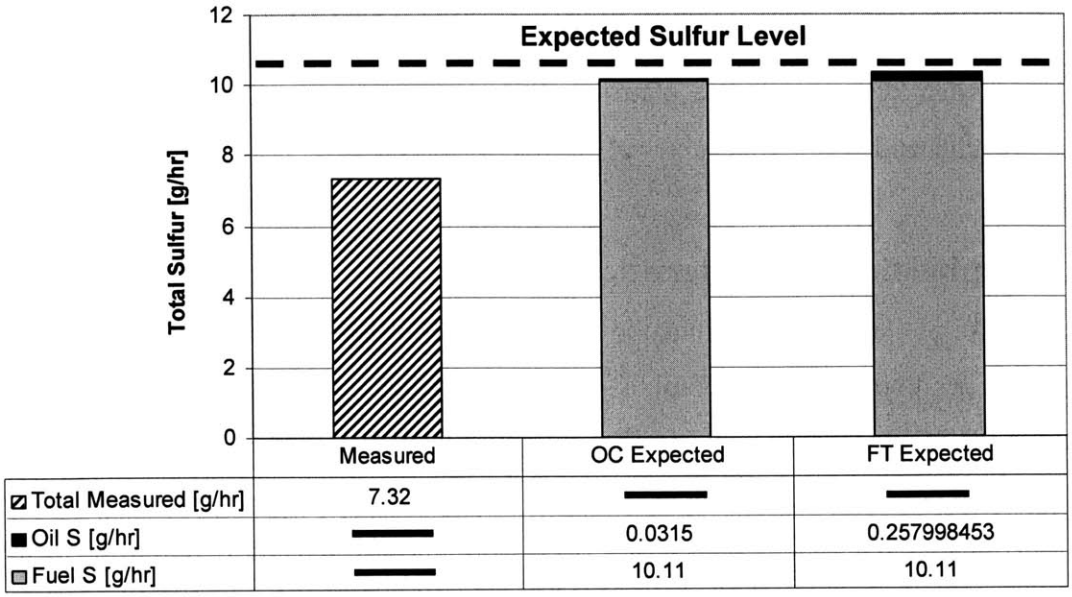

Figure 7.16. Measured and expected sulfur emissions with the 400 PPM low sulfur diesel at 2013 rpm and 1416 kPa BMEP. FT corrected and OC corrected indicate lube oil sulfur contribution estimates based on the measured FT data and oil consumption rates given by Plumley respectively.

Despite differences in the estimation of the lube oil-derived sulfur, the measured exhaust sulfur levels are still 30% to 35% lower than the expected levels. This discrepancy is most likely due to a combination of one of the following causes:

- failure by the Antek SO_2 analyzer to convert and measure all of the gaseous sulfur (SO_2) in the exhaust,
- failure to measure all of the sulfur on the PM via ion chromatography,
- or deposition of the sulfur within the engine/exhaust system.

The first two reasons are the most likely causes, especially since the sulfur content measured on the PM was much smaller than expected. However, if the low PM sulfate content was the only source of the discrepancy, a total PM sulfate content of approximately 25% would be required to make up the difference between the measured and expected exhaust sulfur levels. Since this level of sulfate on the PM is on the high

side for a 400 PPM fuel, low SO_2 readings by the Antek in conjunction with low sulfate measurements are the most likely causes. Nonetheless, deposition of sulfur within the engine/exhaust system is still a plausible factor contributing to the low exhaust sulfur measurements and will be the subject of further investigation.

7.3 Combustion Characteristics

For the sake of clarity, the combustion data for the ultra-low sulfur fuel was not included in the figures comparing the combustion characteristics. It should be noted, however, that the ULSD exhibited very similar combustion characteristics to the standard low sulfur baseline fuel. Thus, the following discussion is focused on comparing the combustion characteristics of the neat FT fuel, low sulfur diesel, and blend of FT/LSD.

7.3.1 Ignition Delay

Figure 7.17 compares the ignition delay of the three fuels. The FT fuel yielded a shorter ignition delay over the range of operating conditions, with the blend exhibiting an ignition delay between that of the FT and LSD.

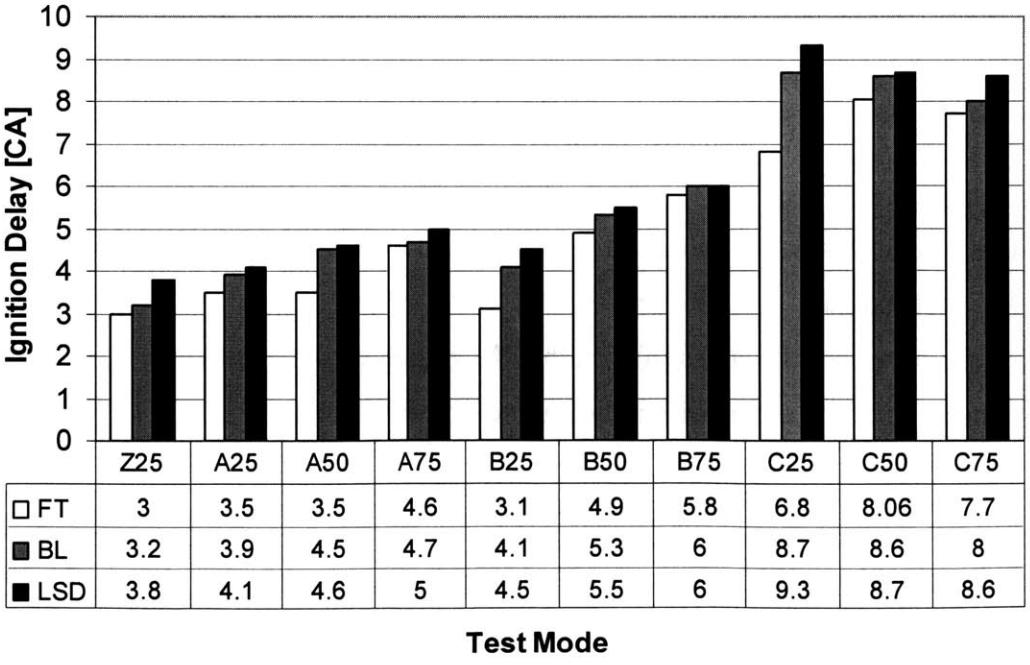

	Z25	A25	A50	A75	B25	B50	B75	C25	C50	C75
FT	3	3.5	3.5	4.6	3.1	4.9	5.8	6.8	8.06	7.7
BL	3.2	3.9	4.5	4.7	4.1	5.3	6	8.7	8.6	8
LSD	3.8	4.1	4.6	5	4.5	5.5	6	9.3	8.7	8.6

Figure 7.17. Ignition delay

The decreased ignition delay for the FT and blend results in less fuel injected during the premixed combustion phase, yielding a more uniform and less rapid temperature rise within the cylinder. This is evidenced by the significantly lower heat release rate in the pilot injection (see Figure 7.21), however the heat release profile of the main injection seemed little affected by the reduced ignition delay.

7.3.2 Burn Duration

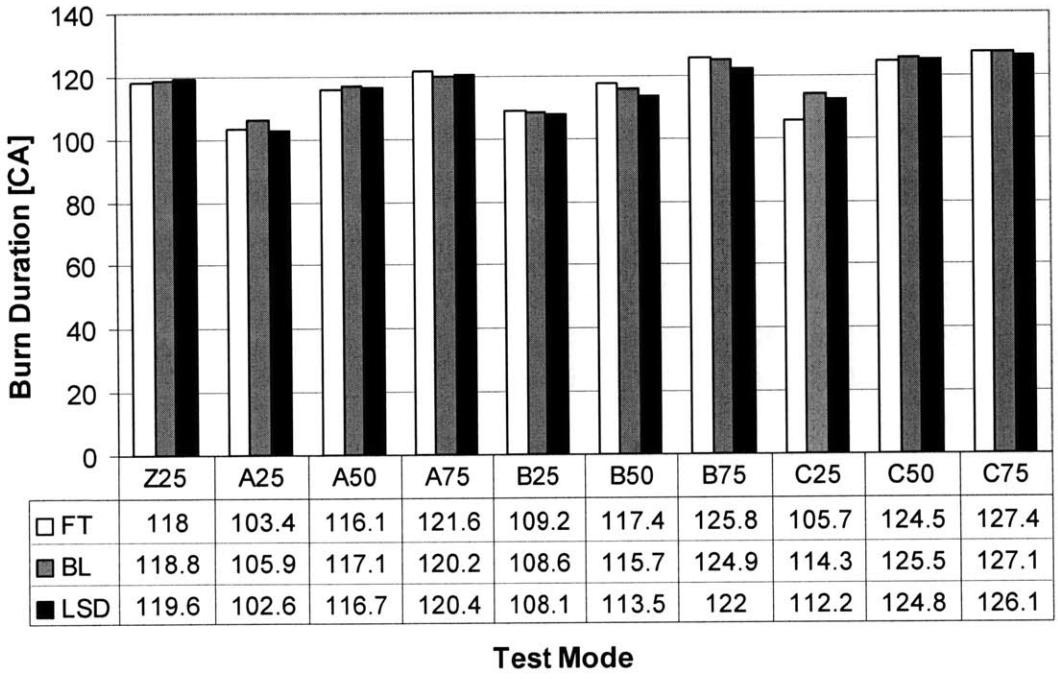

	Z25	A25	A50	A75	B25	B50	B75	C25	C50	C75
FT	118	103.4	116.1	121.6	109.2	117.4	125.8	105.7	124.5	127.4
BL	118.8	105.9	117.1	120.2	108.6	115.7	124.9	114.3	125.5	127.1
LSD	119.6	102.6	116.7	120.4	108.1	113.5	122	112.2	124.8	126.1

Figure 7.18. Start of injection to 99% burn duration

Figure 7.18 depicts the total time from the start of injection (SOI) to the end of combustion (EOC), which is nearly the same for both fuels. Despite the reduced ignition delay of the FT fuel and blend, the fact that the time from SOI to EOC varied little with the three fuels is attributed to the lower density of the FT fuel which results in more fuel injected per cycle (longer injection duration), as well as the slightly longer tale-end burn observed in the FT fuel and blend.

The FT fuel and the blend also exhibited reduced 50% to 90% burn durations, indicating a faster burn rate for the FT fuel during the latter part of the combustion process as shown in Figure 7.19. On average, the FT fuel reduced the diffusion burn duration by approximately 7.4%, with values ranging from a maximum reduction of 20.2% to a slight increase of 1.4% as compared to the low sulfur diesel.

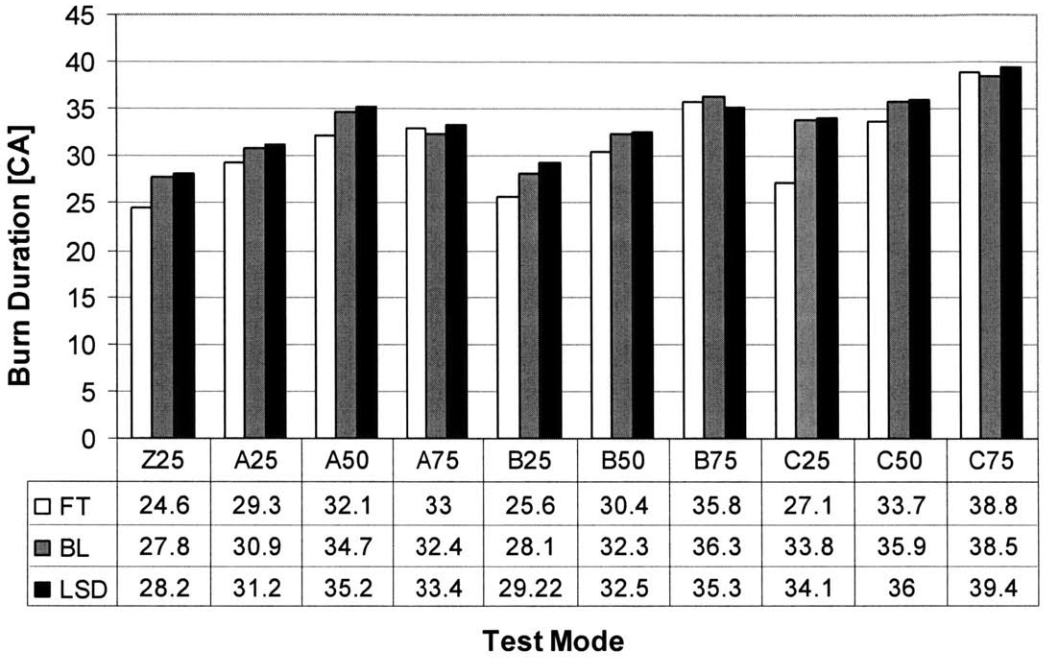

	Z25	A25	A50	A75	B25	B50	B75	C25	C50	C75
FT	24.6	29.3	32.1	33	25.6	30.4	35.8	27.1	33.7	38.8
BL	27.8	30.9	34.7	32.4	28.1	32.3	36.3	33.8	35.9	38.5
LSD	28.2	31.2	35.2	33.4	29.22	32.5	35.3	34.1	36	39.4

Figure 7.19. 50% to 90% burn duration

In addition to exhibiting a faster burn rate during the diffusion burn, the location of the 50% heat release occurred slightly earlier for both the FT and blend as shown in Figure 7.20. This observation is attributed primarily to the reduced ignition delay of the FT fuel and blend, essentially initiating the combustion process earlier and thus liberating more energy faster than the baseline fuel.

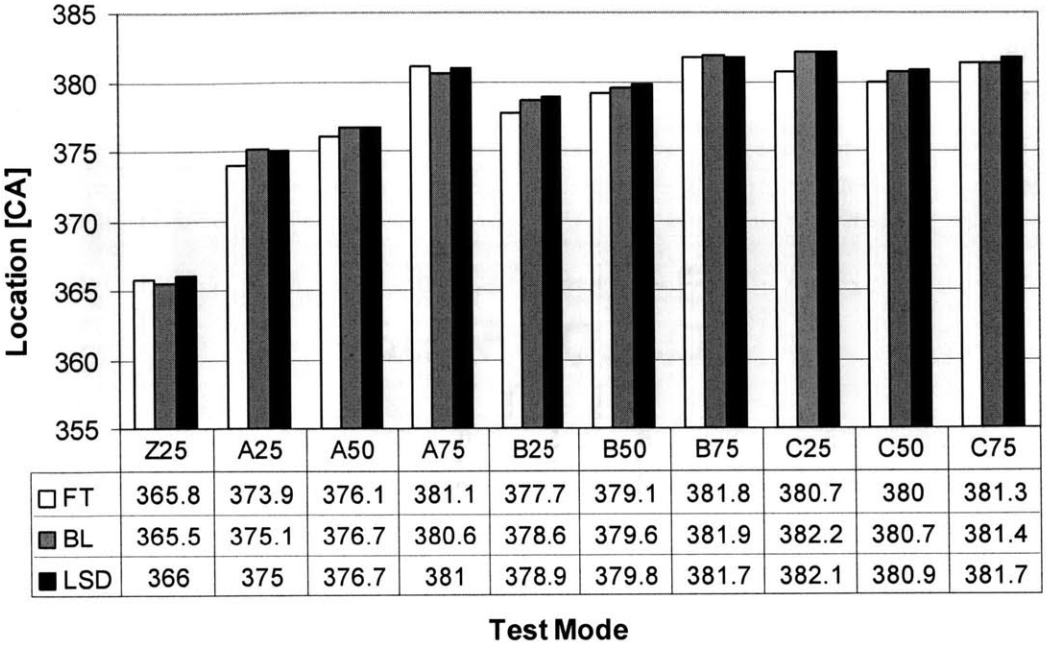

	Z25	A25	A50	A75	B25	B50	B75	C25	C50	C75
FT	365.8	373.9	376.1	381.1	377.7	379.1	381.8	380.7	380	381.3
BL	365.5	375.1	376.7	380.6	378.6	379.6	381.9	382.2	380.7	381.4
LSD	366	375	376.7	381	378.9	379.8	381.7	382.1	380.9	381.7

Figure 7.20. Location of 50% heat release

Figure 7.21 shows the initial 10% to 50% burn duration, which did not vary significantly for the three fuels. The reduced ignition delay for the FT fuel and blend, combined with the lower density of the FT fuel which reduces the amount of fuel injected for a given time interval, may lead to a reduction in the amount of fuel burned during the pre-mixed burn phase and thus contribute significantly to the observed reduction in PM emissions.

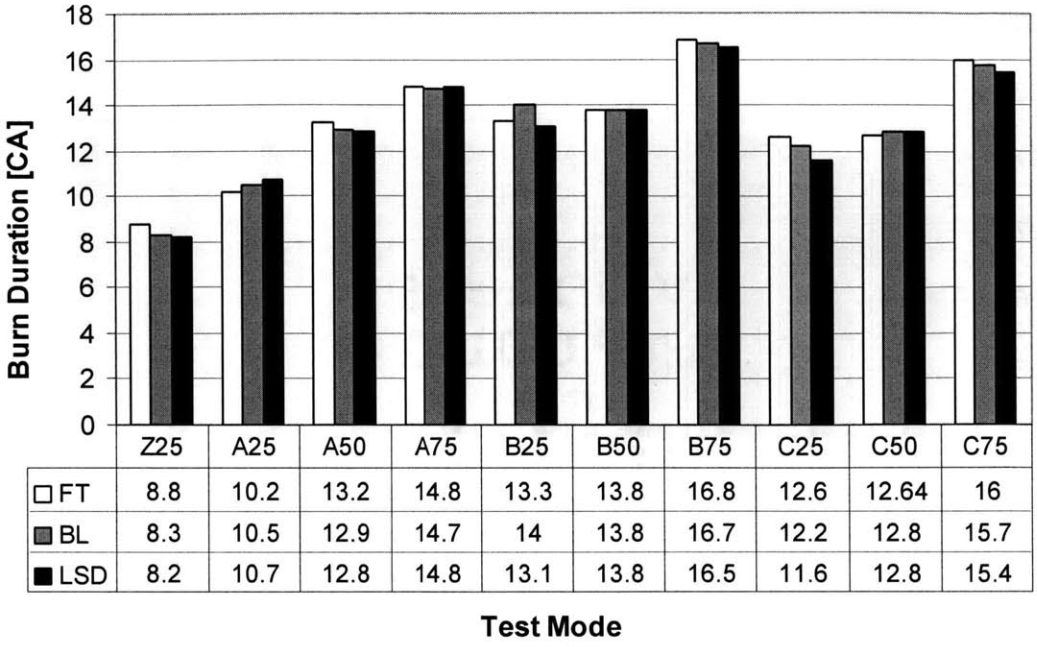

	Z25	A25	A50	A75	B25	B50	B75	C25	C50	C75
FT	8.8	10.2	13.2	14.8	13.3	13.8	16.8	12.6	12.64	16
BL	8.3	10.5	12.9	14.7	14	13.8	16.7	12.2	12.8	15.7
LSD	8.2	10.7	12.8	14.8	13.1	13.8	16.5	11.6	12.8	15.4

Figure 7.21. 10% to 50% burn duration

On the other hand, the FT and blend tended to have a slightly longer tail-end burn as demonstrated in Figure 7.22. The tail-end burn for the FT fuel was approximately 5.3% longer on average, with values ranging from a maximum increase of 10.7% to a minimum of 2.5%. These values should only be taken as approximate, due to the difficulty associated with determining the location of the 99% heat release. In nearly all the cases, the blend exhibited combustion characteristics in between those of the two fuels.

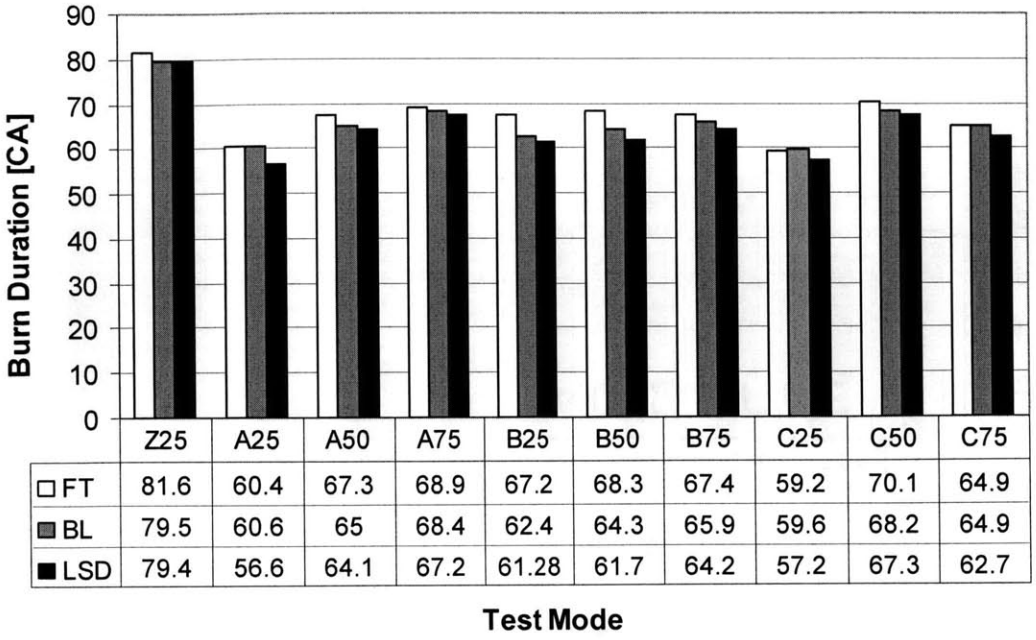

	Z25	A25	A50	A75	B25	B50	B75	C25	C50	C75
FT	81.6	60.4	67.3	68.9	67.2	68.3	67.4	59.2	70.1	64.9
BL	79.5	60.6	65	68.4	62.4	64.3	65.9	59.6	68.2	64.9
LSD	79.4	56.6	64.1	67.2	61.28	61.7	64.2	57.2	67.3	62.7

Figure 7.22. Tail-end burn duration

7.3.3 Maximum In-Cylinder Pressure and Location

Figures 7.23 and 7.24 compare the maximum in-cylinder pressure for each fuel and its associated location. Since torque was held constant at each test condition for each fuel, maximum cylinder pressure and its location remained fairly constant as well. Slight variations between the two fuels can be attributed to small differences in injection timing, which would affect the location and magnitude of the maximum pressure.

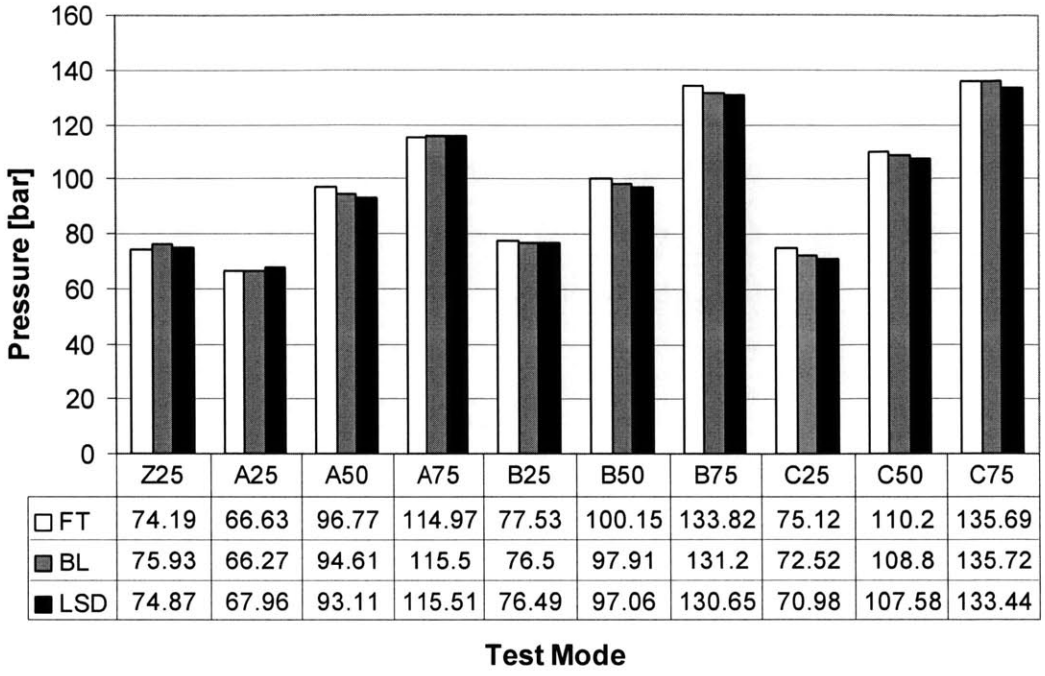

	Z25	A25	A50	A75	B25	B50	B75	C25	C50	C75
FT	74.19	66.63	96.77	114.97	77.53	100.15	133.82	75.12	110.2	135.69
BL	75.93	66.27	94.61	115.5	76.5	97.91	131.2	72.52	108.8	135.72
LSD	74.87	67.96	93.11	115.51	76.49	97.06	130.65	70.98	107.58	133.44

Figure 7.23. Maximum in-cylinder pressure after start of injection

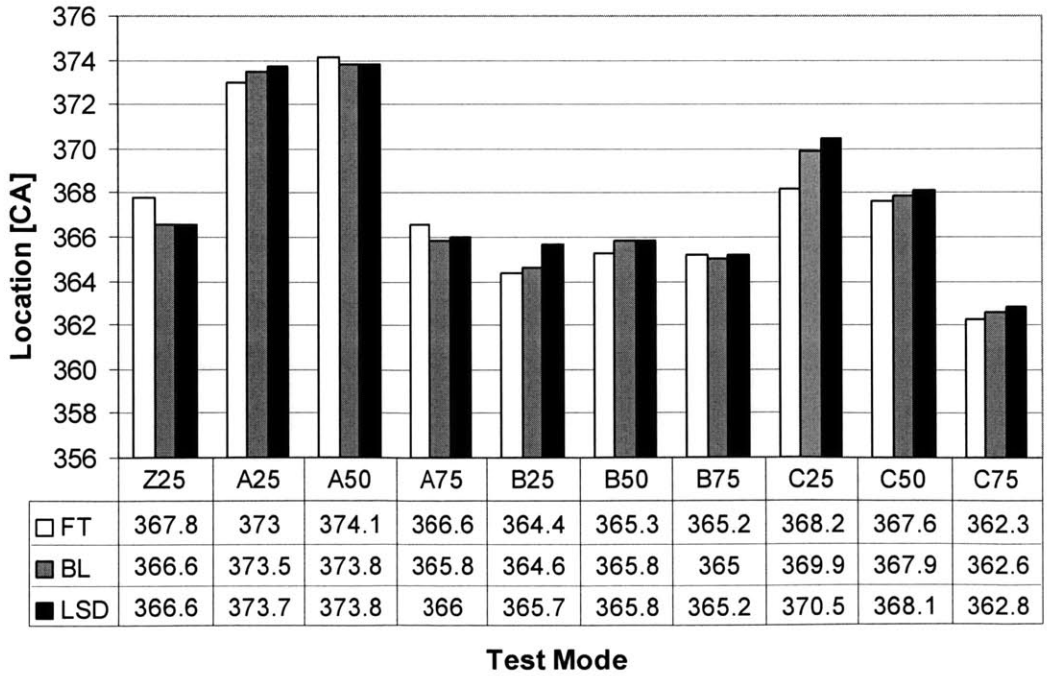

	Z25	A25	A50	A75	B25	B50	B75	C25	C50	C75
FT	367.8	373	374.1	366.6	364.4	365.3	365.2	368.2	367.6	362.3
BL	366.6	373.5	373.8	365.8	364.6	365.8	365	369.9	367.9	362.6
LSD	366.6	373.7	373.8	366	365.7	365.8	365.2	370.5	368.1	362.8

Figure 7.24. Location of maximum in-cylinder pressure after start of injection

7.3.4 Pressure Trace and Heat Release Characteristics

Since the stock engine calibration employs a strategy of severely retarded injection timing to decrease in-cylinder temperatures and reduce NOx emissions, the maximum cylinder pressure for a number of test conditions occurred before TDC and before significant combustion had taken place. For these cases, the maximum cylinder pressure was taken at the 10% heat release location to provide a more representative value of the pressure actually experienced by the fuel [35]. An example of a typical pressure trace for a severely retarded injection timing condition is given in Figure 7.25.

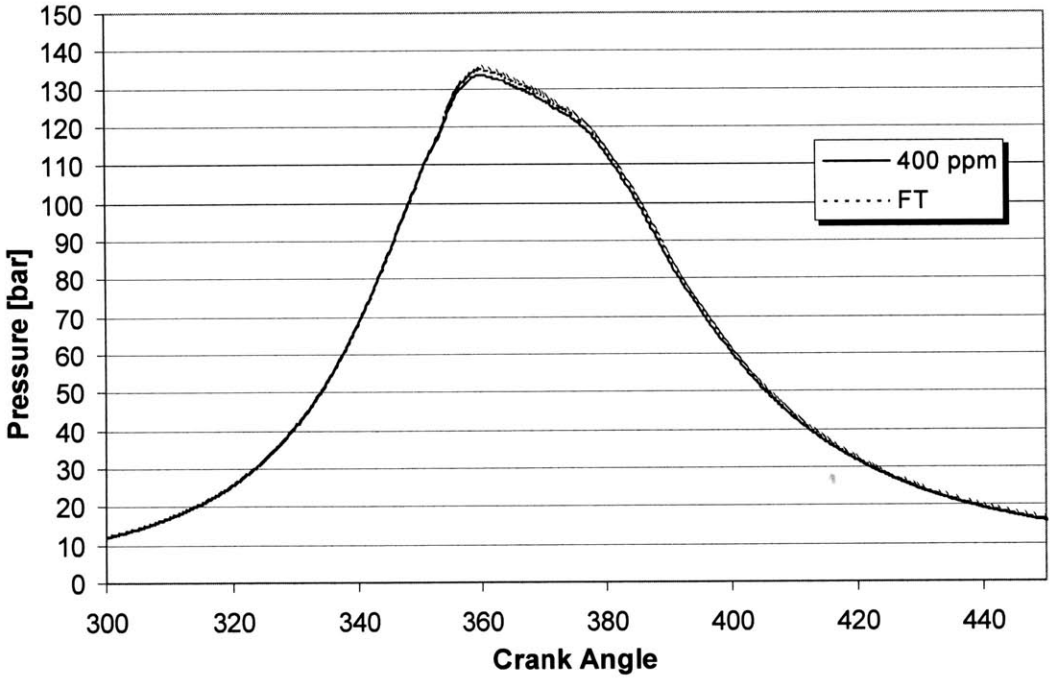

Figure 7.25. Pressure trace for severely retarded timing, 2013 rpm, 1611 kPa IMEP

Figure 7.26 presents the heat release curve corresponding to the pressure trace presented in Figure 7.25 above. The three distinct peaks correspond to the pre-, main-, and post-injection events and their associated heat release profiles.

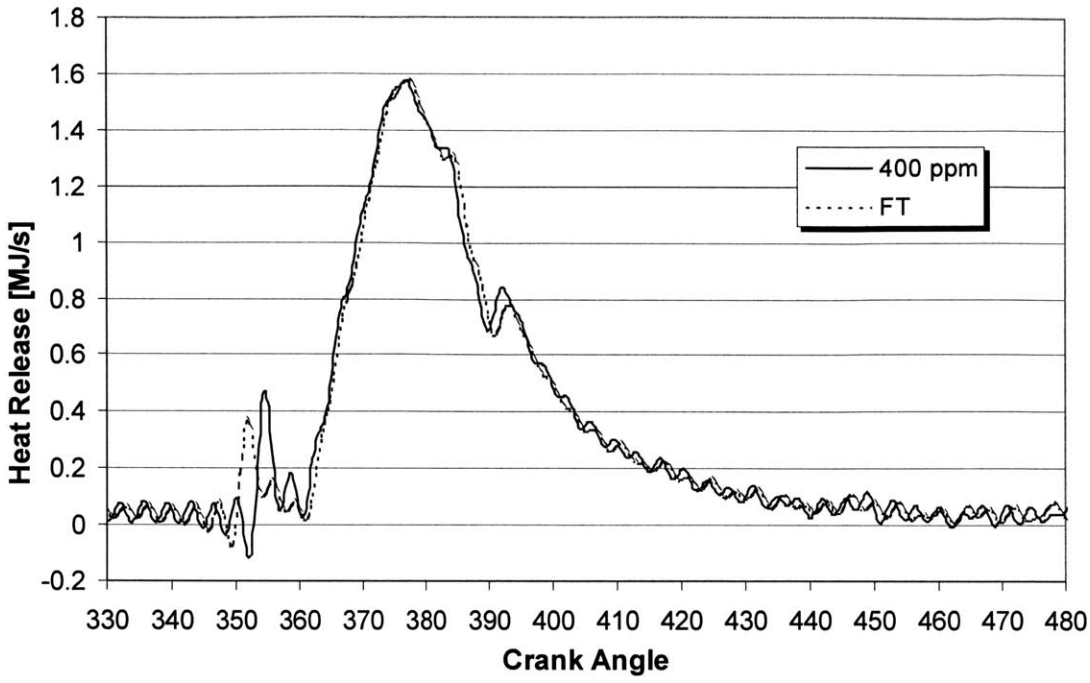

Figure 7.26. Heat release curves corresponding to severely retarded injection timing at an engine operating condition of 2013 rpm, 1611 kPa IMEP

7.3.5 Pilot-Injection Maximum Heat Release Rates and Location

Figures 7.27 and 7.28 depict the maximum heat release rates and corresponding locations for each pilot injection event. In nearly all of the cases, the FT and blend exhibited a lower maximum heat release rate occurring slightly earlier than that of the low-sulfur diesel. The most significant difference between the heat release rates occurred for the pilot injection with the FT fuel. On average the FT reduced the maximum heat released by 24%, once again indicating a reduction in the amount of fuel burned during the pre-mixed combustion phase. The C50 and C75 test conditions were omitted in Figure 7.27 and Figure 7.28 due to the absence of a readily discernible heat release profile for the pilot injection event.

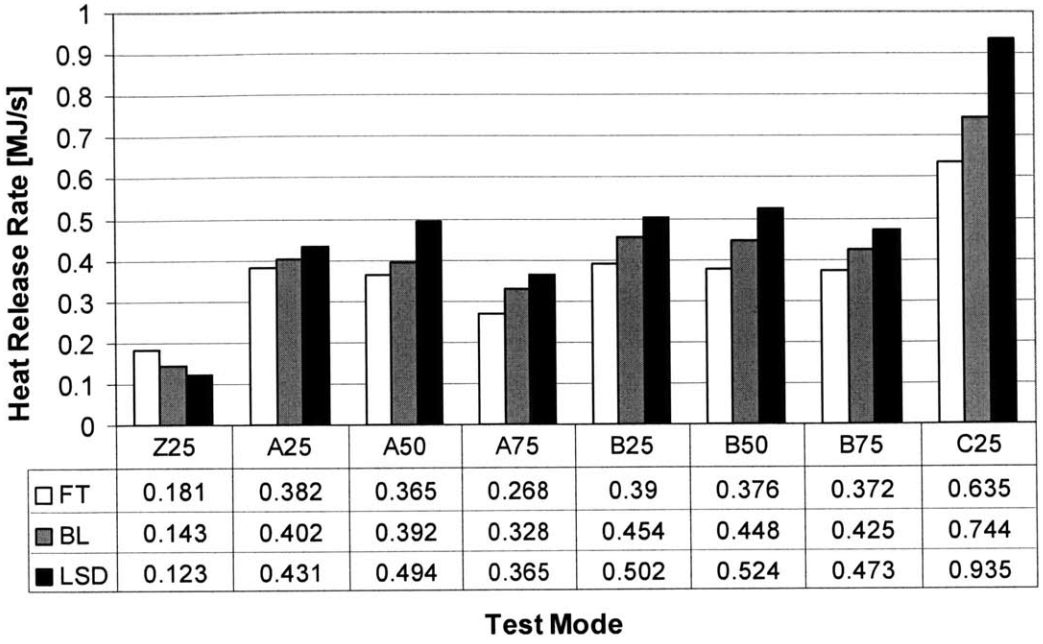

	Z25	A25	A50	A75	B25	B50	B75	C25
FT	0.181	0.382	0.365	0.268	0.39	0.376	0.372	0.635
BL	0.143	0.402	0.392	0.328	0.454	0.448	0.425	0.744
LSD	0.123	0.431	0.494	0.365	0.502	0.524	0.473	0.935

Figure 7.27. Pilot injection maximum heat release rate

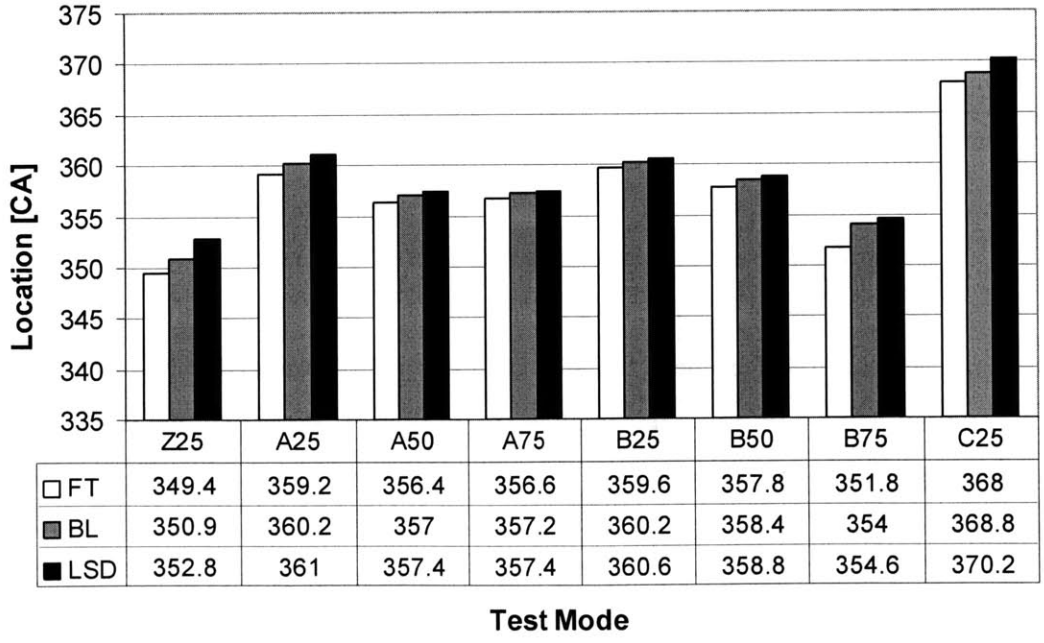

	Z25	A25	A50	A75	B25	B50	B75	C25
FT	349.4	359.2	356.4	356.6	359.6	357.8	351.8	368
BL	350.9	360.2	357	357.2	360.2	358.4	354	368.8
LSD	352.8	361	357.4	357.4	360.6	358.8	354.6	370.2

Figure 7.28. Location of pilot injection maximum heat release

7.3.6 Main-Injection Maximum Heat Release Rates and Location

The differences in the maximum heat released for the main injection are quite small, on the order of 1 to 2%. Typically the location of the maximum heat release rate for the main injection event occurred 1 to 2 crank angle degrees earlier for the FT fuel. Once again, the blend exhibited heat release characteristics between that of the FT and low sulfur diesel. Figure 7.29 compares the heat released during the main injection event for each fuel.

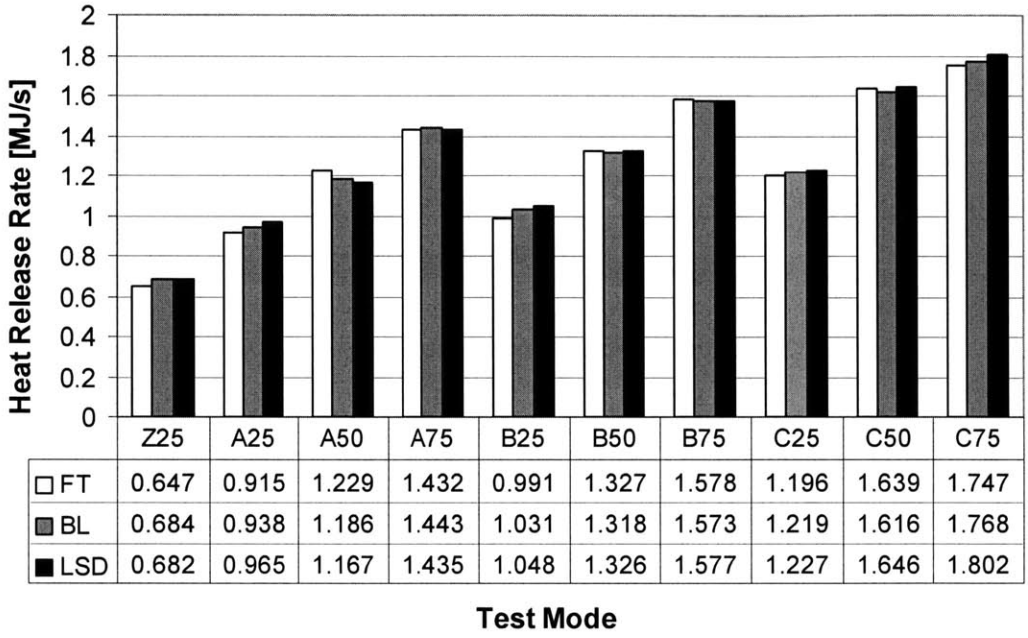

	Z25	A25	A50	A75	B25	B50	B75	C25	C50	C75
FT	0.647	0.915	1.229	1.432	0.991	1.327	1.578	1.196	1.639	1.747
BL	0.684	0.938	1.186	1.443	1.031	1.318	1.573	1.219	1.616	1.768
LSD	0.682	0.965	1.167	1.435	1.048	1.326	1.577	1.227	1.646	1.802

Figure 7.29. Main injection maximum heat release

The fact that the main injection heat release profiles for the various fuels did not differ significantly as reported in previous studies, is primarily attributed to the multiple injection strategy employed by the Cummins ISB. Furthermore, the location of the maximum heat release rates varied less for the higher load conditions, as shown in Figure 7.30.

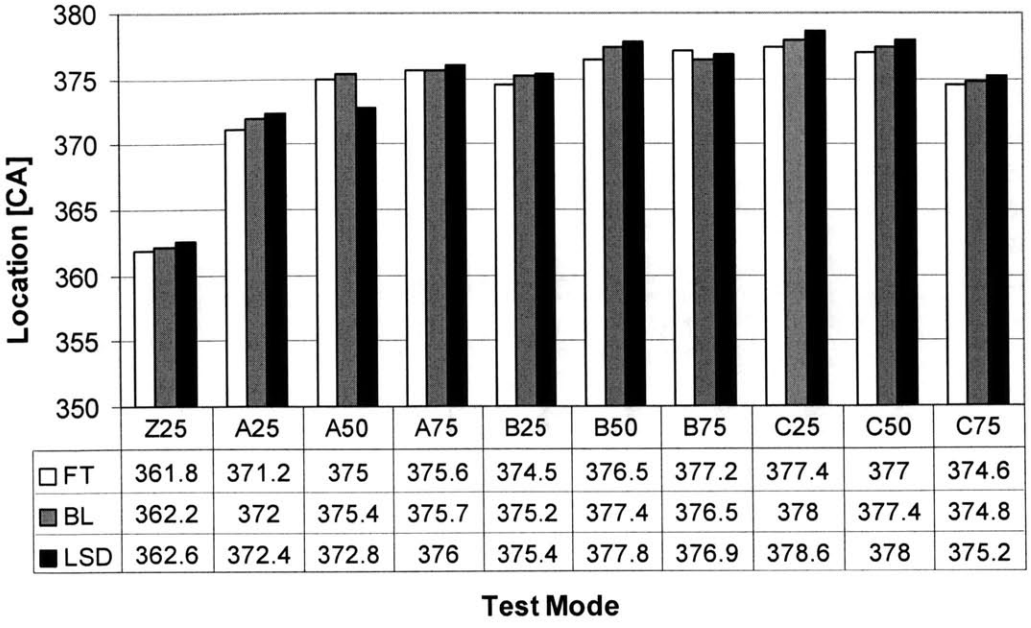

	Z25	A25	A50	A75	B25	B50	B75	C25	C50	C75
FT	361.8	371.2	375	375.6	374.5	376.5	377.2	377.4	377	374.6
BL	362.2	372	375.4	375.7	375.2	377.4	376.5	378	377.4	374.8
LSD	362.6	372.4	372.8	376	375.4	377.8	376.9	378.6	378	375.2

Figure 7.30. Location of main injection maximum heat release

7.3.7 Post-Injection Maximum Heat Release Rates and Location

The post injection maximum heat release rates and corresponding locations are shown in Figure 7.31 and Figure 7.32.

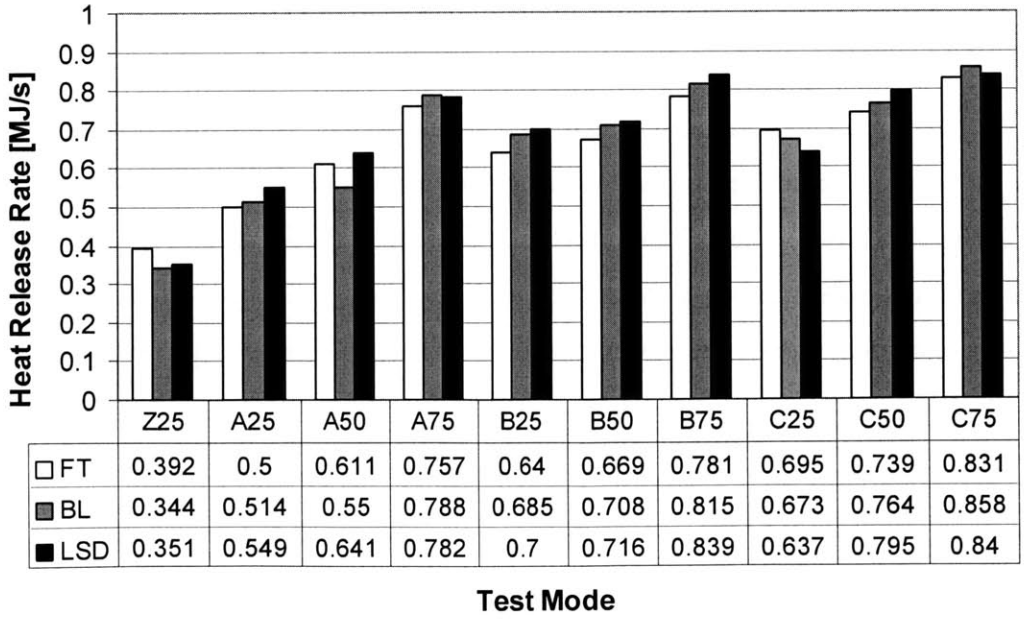

	Z25	A25	A50	A75	B25	B50	B75	C25	C50	C75
FT	0.392	0.5	0.611	0.757	0.64	0.669	0.781	0.695	0.739	0.831
BL	0.344	0.514	0.55	0.788	0.685	0.708	0.815	0.673	0.764	0.858
LSD	0.351	0.549	0.641	0.782	0.7	0.716	0.839	0.637	0.795	0.84

Figure 7.31. Post injection maximum heat release rate

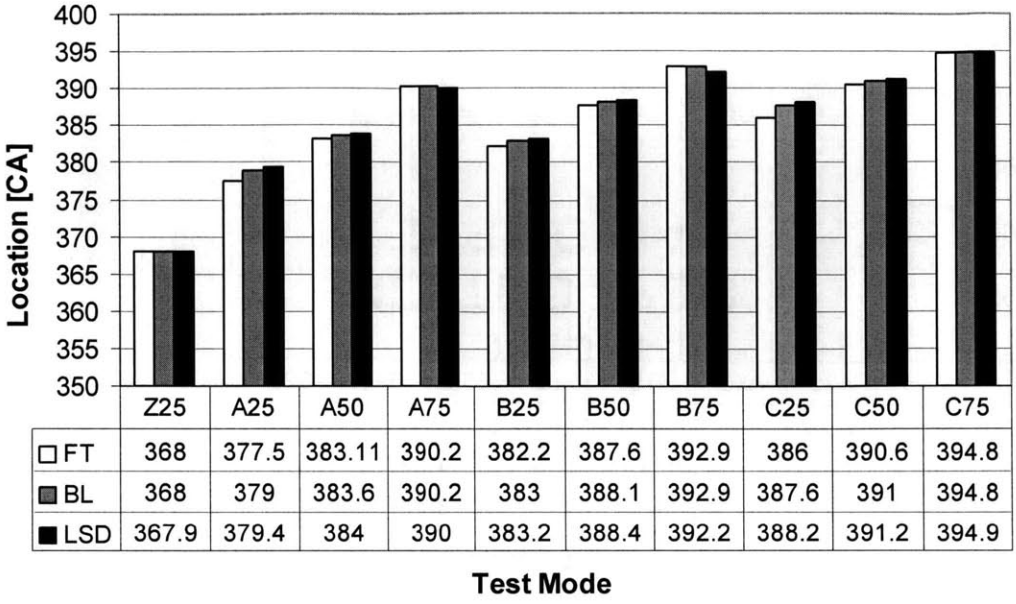

	Z25	A25	A50	A75	B25	B50	B75	C25	C50	C75
FT	368	377.5	383.11	390.2	382.2	387.6	392.9	386	390.6	394.8
BL	368	379	383.6	390.2	383	388.1	392.9	387.6	391	394.8
LSD	367.9	379.4	384	390	383.2	388.4	392.2	388.2	391.2	394.9

Figure 7.32. Location of post injection maximum heat release

The differences in the maximum heat released for the post injection event were slightly greater than those observed in the main injection, with the FT exhibiting a lower average heat release rate for the post injection of approximately 5%. As before, the blend exhibited combustion characteristics between that of the FT and low sulfur diesel.

Unlike the location of the maximum heat release rate for the main injection event, the location of the maximum heat release rate for the post injection event occurred only slightly earlier for the FT fuel. This effect is attributed to the FT fuel's longer tale-end burn duration and subsequently slower tale-end burn rate. In addition, the locations of the post-injection heat release rates were nearly identical for the high load conditions.

8.0 Discussion

The observed emissions behavior of the fuels can be explained by the differences in the fuel properties, combustion characteristics, and impact of the engine technology.

8.1 Fuel effects

The lower density and near zero sulfur and aromatic content of the FT fuel contribute to the reduction in particulate emissions to a certain extent. Furthermore, Lee et al. showed that lower density diesel fuels increase the spray dispersion angle and achieve greater spray penetration in the cylinder, promoting better mixing of the charge and more complete combustion [37]. In addition, the lower C/H ratio of the FT fuel, due to its reduced aromatic content, reduces the amount of carbon in the cylinder and, thus, the amount of solid carbon in the particulates. This fact is further supported by the observed reduction in CO_2 emissions, along with a decrease in the solid fraction (SOL) of the particulates for the FT fuel.

While the reduction in fuel sulfur from 400 PPM in the low-sulfur diesel to 0 PPM in the FT diesel does have some effect in terms of overall PM reduction, the effect is believed to be small. Previous results, most notably reported by Kwon et al. and Lee at al., demonstrate that a reduction in fuel sulfur content below 0.05% yields little incremental benefit in terms of PM emissions reduction [37, 40]. The small overall sulfate content of the particulates, less than 4 % in most cases, further supports this observation. Therefore, a significant non-sulfur effect must be accounted for to explain the observed PM emissions trends.

Interestingly, the blend exhibited the same reduction in HC emissions as the neat FT fuel (Figure 7.4). A number of investigators have attempted to relate total hydrocarbon emissions to fuel properties and combustion characteristics with varying degrees of success. It is widely accepted that cetane number and density are the two fuel properties with perhaps the greatest influence on total hydrocarbon emissions [45]. However, a number of other factors such as mixing, flame quenching, fuel atomization, and combustion rate all play an important role in determining total hydrocarbon emissions as

well. The fact that the ultra-low sulfur diesel has the greatest proportion of light hydrocarbons of all the fuels tested, may partially explain its higher HC emissions. Furthermore, the reduction in T90 and T95 from the LSD to the ULSD by 68°C and 72°C respectively, may also contribute to the large observed increase in HC emissions. A more detailed analysis taking into consideration all of the factors involved is warranted to determine the exact causes of the observed trends in HC emissions.

The detailed particulate analysis carried out by the emission/chemistry laboratory of a major engine manufacturer confirmed the initial observations of the more than proportional benefit of using the FT diesel blend in terms of overall PM reduction. However, since a more than proportional reduction in all of the PM constituents (SOL, SOF, and SO_4) was observed, little insight is gained into this trend based on fuel properties alone. Of interest is the extremely small, almost negligible, contribution of fuel sulfur to the TPM, and while the absolute magnitudes of the numbers are suspect, the observed trend does support the findings presented in [54]. Furthermore, lube oil-derived sulfur was seen to contribute significantly to the PM emissions of fuels containing less than 15 PPM sulfur, with the lube oil-derived sulfur contributing to between 63% to 74% of the SO_4 emissions observed from the ULSD and 100% of the SO_4 emissions for the FT fuel.

8.2 Combustion characteristics

The combustion analysis demonstrated that the significantly higher cetane number of the FT fuel reduced the ignition delay, thus, reducing the amount of fuel vaporized during the pre-mixed phase of combustion. This observation was further supported by the significantly reduced maximum heat release observed in the pilot injection. Furthermore, the lower density and heating value of the FT fuel reduces the amount of fuel injected for a given time interval, and thus, necessitates a slightly longer injection duration in order to achieve the same power output as the baseline fuel. The reduced amount of FT fuel injected during the rich pre-mixed combustion phase may contribute significantly to the reduction in PM formation during this portion of the combustion process. The slightly reduced maximum heat release rates for the main- and post- injections are also indicative

of a slightly more uniform combustion in the case of the FT fuel. However, it should be noted that the extreme differences in the heat release profiles for the FT and baseline fuel observed in other studies [43, 45] were not seen in this investigation. The multiple injection strategy is the most likely cause for this discrepancy.

Since the burn duration is a qualitative indicator of the chemical reaction rates during fuel oxidation, the shorter 50% to 90% burn duration for the FT fuel and blend implies a faster burn rate for these fuels as compared to the low-sulfur diesel. This effect is most likely due to the higher cetane number of the FT coupled with the engine's retarded injection timing. As the fuel is injected later in the expansion stroke, the unburned gas temperature in the cylinder decreases. This decrease in cylinder temperature may affect the auto-ignition chemistry of the fuel. Therefore, a high cetane number fuel injected under these conditions, with auto-ignition characteristics that are less sensitive to cylinder temperature, will ignite more readily and maintain a faster rate of combustion than a lower cetane number fuel [35]. The effect of the faster 50% to 90% burn rate coupled with the slightly longer tail-end burn of the FT fuel and blend on PM emissions is difficult to determine from the present study, although it is possible that the longer tail-end burn may contribute to additional soot oxidation in the cylinder.

The effect of the FT fuel on reducing NOx emissions is somewhat lower than other results reported in the literature. This may be due to the influence of the EGR system, multiple injection strategy, and heavily retarded injection timing on reducing the sensitivity of NOx formation in this engine to the fuel properties. Nonetheless, the reduced exhaust and corresponding cylinder temperatures are most likely the main factors contributing to the observed reduction in NOx emissions for the FT fuel.

The explanations presented above apply equally well to the observed emissions and combustion behavior of the blend. Based on the combustion analysis alone, no specific conclusions can be drawn for the more than proportional reduction in PM emissions of the blend. In most cases the blend exhibited combustion behavior closer to that of the baseline diesel, which is to be expected as the blend contained 75% LSD by volume.

8.3 Engine technology

In addition to the combustion characteristics, a number of engine control parameters such as injection timing, EGR fraction, boost pressure, and the time intervals between the pilot-, main-, and post-injection events were monitored throughout the study. No significant differences were observed between any of the engine control parameters and the fuels used. It is, therefore, unlikely that any significant interactions between the fuels and the various engine sub-systems should influence the observed results.

8.4 Comparison to Cummins Data

In order to verify the NOx and particulate emissions trends for the baseline low sulfur diesel, the Cummins 2002 EPA engine certification emissions levels are presented in Appendix E. Both the NOx and PM emissions levels measured at MIT agree very well with the data provided by Cummins for the baseline fuel, thus confirming the repeatability of the results.

9.0 Conclusions

An investigation into the relationship between fuel properties, combustion characteristics, and exhaust emissions was carried out using a pre-production 2002 Cummins ISB 300 direct injection turbocharged diesel engine. Experimental results indicate that the Syntroleum Fischer-Tropsch gas-to-liquid diesel fuel significantly reduces regulated gaseous and particulate emissions as compared to conventional diesel fuels in a modern direct injection diesel engine.

The advanced subsystems, combustion strategy, and electronic controls employed by the Cummins ISB have a significant effect on the manner in which the fuel properties affect engine-out emissions. The pilot injection, high injection pressures, and retarded injection timing all contribute to reduce the engine's premixed burn fraction, which in turn helps to lower engine-out NOx emissions. Furthermore, these factors reduce the sensitive dependence of NOx emissions on the fuel properties such as cetane number.

A number of thermodynamic indicators, calculated based on the in-cylinder pressure measurements, show that the FT fuel burns faster during the latter part of combustion, as compared to conventional petroleum-based diesel fuels. The faster burn rate of the FT fuel combined with a more uniform heat release profile and longer tail-end burn may help to reduce particulate formation and increase PM oxidation in the power cylinder, thus aiding in the reduction of particulate emissions. Furthermore, previous studies have shown that FT fuel reduces the NOx/PM trade-off, which in conjunction with retarded injection timing and increased EGR rates provide an optimal combination of both NOx and particulate reduction [35, 36]. In addition, the multiple injection strategy employed by the Cummins ISB has a significant effect on the in-cylinder combustion process and plays a significant role in reducing NOx and PM emissions relative to older technology engines.

The experiments performed over the duration of this project include comparisons of the combustion and emissions characteristics of FT fuel with a conventional low sulfur diesel fuel (400 PPM sulfur), ultra-low sulfur diesel (15 PPM sulfur), and a blend of

25%FT/75% LSD by volume. The engine operating conditions included nearly the entire Euro-III 13-mode test cycle with the exception of the 100% load conditions. The data collected over the course of this project leads to the following major conclusions:

- Both the FT diesel and the FT/LSD blend reduced regulated emissions for all test conditions and exhibited similar emissions trends. The FT diesel yielded a reduction in particulate emissions of 54% on average when compared with the low sulfur diesel and 30% on average when compared with the ultra-low sulfur diesel. Furthermore, the blend exhibited a reduction in PM emissions of 28%, nearly the same as the ULSD, when compared with the low sulfur baseline diesel.

- The blend produced a more than proportional reduction in particulate emissions when compared to the reduction obtained using the neat FT fuel alone. A blend of 25% (by volume) FT fuel with 75% 400 PPM sulfur fuel showed that the 25% FT fuel in the blend produced about half of the particulate reduction of using neat FT fuel alone.

- Significant non-sulfur effects are responsible for the large reductions in PM emissions observed for the FT fuel and blends. The results of the PM analysis carried out at the emission/chemistry laboratory of a major engine manufacturer confirms these findings, and demonstrated reductions in the range of 40% to 60% in SOL and SOF for the blend when compared to the reductions observed for the neat FT fuel alone.

- The neat FT diesel reduced NOx emissions by 15% on average over all of the test conditions. The NOx reductions with the ultra-low sulfur diesel and blend were not as significant with the blend reducing NOx emissions by 2% and the ULSD reducing NOx emissions by 4% on average.

- The reduction in NOx emissions for the FT fuel and blend was directly correlated to the measured reduction in exhaust temperatures, shorter diffusion burn, and

reduced pre-mixed heat release. This data confirms that a temperature sensitive extended Zeldovich type mechanism is primarily responsible for NOx formation in the power cylinder [10].

- While emissions of hydrocarbons were low, and typically within acceptable limits, the significantly higher rate of HC emissions from the ultra-low sulfur diesel fuel is most likely due to the fuel's higher volatility and significantly different distillation curve. These two factors may also be responsible for the relatively higher sulfur to sulfate conversion rate observed for the ULSD [10].

- The increased cetane number of the FT and blend decreased the ignition delay compared to the baseline fuel. The shorter ignition delay and lower density of the FT fuel and blend contributed to a significant reduction in the maximum heat release of the pilot injection, thus reducing initial particulate formation [10].

- FT fuel burns faster during the latter part of combustion. The faster 50% to 90% burn duration and longer tail-end burn of the FT fuel may lead to additional particulate oxidation in the power cylinder [10].

- The contribution of the sulfur in the lubricant oil to the total particulate sulfates increases substantially as the fuel sulfur levels decrease. For the 15 PPM ULSD, the contribution of the sulfur in the lubricant oil made up 63% to 74% of the total PM sulfates. Furthermore, the sulfur in the lubricant oil made up 100% of the PM sulfates for the FT fuel.

- The zero sulfur content of the FT fuel allows for the determination of the lubricant oil sulfur contribution to the total engine-out sulfur levels (gaseous and particulate). Despite this fact, not all of the fuel and oil sulfur could be accounted for in the exhaust.

The major conclusions supported by the experimental data listed above contribute significantly to a fundamental understanding of the emissions behavior of Syntroleum FT fuel in an unmodified modern diesel engine. The differences in the fuel's chemical and physical composition, combustion characteristics, and interaction with the engine technology explain fairly well the observed emissions trends. However, despite much of the progress in expanding the fundamental knowledge base of FT fuels and their effect on emissions, the experimental results raise a number of additional questions as well.

It is, therefore, proposed that further studies be undertaken to investigate the observed discrepancy between the measured and expected exhaust sulfur levels. A mass balance taking into consideration the lubricant oil and fuel sulfur contributions, as well as the mechanisms for the consumption and transport of lube oil- and fuel- derived sulfur through the power cylinder, lubricant, engine, and exhaust systems should provide further insight into the actual processes involved. Furthermore, as fuel sulfur levels continue to decline, the relative magnitude of the contribution of lube oil-derived sulfur to the total particulate mass increases significantly, as do the detrimental effects of sulfated ash on the long term performance and service life of diesel aftertreatment systems.

Lastly, this report has demonstrated the significant improvements in engine performance and emissions reduction that can be achieved when Fischer-Tropsch fuels are used in modern diesel engines. However, additional improvements in performance and further reductions in emissions can be realized by calibrating the engine to take advantage of the FT fuel's properties, along with the addition of exhaust aftertreatment systems. Furthermore, the sulfur-free nature of the FT fuel allows for the use of additional and more aggressive exhaust aftertreatment devices, previously impossible due to the deleterious effects of fuel sulfur on the catalyst. Thus, further investigation into the potential benefits of Fischer-Tropsch fuels used in conjunction with advanced aftertreatment devices should be the subject of future studies.

10.0 References

1. Heywood, J. B., Internal Combustion Engine Fundamentals, McGraw-Hill, Inc., New York, 1988.
2. Adler, U., Editor-in-Chief, Bosch Automotive Handbook, 2nd Edition, Robert Bosch GmbH, Stuttgart, 1986.
3. DieselNet Technology Guide, http://www.dieselnet.com/tg.html/, 2005.
4. Diesel Technology Forum, "Where is Diesel: Cars, Trucks, and SUVs," http://www.dieselforum.org/where-is-diesel/cars-trucks-suvs/, 2005.
5. Sappok, A.G., and Wong, V.W., "Comparative Particulate Trap Performance using Fischer-Tropsch and Conventional Diesel Fuels in a Modern CI Engine," ASME paper ICES2006-1345, 2006.
6. Charles River Associates, "Diesel Technology and the American Economy," Diesel Technology Forum Report no. D02378-00, 2000.
7. R.L. Polk and Company, "Make/Model Registration Volume by Fuel, Industry Registration Volume by Fuel: 2000-2004," Polk® Automotive Intelligence, 2004.
8. Frank, H.J., "Germany's Auto Industry: Upbeat on 2004 – Will the Diesel Boom Continue?," Deutsche Bank Research, http://www.dbresearch.com, 2003.
9. Swiss Agency for the Environment, Forests and Landscape, "Vert-Filterliste: Gepruefte und erprobte Partikelfilter-Systeme fuer die Nachruestung von Dieselmotoren," Bern, Switzerland, 2005.
10. Sappok, A., Llaniguez, J., Acar, J., and Wong, V., "Emissions and In-Cylinder Combustion Characteristics of Fischer-Tropsch and Conventional Diesel Fuels in a Modern CI Engine," ASME Paper ICEF2005-1326, 2005.
11. EPA Office of Transportation and Air Quality, "Mobile Source Black Carbon Emissions," Black Carbon Emissions and Climate Change: A Technical Workshop, San Diego, http://www.nrel.gov/vehiclesandfuels/nfti/pdfs/bc12_j_somers.pdf, 2004.
12. Klanner, W., "Car Emissions and Euro 5 Consumers View," ADAC Workshop, Brussels, http://www.fiafoundation.com/, 2005.
13. Johnson, J.H., Bagley, S.T., Gratz, L.D., and Leddy, D.G., "A review of Diesel Particulate Control Technology and Emissions Effects," SAE paper 940233, 1994.
14. Schweizerischen Krebsliga "Dieselpartikel Luftschadstoff Nr. 1: Wirkungen auf den menshclichen Organismus und technische Loesungen zur Eliminierung dieses Schadstoffs," 2004.
15. Dorenkamp, R., "Dieseltechnologien fuer zukunftige Emissionserfuellung," Third FAD Conference, Dresden, Germany, 2005.
16. Thompson, N., Stradling, R., Zemroch, P.J., Sams, T., and Neuntefel, A., "Fuel Effects on Regulated Emissions from Advanced Diesel Engines and Vehicles," SAE paper 2004-01-1880, 2004.
17. Frank, B.P., Tang, S., Lanni, T., Rideout, G., Beregszaszy, C., Meyer, N., Chatterjee, S., Conway, R., Lowell, D., Bush, C., and Evans, J., "A Study of the Effects of Fuel Type and Emission Control Systems on Regulated Gaseous Emissions from Heavy-Duty Diesel Engines," SAE paper 2004-01-1085, 2004.

18. Alleman, T. L. and McCormick, R. L., "Fischer-Tropsch Diesel Fuels – Properties and Exhaust Emissions: A Literature Review," SAE Paper 2003-01-0763, 2003.
19. Schaberg, P. W., Myburgh, I. S., Botha, J. J., Roets, P. N., Viljoen, C. L., Dancuart, L. P., and Starr M.E., "Diesel Exhaust Emissions Using Sasol Slurry Phase Distillate Process Fuels," SAE Paper 972898, 1997.
20. Sirman, M.B., Owens, E.C., and Whitney, K.A., "Emissions Comparison of Alternative Fuels in an Advanced Automotive Diesel Engine," SAE paper 2000-01-2048, 2000.
21. Fanick, E.R., Schubert, P.F., Russell, B.J., and Freerks, R.L., "Comparison of Emission Characteristics of Conventional Hydrotreated, and Fischer-Tropsch Diesel Fuels in a Heavy-Duty Diesel Engine," SAE paper 2001-01-3519, 2001.
22. May, M. P., Vertin, K., Ren, S., Gui, X., Myburgh, I. And Schaberg, P., "Development of Truck Engine Technologies for Use with Fischer-Tropsch Fuels," SAE Paper 2001-01-3520, 2000.
23. Mallmo, F., Badami, M., and Millo, F., "Analysis of Multiple Injection Strategies for the Reduction of Emissions, Noise and BSFC of a DI CR Small Displacement Non-Road Diesel Engine," SAE paper 2002-01-2672, 2002.
24. Tilch, B., and Seiler, V., "Messtechnik zur Erfassung der Partikelemission im Abgasstrang eines Dieselmotors," Technische Universitaet Braunschweig, Institut fuer Verbrennungskraftmashinen, 2005.
25. EPA Test Procedure TP 713D, "Sample Collection, Continuous Hydrocarbon Analysis and Particulate Collection of the Light Duty Diesel Test Procedure."
26. Plumley, M.J., "Lubricant Oil Consumption Effects on Diesel Exhaust Ash Emissions using a Sulfur Dioxide Tracer Technique and Thermogravimetry", Master's thesis, Massachusetts Institute of Technology, Cambridge, MA, 2005.
27. Bechmann, O., Carli, S., Engeler, W., Garbe, T., Lach, G., Ryan, L., and Schindler, K.P., "Partikelemission und –messung aus Sicht des Anwenders: heute und morgen," Organisation Internationale des Constructeurs D'Automobiles, http://www.oica.net, 2002.
28. Norton, P., Vertin, K., Bailey, B., Clark, N. N., Lyons, D. W., Goguen, S., and Eberhardt, J., "Emissions from Trucks using Fischer-Tropsch Diesel Fuel," SAE Paper 982526, 1998.
29. Clark, N. N., Atkinson, C. M., Thompson, G. J. and Nine, R. D., "Transient Emissions Comparisons of Alternative Compression Ignition Fuels," SAE Paper 1999-01-1117, 1999.
30. Atkinson, C. M., Thompson, G. J., Traver, M. L., and Clark, N. N., "In-Cylinder Combustion Pressure Characteristics of Fischer-Tropsch and Conventional Diesel Fuels in a Heavy-duty CI Engine," SAE Paper 1999-01-1472, 1999.
31. Springer, P. S., Hugman, R. H., Costiness, M. J., Vidas, E. H., "Chemical Composition of Discovered and Undiscovered Natural Gas in the Continental United States – 1998 Update. Project Summary," Gas Research Institute, 1998.
32. McMillian, M. H. and Gautam, M., "Consideration for Fischer-Tropsch Derived Liquid Fuels as a Fuel Injection Emission Control Parameter," SAE Paper 982489, 1998.

33. Cheng, A. S. and Dibble, R. W., "Emissions Performance of Oxygenate-in-Diesel Blends and Fischer-Tropsch Diesel in a Compression Ignition Engine," SAE Paper 1999-01-3606, 1999.
34. Schaberg, P. W., Myburgh, I. S., Botha, J. J. and Khalek, I. A., "Comparative Emissions Performance of Sasol Fischer-Tropsch Diesel Fuel in Current and Older Technology Heavy-Duty Engines," SAE Paper 2000-01-1912, 2000.
35. Llaniguez, J.T., "A Fundamental Study of Relationships Among Fuel Properties, Combustion Characteristics, and Emissions with Normal and Synthetic Diesel Fuel", Master's thesis, Massachusetts Institute of Technology, Cambridge, MA, 2003.
36. Acar, J., 2003, "Effect of Engine Operating Parameters and Fuel Characteristics on Diesel Engine Emissions", Master's thesis, Massachusetts Institute of Technology, Cambridge, MA, 2005.
37. Lee, R., Pedley, J., and Hobbs, C., "Fuel Quality Impact on Heavy-duty Diesel Emissions: - A Literature Review," SAE paper 982649, 1998.
38. Thomas, R.W., Buckingham, J., Dodge, L.G., and Olikara, C., "The Effects of Fuel Properties on Emissions from a 2.5gm NOx Heavy-duty Diesel Engine," SAE paper 982491, 1998.
39. Cowley, L.T., Stradling, R.J., and Doyon, J., "The Influence of Composition and Properties of Diesel Fuel on Particulates Emissions from Heavy-duty Engines," SAE paper 932732, 1993.
40. McKinley, T., "Modeling Sulfuric Acid Condensation in Diesel Engine EGR Coolers", SAE paper 970636, 1997.
41. Alleman, T.L., and McCormick, R.L., "Fischer-Tropsch Diesel Fuels – Properties and Exhaust Emissions: A Literature Review," SAE paper 2003-01-0763, 2003.
42. Kwon, Y., Mann, N., Rickeard, D.J., Haugland, R., Ulvund, K.A., Kvinge, F., and Wilson, G., "Fuel Effect on Emissions- A New Understanding", SAE paper 2001-01-3522, 2001.
43. Rickeard, D.J., Bonetto, R., and Signer, M., "European Programme on Emissions, Fuels and Engine Technologies (EPEFE) – Comparison of Light and Heavy-duty Diesel Studies", SAE paper 961075, 1996.
44. Atkinson, C.M., Thompson, G.J., Traver, M.L., and Clark, N.N., "In-Cylinder Combustion and Pressure Characteristics of Fischer-Tropsch and Conventional Diesel Fuels in a Heavy-duty CI Engine," SAE paper 1999-01-1472, 1999.
45. McMillian, M.H., and Gautam, M., "Combustion and Emission Characteristics of Fischer-Tropsch and Standard Diesel Fuel in a Single-Cylinder Diesel Engine," SAE paper 2001-01-3517, 2001.
46. Mann, N., Kvinge, F., and Wilson, G., "Diesel Fuel Effects on Emissions – Towards a Better Understanding," SAE paper 982486, 1998.
47. Liu, Y., and Reitz, R.D., "Optimizing HSDI Diesel Combustion and Emissions Using Multiple Injection Strategies", SAE paper 2005-01-0212, 2005.
48. Gill, K., Marriner, C., Sison, K., and Zhao, H., "In-Cylinder Studies of Multiple Diesel Fuel Injection in a Single Cylinder Optical Engine", SAE paper 2005-01-0915, 2005.
49. "Syntroleum S-2 Synthetic Diesel: Driving Clean-Fuel Innovation," http://www.syntroleum.com/media/syntroleum_s2.pdf, Syntroleum Corporation, 2002.

50. EPA Test Procedure TP 714C, "Diesel Particulate Filter Handling and Weighing Procedure."
51. Kweon, C.B., Foster, D.E., Schauer, J.J., and Okada, S., "Detailed Chemical Composition and Particle Size Assessment of Diesel Engine Exhaust", SAE paper 2002-01-2670, 2002.
52. Assanis, D. N., "A Computer Simulation of the Turbocharged Turbocompounded Diesel Engine System for Studies of Low Heat Rejection Engine Performance," Ph.D. Thesis, MIT, 1985.
53. Warner, J., Johnson, J., Bagley, S., and Huynh, C., "Effects of a Catalyzed Particulate Filter on Emissions from a Diesel Engine: Chemical Characterization Data and particulate Emissions Measured with Thermal Optical and Gravimetric Methods," SAE Paper 2003-01-0049, 2003.
54. Frank, B., Tang, S., Lanni, T., Rideout, G., Beregszaszy, C., Meyer, N., Chatterjee, S., Conmway, R., Lowell, D., Bush, C., Evans, J., "A Study of the Effects of Fuel Type and Emission Control Systems on Regulated Gaseous Emissions from Heavy-Duty Diesel Engines," SAE paper 2004-01-1085, 2004.

Appendix A Experimental Setup

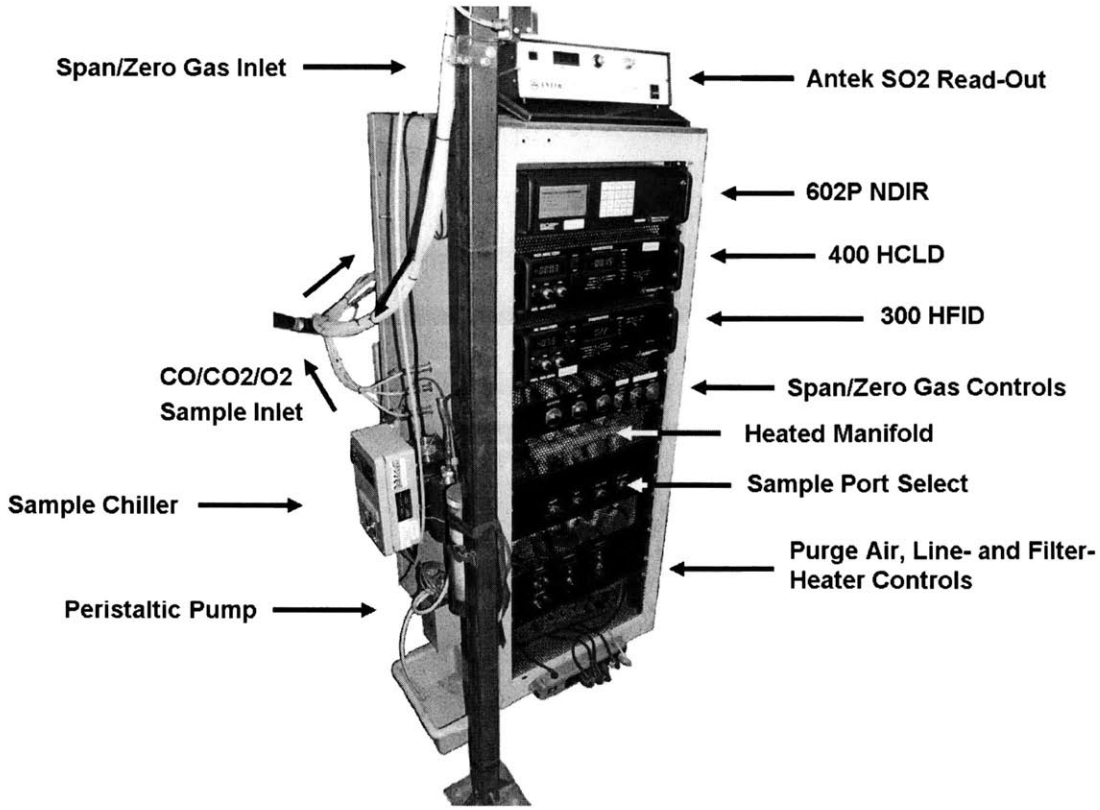

Figure A.1. Gaseous emissions analyzer rack

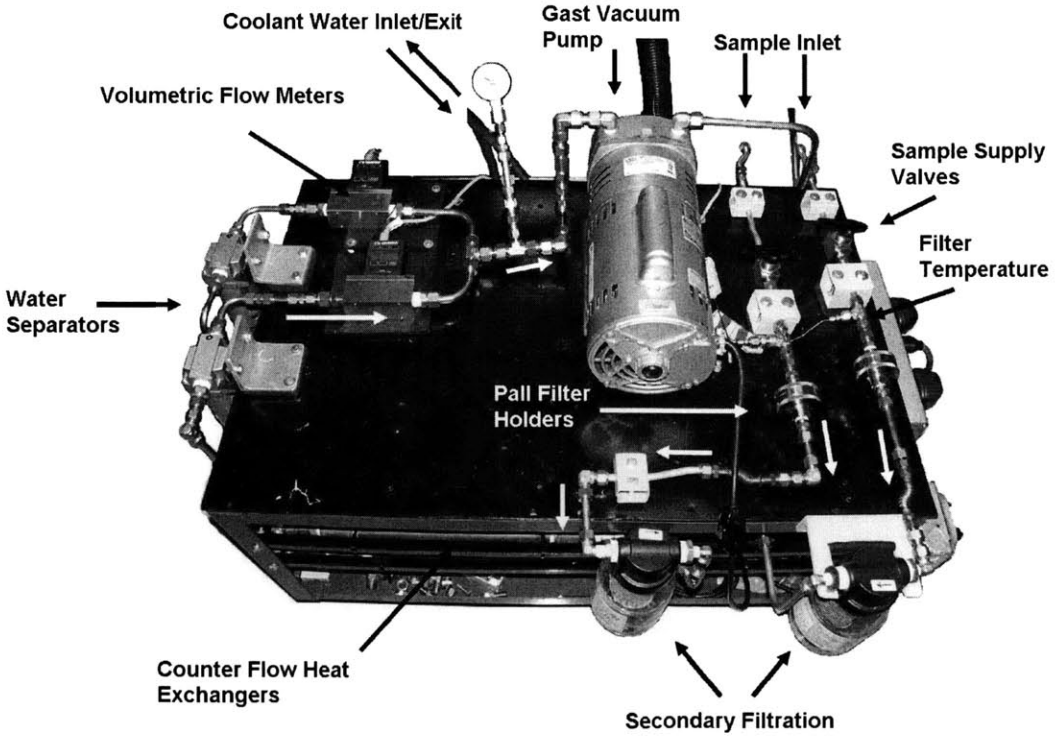

Figure A.2. Particulate sampling system

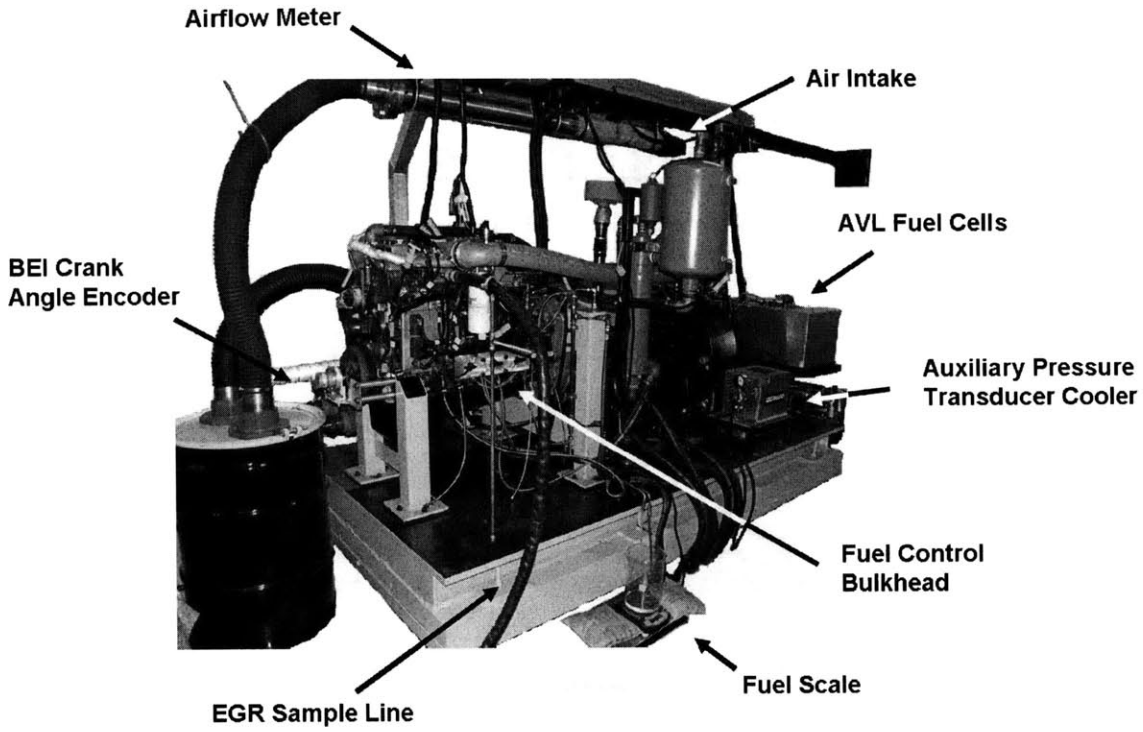

Figure A.3. Cummins ISB 300 on test bed. Note fuel container and balance for measuring fuel flow as well as heated sample line to measure EGR fraction in the intake manifold in the foreground.

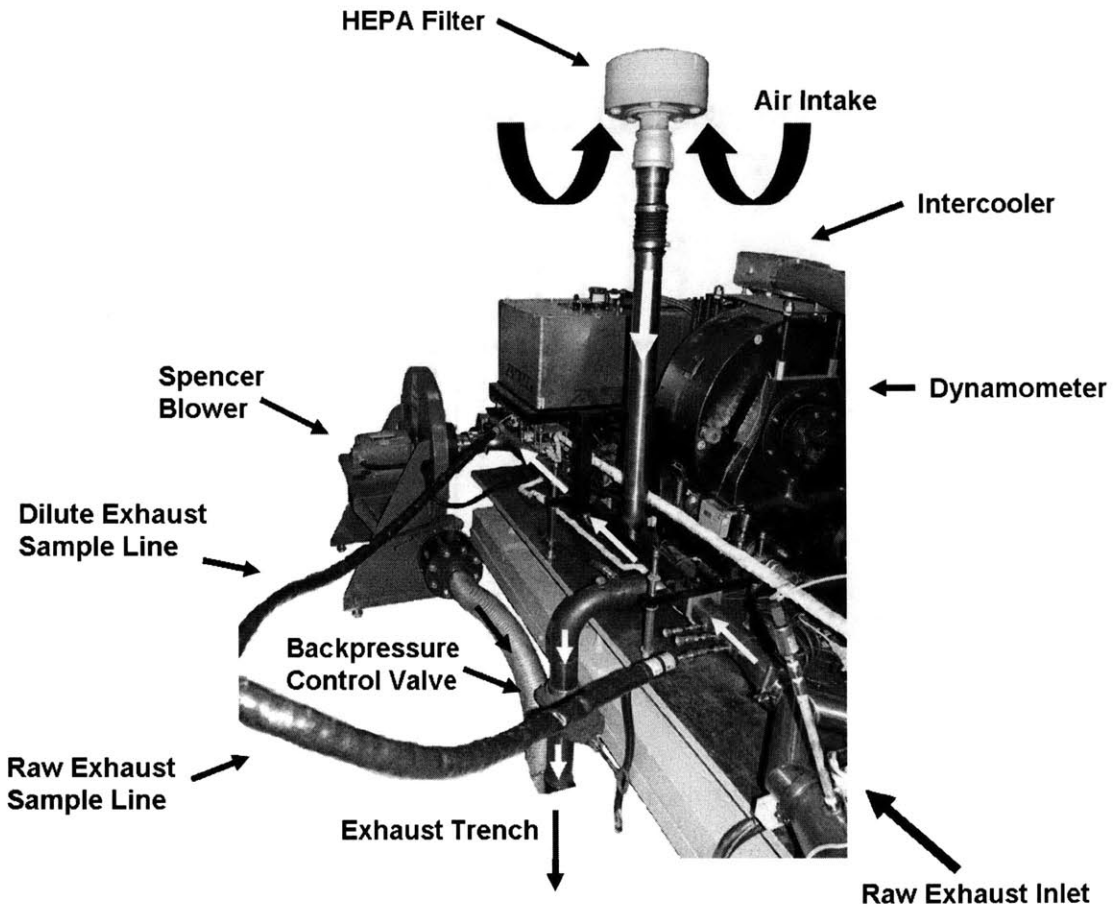

Figure A.4. Mini dilution tunnel and associated hardware showing heated sample lines used to sample gaseous emissions before and after the tunnel.

Appendix B ISB 300 Performance Data

FTP / SET Emissions Zone Calculations:					
Description:	RPM	25%Torque	50%Torque	75%Torque	100%Torque
"A" (25%RPM)	1682	165	330	495	660
"B" (50%RPM)	2013	165	329	494	658
"C" (75%RPM)	2345	160	320	479	639

Table B.1. Euro-III 13-mode test conditions for the Cummins ISB 300

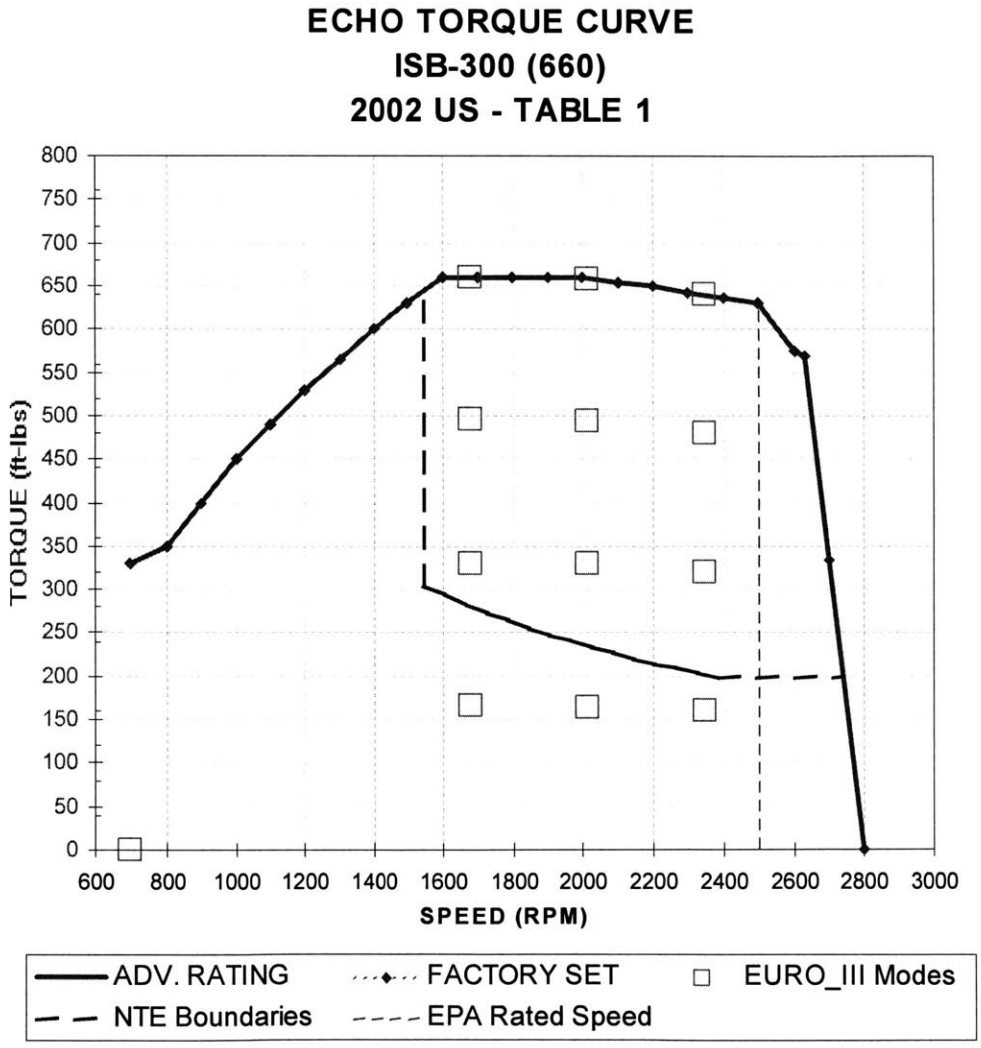

Figure B.1. Cummins ISB 300 2002 EPA certification torque curve

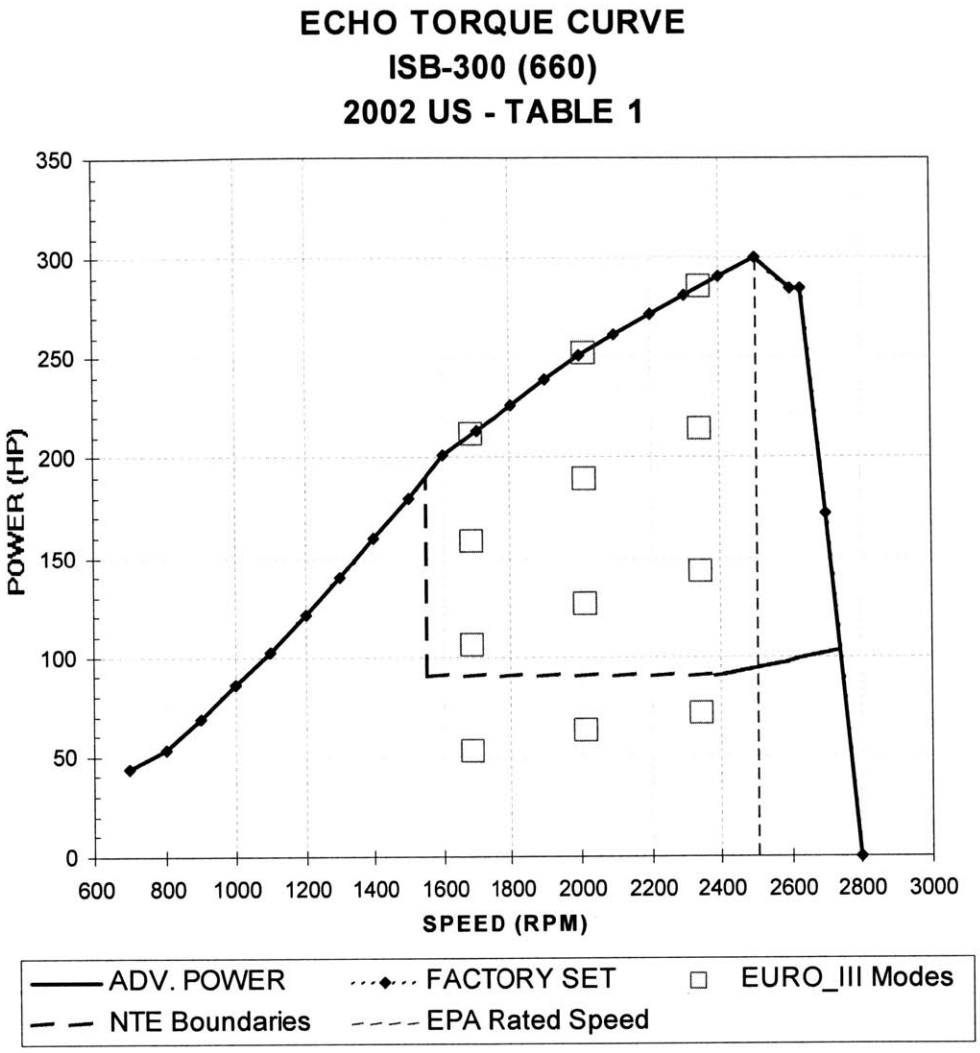

Figure B.2. Cummins ISB 300 2002 EPA certification power curve

(This page intentionally left blank)

Appendix C Measurement and Data Acquisition Systems

Measurement	Instrument Type	Device: 1102B (1)	Device: 1100	Device: 1102B (2)	Device: PCI-6024E
Cylinder 1 Exhaust TC	Type K TC	0	--	--	--
Cylinder 2 Exhaust TC	Type K TC	1	--	--	--
Cylinder 3 Exhaust TC	Type K TC	2	--	--	--
Cylinder 4 Exhaust TC	Type K TC	3	--	--	--
Cylinder 5 Exhaust TC	Type K TC	4	--	--	--
Cylinder 6 Exhaust TC	Type K TC	5	--	--	--
EGR TC: Before Cooler	Type K TC	6	--	--	--
EGR TC: After Cooler	Type K TC	7	--	--	--
Heat Exchanger: City Water Outlet	Type K TC	8	--	--	--
Heat Exchanger: City Water Inlet	Type K TC	9	--	--	--
Turbine Outlet TC	Type K TC	10	--	--	--
Intake Manifold TC	Type K TC	11	--	--	--
Exhaust Manifold TC	Type K TC	12	--	--	--
Coolant Reservoir TC	Type K TC	13	--	--	--
Heat Exchanger: Engine Coolant Outlet	Type K TC	14	--	--	--
Heat Exchanger: City Water Inlet	Type K TC	15	--	--	--
Engine Block Oil TC	Type K TC	16	--	--	--
Compressor Outlet TC	Type K TC	17	--	--	--
Fuel Supply TC	Type K TC	18	--	--	--
Dynamometer TC: Inner Loss Plate	Type K TC	19	--	--	--
Dynamometer TC: Outer Loss Plate	Type K TC	20	--	--	--
Dynamometer TC: Bearing no. 1	Type K TC	21	--	--	--
Dynamometer TC: Bearing no. 2	Type K TC	22	--	--	--
Dynamometer Water Pressure	Pressure Transducer	23	--	--	--
Thermo-Hygrometer	0-10 VDC	24	--	--	--
Exhaust Pressure	Pressure Transducer	25	--	--	--
Engine Block Oil Pressure	Pressure Transducer	26	--	--	--
Turbine Exhaust Pressure	Pressure Transducer	27	--	--	--
Intake Manifold Pressure	Pressure Transducer	28	--	--	--
Fuel Lift Pump Pressure	Pressure Transducer	29	--	--	--
Exhaust Manifold Pressure	Pressure Transducer	30	--	--	--
Coolant Reservoir Pressure	Pressure Transducer	31	--	--	--
Cylinder 6 Pressure Transducer	Pressure Transducer	--	0	--	--
Fluke Current Probe	Hall-Effect Sensor	--	1	--	--
Intake Air Flow Meter	Dual RTD	--	2	--	--
Dilution Tunnel: Pre-Dilution	Type K TC	--	3	--	--
Dilution Tunnel: Post-Dilution	Type K TC	--	4	--	--
Ambient Temperature	Type K TC	--	5	--	--
Post-Filter TC	Type K TC	--	6	--	--
Pre-Filter TC	Type K TC	--	7	--	--
Engine Torque	Digalog Controller	--	10	--	--
Engine RPM	Digalog Controller	--	11	--	--
Charge Air Cooler	Type K TC	--	13	--	--
PM Sample Flow 2	0-5 VDC	--	14	--	--
Exhaust Temperature	Type K TC	--	15	--	--
HFID Range 1-8	0-5 VDC	--	16-23	--	--
HFID Voltage	0-5 VDC	--	25	--	--
HFID Oven Temperature	0-5 VDC	--	26	--	--
PM Sample Flow 1	0-5 VDC	--	29	--	--
NOx Voltage	0-10 VDC	--	30	--	--
NO Voltage	0-10 VDC	--	31	--	--
Crankshaft Sensor	Hall-Effect Sensor	--	--	--	2
Exhaust TR TC	Pressure Transducer	--	--	0-9	--
Exhaust TL TC	Pressure Transducer	--	--	10-17	--
Exhaust TP	Pressure Transducer	--	--	19-21	--
CO2 Voltage	0-10 VDC	--	--	23	--
CO Voltage	0-10 VDC	--	--	24	--
O2 Voltage	0-10 VDC	--	--	25	--

Table C.1. Measured parameters and corresponding instruments and DAQ channels

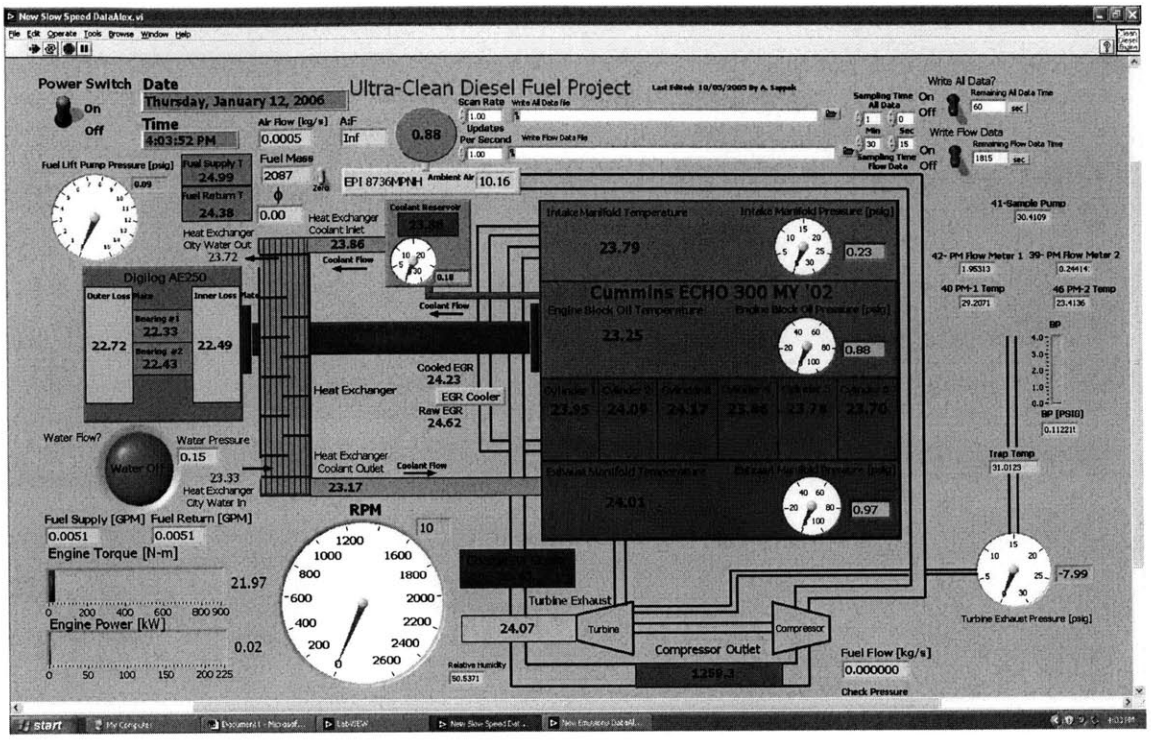

Figure C.1. Slow-speed data acquisition VI

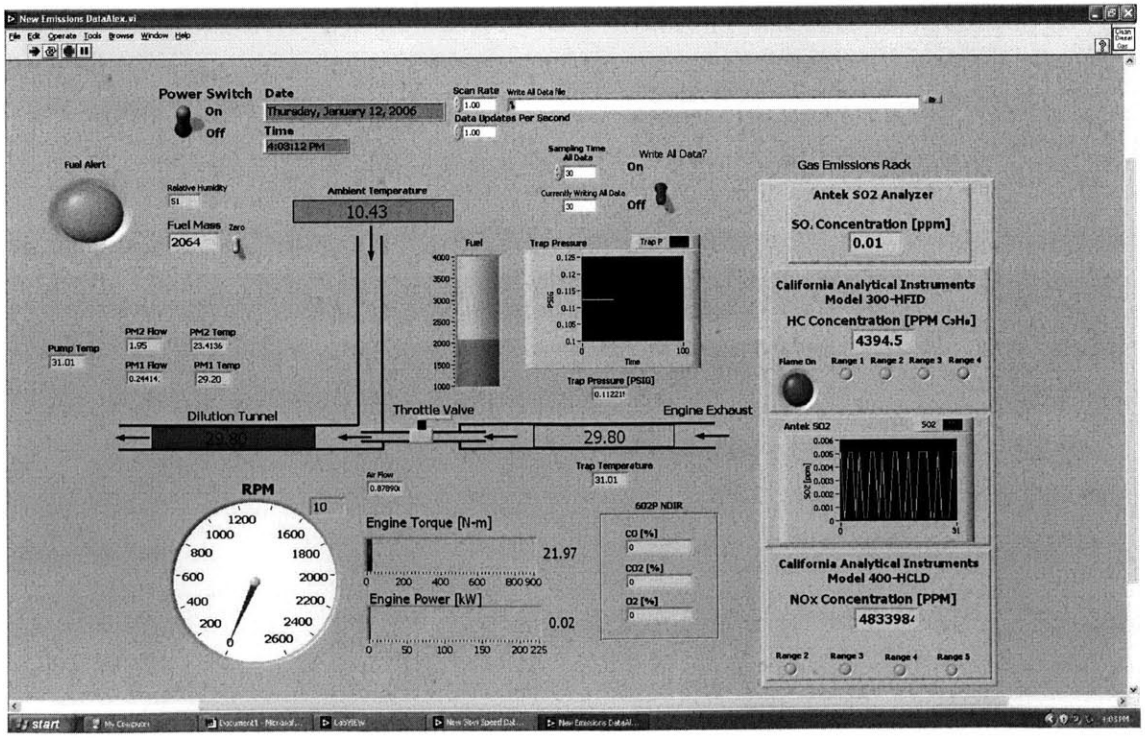

Figure C.2. Emissions data acquisition VI

(This page intentionally left blank)

Appendix D Data Analysis Code

Appendix D.1. MatLab program used to filter in-cylinder pressure data prior to processing with heat release program.

```
%Function Written To Load High-Speed Data Taken From National
Instruments SCXI DAQ System.
%Also, Filters Pressure Data

%High-Speed Data File Format

%Column 1              Column 2                Column 3
%Pressure          Crankshaft Sensor      Intake Manifold Pressure
% [Bar]                [Volts]                 [PSIG]

%If Data Format Does Not Match Above, Change The Following To Reflect
The Proper Column

Pcolumn = 1;
Crankcolumn = 2;
MAPcolumn = 3;

file=inputdlg({'Enter file name of input data:','Enter engine
RPM:','Enter low-pass cut-off as multiple of RPM:'},...
'YA RIGHT Data Analysis',1,{'C25pcp10.txt','2342','100'});
data = load(char(file{1}));
%Load High-Speed Data File)
Pdata = data(:,Pcolumn);
%Create Pressure Vector
Crankdata = data(:,Crankcolumn);
%Create Crankshaft Voltage Vector
MAPdata = data(:,MAPcolumn);
%Create MAP Vector
RPM=str2num(file{2});
cutoff=str2num(file{3});
clear w; clear s; clear s1; clear S; clear S1;
format long e
%count the number of cycles in input data
%(count on high-to-low shift of crank column)
low=1.;
iflip=0;
nrev=0;
n=0;
N=length(Crankdata);
tooth=zeros(N,1);
 for i=1:N
     if(Crankdata(i,1)<low)
         if(iflip==0)
             itemp=i;
         end
         iflip=1;
         n=n+1;
     end
     if((Crankdata(i,1)>=low)&(iflip==1))
         iflip=0;
         if(n>25)
             nrev=nrev+1;
             tooth(nrev,1)=itemp;
```

```
        end
        n=0;
    end
  end
  tooth=tooth(1:nrev,1);
  n=tooth(nrev,1)-tooth(1,1);
  nrev=nrev-1;
  %sampling period, dt, and sampling freq., fsample
  dt=nrev/n*2*60/RPM;
  %sampling frequency in Hz
  fsample=1/dt;
  %truncate data to begin and end at TDC intake
  %number of data points per degree of crankshaft rotation
  ndeg=n/nrev/360;
  %check to see if first notch on compression or exhaust stroke
  %assume falling edge of notch at 280 degrees after TDC intake
if(Pdata(round(tooth(1,1)+60*ndeg))>Pdata(round(tooth(2,1)+60*ndeg)))
      ifirst=round(tooth(2,1)+79.6*ndeg);
      nrev=nrev-2;
  else
      ifirst=round(tooth(1,1)+79.6*ndeg);
      nrev=nrev-1;
  end
  %throw out first and last cycle and start and end at TDC intake
  if(rem(nrev,2)~=0)
      nrev=nrev-1;
  end
  ilast=round(ifirst+(nrev)*ndeg*360);
  Pdata=Pdata(ifirst:ilast,1);
  Punfiltered = Pdata;
  %Convert From Time To Frequency Domain.
  transform=fft(Pdata);
  N=length(Pdata);
  %Finite Fourier Transform On Data
  f=fsample*(1:N)/N;
  %frequencies above Nyquist frequency are redundant
  %Nyquist frequency is 0.5*fsample
  fNyquist=0.5*fsample;
  %look at power spectrum
  %P=transform.*conj(transform)/N;
  %Assume frequencies above 'high' are noise
  high=cutoff*RPM/60/2;
  %Upper Limit Of Frequencies
  %Eliminate Frequencies Above High
  for i=1:(N+1)/2
      if (f(i)>=high)
          transform(i,:)=0;
          transform(N+1-i,:)=0;
      end
  end
  %Convert From Frequency Domain To Time Domain
  time=ifft(transform);
  %Combine Magnitude And Phase To 'Recreate' P
  Pdata = abs(time).*cos(angle(time));
  %linearly interpolate pressure data to be at 0.2 degree steps
  t=[0:1/ndeg:(N-1)/ndeg]';
  tnew=[0:0.2:nrev*360]';
```

```
    tnew=tnew(1:(size(tnew)-1),1);
    Pdata2=zeros(length(tnew),1);
    Pdata2=interp1(t,Pdata,tnew);
    plot(Punfiltered);
    hold; plot(Pdata,'r');
%data = [Pdata Crankdata MAPdata];
save filtered.txt Pdata2 -ASCII -TABS
msgbox(['The Nyquist frequency is ',num2str(fNyquist),' Hz',...
       ' and the cutoff frequency is ',num2str(high),' Hz. There are
',num2str(nrev/2),' cycles. ',...
       'Number of data points per cycle is ',num2str(ndeg*720)],'YA
RIGHT Data Analyzer');
%clear data
```

Appendix D.2. Relevant portions of the heat release program used in the calculation of the thermodynamic indicators to quantify the combustion characteristics of the fuels.

```
C*************************************************************************
C*          Simple Heat Release Analysis Based on First Law
C*                          Written By: Dr. Victor Wong
C*                          Modified by: Jeremy Llaniguez, Jeff Jocsak, Alexander Sappok
C*************************************************************************
logical pcal
dimension psd(3600),hrg(3600),qiallw(3600),volca(3600),
&tbulk(3600),pdsyn(3600),cumhr(3600),hrn(3600)
common bore,stroke,crl,cr,viarea,vearea,cdin,cdex,rpm,tin,pin,
&      pcrmax,SOImain
common /filter/ w1,w2,w3,w4,mfl,ktype,hfir
common /mnfold/ pim,tim,pem,tem
common /gas/ rgas, cp, cv, gamma
common /valtim/ caivc,caevo,caeend,caend, castep, cpstep
common /valflo/nin,nex
common /eff/effc,efft,effm
common /burn/casoc,burn90,fpower,qlower,fpc
common /heat/temp,alinr,pspeed,ahdpst,re,prandl,cmuprl,twal, hcoef
common /hwalls/hcst(3),twalli(3),twallp(3),twallh(3)
common /change/cm(3),par(3),parout,ch(3),pah(3),pahout
common /conduc/condin(3),din(3),cndout(3),dout(3),hext(3),text(3)
common /ddd1/caivo,caevc,icycnum,timc,trqini
common /prdata/ca(3600),p(3600),dnl(3600),cca(3600),ps(3600),
&            pfil(3600)
common /ativc/pinit,vinit,tinit,trapm,pi,avpspd,hbore
common /burnsp/cainj,caignd,cabdur,abeta,bbeta,cbeta,c1pmix,
& c2pmix,c1diff,c2diff,c3diff,c4diff,afstoi,betasp,pcal
real Pmax, CApmax(3600)
external pderiv
C
C  Read general inputs
C
call readin
C
C  Read pressure data
C
call readp
C
C  Prepare initial variables used in the calculation
C
     avpspd=stroke*rpm/30.                    !Mean Piston Speed [m/s]
     rgas=8314.3/28.962                       !Universal Gas Constant [J/kg-K]
     cv=rgas/(gamma-1.)                       !Constant Volume Specific Heat
     cp=gamma*cv                              !Constant Pressure Specific Heat
     pi=3.14159265                            !pi
     ahdpst=pi*bore**2/4.                     !Piston Head Area [m^2]
     alner=pi*bore*stroke*cr/(cr-1.)          !Cylinder Liner Area [m^2]
     hbore=bore/2.                            !Half Of Bore, Radius [m]
     vdispl=pi/4.*bore*bore*stroke            !Displaced Volume [m^3]
```

```
      vc=vdispl/(cr-1.)                                    !Clearance Volume [m^3]
      fpc=fpower/qlower*120./rpm/float(icycnum)            !Fuel Per Cycle Per Cylinder
C
write (6,*) 'Fuel Energy =',fpower,'kW','Fuel Per Cylinder=',fpc
C
tstep=castep/rpm/6.                                        !Time Steps For Integration
C
C  Add Reference Pressure To Raw Data, Assuming Average p Before IVC = IMP
C
if ((caivc.lt.90.).or.(caivc.gt.270.)) then
write(6,*)'Check intake valve closing timing convention(90-270)'
stop
endif
nivc=ifix(caivc*5.+0.0001)                                 !IVC Reference
nevo=ifix(caevo*5.+0.0001)                                 !EVO Reference
sumip=0.                                                   !Initialize Intake Pressure Variable
          do 20 i=1,nivc                                   !Loop To Average Pressure
 20       sumip=sumip+p(i)                                 !Cumulative Presesure
          pinavg=sumip/float(nivc)                         !Average Pressure
C
C  Calculate Scaled Pressure For Each Crank Angle
C  All Units Should Be In SI, Thus Pressure Should Be In Pascal, Except Jeremy's Data
C
     do 30 i=1,3600                                        !Loop To Convert Pressure
30        ps(i)=(p(i)-pinavg)*1.0e5+pim                    !Conversion Calculation
C
C  Get pressure time derivatives
C
call deriv5p(ps,tstep,3600,psd)
C
C  Set Initial Cylinder Conditions At IVC
C
          pinit=ps(nivc)                                   !Pressure At IVC
          pinitkPa = pinit/1000                            !Pressure At IVC in kPa
          tinit=tim                                        !Temperature At IVC
          call engvol(caivc,vinit,vdot,spdum,alndum)
          trapm=pinit*vinit/rgas/tinit                     !Trapped Cylinder Mass
          rhoint=trapm/vinit                               !Initial Gas Density
          pvgini=pinit*vinit**gamma                        !Initial PV^gamma
          write(7,*)
          write(7,950) pinitkPa
          write(7,951) tinit
          write(7,952) vinit
          write(7,953) pvgini
 950      format('Pressure At IVC [kPa] = ',f12.3)
 951      format('Temperature At IVC [K] = ',f6.1)
 952      format('Volume At IVC [m^3] = ',e12.3)
 953      format('PV^gamma At IVC = ',f6.3)
C
C  Start cycle calculation loop
C
smwork=0.                                                  !Initialize Work Variable
smhrel=0.                                                  !Initialize Heat Release Variable
smhxfer=0.                                                 !Initialize Heat Transfer Variable
C
do 40 i=nivc, nevo                          !Heat Release Done During "Closed" System
```

```
theta=ca(i)                                    !Index For Current Crank Angle In Loop
C
C  Call engvol To Get Various Engine Geometry Information At Each CA
C
call engvol(theta,vol,vdot,pspeed,alinr)
C
rho=trapm/vol                                  !Gas Density At Any Crank Angle
temp= tinit*ps(i)/pinit*vol/vinit              !Cylinder Average Temperature
tbulk(i)=temp                                  !Bulk Temperature
C
C  Calculate Some Heat Transfer Parameters
C  Heat Transfer Theory Based On Nusselt-Reynolds Correlation:
C  Nu = Constant * Re^d * Pr^e
C  Constant Stored As hcst Array, With All 3 Values = 0.05 (See Input)
C  Prandtl Number Dependence Removed Below Sine Pr ~ Unity
C  For More Information, See Ph.D Thesis By Assanis, 1980
C  Assanis Uses Characteristic Velocity Equation Incorporating Turbulence
C  Models.  More Simplified Approach Applied Here.
C
scale=alinr/pi/bore                            !Characteristic Length Scale
if (scale.ge.hbore) scale=hbore                !Length Scale Restriction
vis=3.3e-4*temp**.7                            !NASA Equilibrium Program
charv=max(abs(pspeed),avpspd/2.)               !Simple Characterisitc Vel.
re=charv*scale*rho/vis                         !Definition Of Re
congas=vis*cp/prandl                           !Conductivity Of Gas
cmuprl=congas/scale                            !Inverse Of RHS Of Nu
 rnuslt=hcst(2)*re**.7                         !Nusselt Number, As Above
 hcoef=cmuprl*rnuslt                           !Solving For h
C
C  Calculate Heat Transfer From Various Parts Of Cylinder
C
qipist=ahdpst*hcoef*(temp-twallp(2))           !Piston Heat Transfer
qihead=ahdpst*hcoef*(temp-twallh(2))           !Heat Heat Transfer
qilinr=alinr*hcoef*(temp-twalli(2))            !Liner Heat Transfer
qiallw(i)=qipist+qihead+qilinr                 !All Wall Heat Transfer
C
C  Calculate Gross Heat Release
C
hrg(i) = qiallw(i)+(cv/rgas+1.)*ps(i)*vdot+cv/rgas*vol*psd(i)
C
C  Calculate Net Heat Release
C
hrn(i) = hrg(i) - qiallw(i)
C
C  Further Calculations For Various Heat Release Characteristics
C
volca(i)=vol
C
C  pdsyn(i) Is P*dV Term In Burn Rate Analysis Mode
C
pdsyn(i)=ps(i)*vdot                            !P*dV Term
C
smwork=smwork+pdsyn(i)*tstep                   !Work
smhrel=smhrel+hrg(i)*tstep                     !Heat Release Up To CA
cumhr(i)=smhrel                                !Cumulative Heat Release
smhxfer=smhxfer+qiallw(i)*tstep                !Cumulative Heat Transfer
```

```
40        continue
C
C  Find where heat release crosses 10%, 50%, and 90%
C
 c10par=0.
c50par=0.
c90par=0.
C
do 45 i=nivc,nevo
hrfrac=cumhr(i)/smhrel
C
C  Find 10% Cross-Over Point
C
if (hrfrac.gt.0.1) then
if (c10par.lt.0.5) ca10=ca(i)
c10par=1.
endif
C
C  Find 50% Cross-Over Point
C
if (hrfrac.gt.0.5) then
if (c50par.lt.0.5) ca50=ca(i)
c50par=1.
endif
C
C  Find 90% Cross-Over Point
C
if (hrfrac.gt.0.9) then
if (c90par.lt.0.5) ca90=ca(i)
c90par=1.
Endif
 45   continue
C
C  Get Pumping Work Integrated Data
C
prewrk=0.
pstwrk=0.
do 60 i=1,nivc
theta=ca(i)
call engvol(theta,vol,vdot,pspeed,alinr)
 60        prewrk=prewrk+ps(i)*vdot*tstep
do 70 i=nevo+1,3600
theta=ca(i)
call engvol(theta,vol,vdot,pspeed,alinr)
 70   pstwrk=pstwrk+ps(i)*vdot*tstep
C
C  Expressed in kW basis at that rpm (ihp):
C
prewkw=prewrk*rpm/120./1000.
pstwkw=pstwrk*rpm/120./1000.
C
C  Expressed in kW basis at that rpm:
C
work=smwork*rpm/120./1000.
hrel=smhrel*rpm/120./1000.
hxfer=smhxfer*rpm/120./1000.
```

```
C  Calculate The Maximum Pressure, It's Location, And The Corresponding
C  Bulk Temperature Of The Cylinder.
C  It Is Unlikely That The Pressure Derivative Will Be Exactly Zero, So
C  Code Computes Where The Derivative Goes Through Zero, Then Checks The
C  Pressure At These Two Crank Angles.
C  Lastly, The Maximum Pressure Locations Are Compared To The Pressure At
C  TDC.  If TDC Is The Maximum Pressure, Then The Next Maximum Pressure
C  At A Crank Angle Greater Than 360 Is Searched For.  This Is Done Since
C  The Clean-Diesel Engine Is Run With Retarded Timings
C
k = 1                                                    !Index For Writting To CApmax
do j = nivc, nevo - 1          !Search Only Within "Closed" System
if ((psd(j)*psd(j+1).LT.0).and.(ca(j).GT.330)) then
CApmax(k) = int(ca(j))     !Array Of CA Where dP Goes Through Zero.
k = k + 1
CApmax(k) = int(ca(j+1))
k = k + 1
endif
enddo
Pmax = 0.                                                !Initialization Of Pmax.
do m = 1,k
n = int(CApmax(m) * 5)   !Reference Back To Heat Release Index
if ((ps(n).GT.Pmax).and.(CApmax(m).GT.360)) then
Pmax = ps(n)
PmaxCA = CApmax(m) + 0.1
Pmaxloc = n
call engvol(CApmax(m),vol,vdot,pspeed,alinr)
rho=trapm/vol                                            !Gas Density At Any Crank Angle
TatPmax=tinit*ps(n)/pinit*vol/vinit   !Cylinder Average Temperature
endif
enddo
PmaxkPa = Pmax/1000
C
C  Find Ignition Delay
C  Ignition Delay Is Defined As The Time Between The Start Of Injection Of
C  The Main Fuel Pulse And When The Heat Release Goes Through Zero From
C  Being Negative.
C  The Main SOI In The Input File Should Reflect The Cummins Covention Found
C  In CalTerm:  Timing in Degrees Before Top Dead Center [°bTDC]
C
k  = 1                                                   !Reinitialize Index
SOIindex = (360 - SOImain) * 5
do j = SOIindex + 50,SOIindex,-1   !Backward Search Algorithm
if (hrg(j)*hrg(j+1).LT.0) then
SOCindex = j
SOC = SOCindex/5 - 0.1
goto 999
endif
enddo
999       SOImain = 360 - SOImain
Delay = SOC - SOImain
C
C  Compute Various Burn Durations
b10t90=ca90-ca10
EOC = ca90
BurnDur = EOC - SOC
```

&input	cbeta=0.38
rpm=1677.	c1pmix=1.0
tim=310.4	c2pmix=1.0
pim=1.822e5	c1diff=9.95
torque=462.8	c2diff=0.63
SOImain=0.65	c3diff=0.98
bore=0.10202	c4diff=0.19
stroke=0.120	afstoi=14.9
icycnum=6	betasp=0.
crl=0.192	pcal=false
cr=17.184	///////
viarea=0.0012	&end
vearea=0.001	&hxfer
gamma=1.3	hcst=0.05,0.05,0.05
caivo=710.5	twallp=450., 450., 450.
caivc=204.	twallh=450., 450., 450.
caevo=502.	twalli=375., 375., 375.
caevc=18.	prandl=0.67
caend=720.0001	///////
castep=0.2	&end
cpstep=0.2	&modify
effc=0.7	cm=335.,410.,520.
efft=0.7	par= 0.,0.,0.
effm=0.8	parout=0.
pcrmax=3.	ch=330.,360.,390.
timc=0.	pah=1.,1.,1.
tin=300	pahout=1.
pin=1.01325e5	//////
//////	&end
&end	&wall
&comb	condin=80., 80., 80.
casoc=355.	cndout=80., 80., 80.
burn90=42.	din=.508e-3, .508e-3, .508e-3
qlower=43.7e6	dout=2.e-2, 2.e-2, 2.e-2
fpower=200.e3	hext=0.,0.,0.
///////	text=350., 350., 350.
&end	//////
&combsp	&end
cainj=360.	&engmap
caignd=10.	spdran=701.,1000.,1500.,2000.,2500.,3000.,3500.,4000.,4500.,5000.,5500.,0.,0.,0.,0.
cabdur=80.	trqran=135.81,115.46,97.68,78.55,58.47,40.,20.,5.,0.,0.,0.,0.,0.,0.,0.
abeta=0.71	/////
bbeta=0.35	&end

Table D.1. Heat release program input parameters. Highlighted values are dependent upon engine operating conditions and fuel type.

Appendix E Comparison to Cummins Emissions Data

MODE No.	SPEED (rpm)	TORQUE (N-m)	NOx (g/hr)	Particulate (g/hr)
1	750	95	**129.6**	**0.0**
2	1682	895	**388.8**	**17.3**
3	2013	446	**242.1**	**7.8**
4	2013	669	**357.5**	**12.7**
5	1682	447	**216.6**	**7.2**
6	1682	671	**328.1**	**9.5**
7	1682	224	**105.7**	**8.8**
8	2013	892	**587.6**	**19.2**
9	2013	223	**148.2**	**6.6**
10	2345	866	**747.4**	**16.3**
11	2345	217	**144.8**	**7.7**
12	2345	650	**425.7**	**12.2**
13	2345	433	**328.0**	**6.0**

Table E.1. Cummins EPA certification NOx and PM emissions

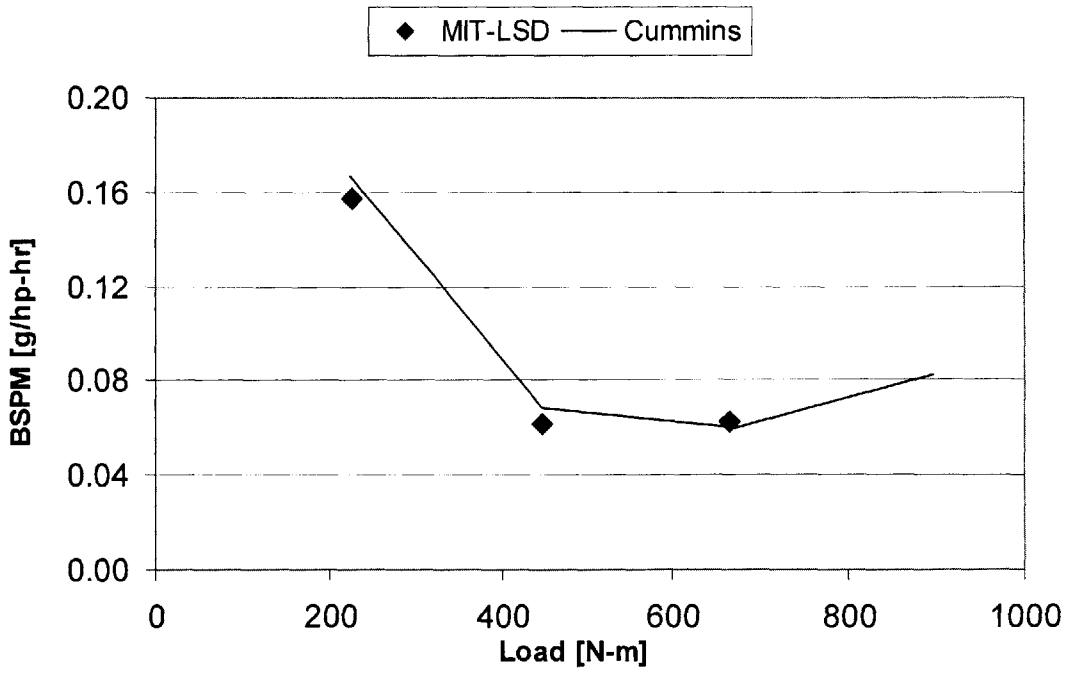

Figure E.1. Comparison of MIT PM emissions to Cummins PM emissions at an engine speed of 1682 rpm

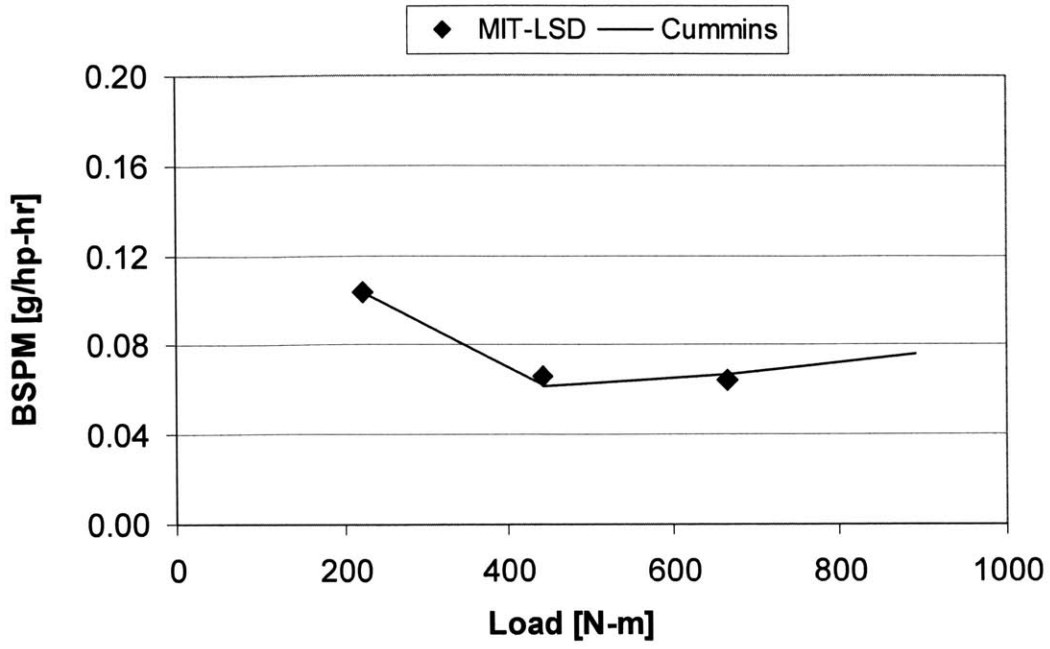

Figure E.2. Comparison of MIT PM emissions to Cummins PM emissions at an engine speed of 2011 rpm

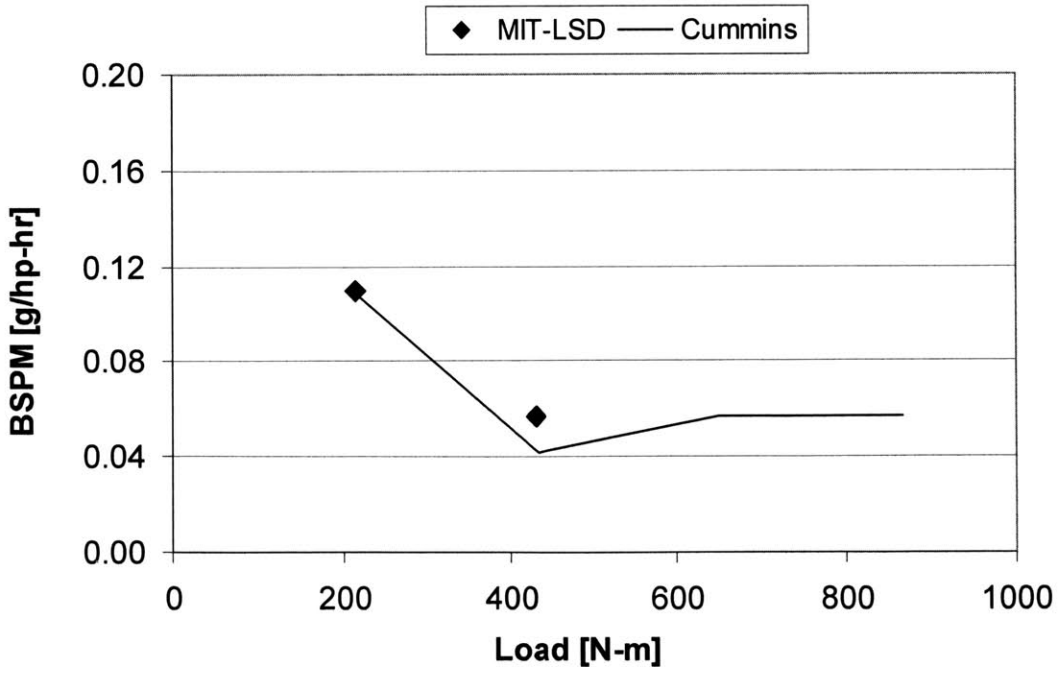

Figure E.3. Comparison of MIT PM emissions to Cummins PM emissions at an engine speed of 2345 rpm